Project THEMIS
Technical Report No. 22

PREDICTION OF THE TURBULENT BOUNDARY LAYER SEPARATION

by

Fang-Kuo Chou
and
Virgil A. Sandborn

Prepared under

Office of Naval Research

Contract No. N00014-68-A-0493-0001

Project No. NR 062-414/6-6-68(Code 438)

U.S. Department of Defense

Washington, D.C.

Fluid Dynamics and Diffusion Laboratory
College of Engineering
Colorado State University
Fort Collins, Colorado

July 1973

CER73-74FKC-VAS3

ABSTRACT

PREDICTION OF THE TURBULENT BOUNDARY LAYER SEPARATION

A method for the prediction of the location of turbulent boundary layer separation is developed. The method is based on the inner and outer velocity distributions technique developed by Stratford, together with a separation criterion which applies directly to the separation position.

For the inner region, the model employs the empirical one-parameter boundary layer separation profiles proposed by Sandborn and Kline. For the outer region the equivalent velocity distribution for the flow on a flat plate has been used. The resulting formula for predicting the separation position is a simple non-linear algebraic equation.

The method is tested by comparing with several well documented separation measurements. The results show a good agreement in the prediction of the position of turbulent separation. The calculated pressure rise to separation is also in good agreement with experimental results.

An experimental study for a turbulent boundary layer up to and through the separation region has been made to further demonstrate the present method. The measurements were taken along the test wall of a two dimensional diffuser. Mean quantities, turbulent intensities and the wall shear stresses were measured. The velocity profile integral parameters were evaluated from the measured data. The results are also compared with the separation model suggested by Sandborn and Kline. At the start of the separation region, the velocity profile correlation falls approximately on the unrelaxed separation correlation curve given

by Sandborn and Kline. The velocity profiles in the separation region are well represented by the two-parameter separation profiles suggested by Sandborn.

ACKNOWLEDGMENT

This work was supported by the Office of Naval Research, U.S. Department of Defense under contract No. N00014-68-A-0493-0001, project No. NR062-414/6-6-68 (Code 438). The authors gratefully acknowledge this support.

TABLE OF CONTENTS

LIST OF TABLES

LIST OF FIGURES

LIST OF SYMBOLS

Symbol	Definition
a	Constant
A	Constant
b	Constant
B	Constant
C	Constant
C_2	Constant
C_f	Skin-friction coefficient $\frac{\tau_w}{1/2\ \rho U^2}$
C_p	Pressure coefficient $1 - \frac{U^2}{U_o^{\ 2}}$
E_m	Mean voltage
h	Distance normal to wall
H	Velocity form factor $\frac{\delta^*}{\theta}$
H^*	Ratio of the energy-dissipation thickness to the momentum thickness $\frac{\theta^*}{\theta}$
I	Current
K	Karman constant
K_1	Constant
L	Shape factor $\int_{1.73}^{H^*} \frac{dH^*}{(H-1)\ H^*}$
m	Separation profile parameter
m_1	Separation profile parameter
n	Exponent in power law equation
p	Static pressure
p_o	Minimum static pressure
q	Dynamic pressure outside boundary layer
Q	Heat transfer of the hot wire

LIST OF SYMBOLS - Continued

Symbol	Definition
R	Resistance of the hot wire
R_a	Cold resistance of the hot wire
R_e	Reynolds number $\frac{U_o x}{\nu}$
R_θ	Reynolds number based on the momentum thickness $\frac{U\theta}{\nu}$
u	Mean velocity in x-direction
u_t	Total velocity
u'	Turbulent fluctuation in x-direction
U	Free stream velocity
U_o	Peak free stream velocity
v'	Turbulent fluctuation in y-direction
w'	Turbulent fluctuation in z-direction
x	Longitudinal coordinate parallel to wall
x_o	Point of maximum velocity
X	Equivalent coordinate
X_o	Point of maximum velocity from the equivalent leading edge
y	Coordinate normal to wall
z	Lateral coordinate parallel to wall
α	Angle of attack
γ	Shape parameter $\frac{u\|y=\theta}{U}$
Γ	Shape factor $\frac{\theta}{U}\ \frac{dU}{dx}\ \left(\frac{U\theta}{\nu}\right)^4$
δ	Boundary layer thickness
δ^*	Displacement thickness $\int_o^\infty (1 - \frac{u}{U})\, dy$
η	Shape factor $1-\left(\frac{u\|y=\theta}{U}\right)^2$

LIST OF SYMBOLS

Symbol	Definition
ζ	Separation profile slip parameter
θ	Momentum thickness $\int_o^\infty \frac{u}{U}(1 - \frac{u}{U})\, dy$
θ^*	Dissipation-energy thickness $\int_o^\infty \frac{u}{U}(1 - \frac{u^2}{U^2})\, dy$
λ_δ	Pohlhausen pressure parameter $-\frac{\delta^2}{\nu}\frac{dU}{dx}$
μ	Dynamic viscosity
ν	Kinematic viscosity
ρ	Density of fluid
σ	Free stream flow parameter $\frac{1}{(x_s - t_o)}\left[\int_{x_o}^{x_s} xC_p \frac{dC_p}{dt}\right]^{1.2} / \frac{1}{(x_s - x_o)}\int_{x_o}^{x_s} C_p\, dx$
σ^2	Variance
$\psi^{\cdot}$	Stream function $\int_o^y u\, dy$
ψ_i	Stream function in the inner layer
τ	Shear stress
τ_w	Shear stress at wall

Suffixes

o	Conditions at the position of the peak velocity
'	Velocity fluctuations
'	Derivative with respect to x
'	Denotes value for the comparison profile of constant pressure in flat plate case
s	Denotes value evaluated at separation
t	Denotes value evaluated at transition position
w	Denotes value evaluated at the wall

Chapter I

INTRODUCTION

Separation is mostly an undesirable phenomenon because it is associated with large energy losses. Most conventional aerofoil sections are designed with a flow configuration such that separation occurs just prior to the trailing edge to provide optimum performance. For this reason it is an important problem in the boundary layer application to determine whether the flow will separate from a specific surface of body; and if it does, it is essential to know where the point of separation occurs.

In the past a considerable amount of effort has been made to develop methods for calculating the turbulent boundary layer. Because of the complicated phenomena associated with the formation of the turbulent boundary layer, all existing methods are empirical or semi-empirical. Most of the methods are based on the momentum or energy integral equations in conjuction with empirical expressions representing the shape and the behavior of the velocity profile. Gruschwitz (1931) introduced a shape factor η , which was related to the velocity at a distance equal to the momentum thickness from the wall, and found that separation occurred for $\eta \approx 0.8$. Doenhoff and Tetervin (1943) chose the form factor H , which is the ratio of the displacement thickness to the momentum thickness of the boundary layer, as a single parameter in the development of the turbulent boundary layer. The criterion for separation was that H should lie between 1.8 and 2.6. Truckenbrodt (1952) suggested a shape factor L , which was a function of both H and H^* , the latter is the ratio of the energy-dissipation thickness to the momentum thickness. Separation occurs for $L = -0.13$ to -0.18.

These methods and others (Ref. 17) are reasonably accurate except near separation where none of the predictions appear to approach the separation criterion, as was indicated by Sandborn (1971). Furthermore, the mathematical complexities associated with these methods are considerable. Since these numerical or step-by-step methods require an amount of work which is not practical in actual applications, it is therefore important to devise a simple technique which would quickly lead to a reasonably accurate prediction.

Stratford (1959A) developed a rapid method for the prediction of flow separation which can be applied directly to the separation position. The equation of motion was integrated by a modified inner and outer solutions technique. Near the wall it was assumed that the velocity was proportional to the square root of the distance from the wall when the flow approached separation. For the outer region, since the losses due to the shear stresses are almost the same as for the flow on a flat plate, a solution was obtained in terms of flat plate flow. According to Stratford, the accuracy of the prediction in the pressure coefficient at separation is about 0 to 20 percent. Sandborn and Liu (1968) obtained results similar to those of Stratford by using both linear and parabolic velocity distributions in the inner region. Results from these highly approximate velocity distributions suggest that more accurate predictions of separation may be possible by using more accurate empirical velocity distribution relations.

The purpose of the present study is to develop a method to improve the prediction of the separation by using more realistic separation profiles. The one parameter family of separation velocity profiles proposed by Sandborn and Kline (1961) was employed together with Stratford's two layer concept. Although the Sandborn and Kline's model is also inadequate to represent the velocity distribution in detail, it has been shown to fit most separation measurements in the overall integral effects. Data from various sources and from the measurements in the CSU separation wind tunnel were analyzed to test the present method. The results show a good agreement in the prediction of the position of turbulent separation and in the pressure rise to separation. The separation profile parameter can be expressed as a unique function of non-dimensional pressure coefficient of the flow field.

Chapter II

REVIEW OF LITERATURE

2.1 Definitions and Concepts

Boundary layer flow has the property that under certain conditions the flow in the neighborhood of a wall becomes reversed causing the boundary layer to separate. Prandtl first explained the phenomenon of separation of a two-dimensional boundary layer as shown in Fig. 1. A fluid particle moving in the immediate vicinity of the wall is retarded by the friction of the wall. If the pressure increases downstream the particle may not have sufficient momentum to move farther into the region of the increasing pressure, and its motion will be brought to rest at some point S . Further downstream of this point, the external pressure will cause it to move in the opposite direction. The point of separation was defined in Prandtl's concept as the limit between forward and backward flow in the immediate neighborhood of the wall, or the wall shear stress.

$$\tau_w = \mu \frac{\partial u}{\partial y} \Big|_w = 0 \qquad (2\text{-}1)$$

It is now evident that Prandtl's model of boundary layer separation is too idealized for general engineering applications, since much of the undesirable features of turbulent boundary layer separation are associated with unsteady character. Kline's flow visualization studies (1957) showed that turbulent separation began as a local, unsteady, three-dimensional phenomenon. The separation was seen to develop into what was thought to be a statistically "steady" type of separation. These flow visualizations indicate that turbulent separation is not always an abrupt event as implied in the classical model of separation. Sandborn and Kline (1961) suggested that a transition region existed where the flow changed from the "unsteady" to the "steady" type separation. The experimental measurements by Liu (1967) demonstrate the existence of the transition region in the turbulent boundary layer separation. Liu's measurements indicate that at the start of the transition region a small positive mean wall shear stress exists. Only at the end of the transition region does the time average of the wall shear appear to vanish. Recently, Sandborn (1971) proposed a more general model for boundary layer separation to include time dependent boundary layers in the framework. The new model is based on the concept of an adjustment time for the boundary layer, and separation was defined as the removal of viscous restraints at the wall. Thus, the transition region was viewed as a region over which the flow adjusts to the removal of viscous restraints at the wall. At the start of the separation region, boundary conditions are such that viscous effects at the surface are negligible. At the end of the region the complete velocity distribution has adjusted to the surface condition. If a laminar boundary layer approaches separation in a sufficiently mild pressure gradient, the whole layer can adjust to the boundary conditions. In this case the transition region reduces to a point. On the other hand, if the approach to separation is very rapid, or for a turbulent boundary layer, the velocity distribution does not adjust to the wall conditions and a transition region exists. The nature of the turbulent boundary layer is such that a transition region would be expected. Fig. 2 shows a sketch of the proposed general model of the separation region. Experimentally, the start of the separation can be identified by the flow visualization technique. Tufts, smoke and other chemical compounds have been used for this purpose. It is believed that most turbulent boundary layer separation measurements were made at or near the start of the separation region.

2.2 Calculation of Turbulent Boundary Layer Separation

Since the complete phenomena associated with the formation of turbulent boundary layer are far from understood at the present time, all existing methods for the calculation of turbulent boundary layers are either empirical or semi-empirical. These methods are based mainly on the integral forms of the momentum and energy equations using empirical expressions for shear and dissipation in turbulent flow.

2.2.1 Methods based on the momentum integral equation

The momentum integral equation was first derived by von Karman by integrating the boundary layer equation from $y = 0$ to $y = h > \delta(x)$. For steady, two-dimensional, incompressible flow it assumes the form

$$\frac{d\theta}{dx} + (H+2)\frac{\theta}{U}\frac{dU}{dx} = \frac{\tau_w}{\rho U^2} \tag{2-2}$$

where H is the form factor defined as the ratio of displacement δ^* to momentum thickness θ, thus

$$H = \frac{\delta^*}{\theta}$$

and

$$\delta^* = \int_o^\infty (1 - \frac{u}{U})\, dy$$

$$\theta = \int_o^\infty \frac{u}{U}(1 - \frac{u}{U})\, dy$$

In order to determine the variations of momentum thickness along the contour of the body, data on the form factor H and the shear stress at the wall $\frac{\tau_w}{\rho U^2}$ are needed. This information was obtained by each author in a different way. In spite of the different assumptions for the shear stress τ_w and form factor H , most of the methods led to the following equation. (See for example Rotta, 1962)

$$\theta \left(\frac{U\theta}{\nu}\right)^{\frac{1}{n}} = U^{-b} \left(C + a \int_{x=x_t}^{x} U^b \, dx\right) \tag{2-3}$$

where C is a constant to be determined from the laminar boundary layer at point of transition $x=x_t$, and n, a, b are constants. The constants are slightly different for different methods.

For the prediction of separation a second equation, the so called shape parameter equation is needed. Various authors used different shape factors for the turbulent velocity profiles and established differential equations for them as well as for the momentum thickness. Gruschwitz (1931) introduced the shape factor

$$\eta = 1 - \left(\frac{u|y=\theta}{U}\right)^2$$

where $u|y=\theta$ denotes the velocity in the boundary layer at a distance $y=\theta$ from the wall. Separation occurs for $\eta \approx 0.8$. Buri (1931) chose for this purpose the dimensionless quantity

$$\Gamma = \frac{\theta}{U} \frac{dU}{dx} \left(\frac{U\theta}{\nu}\right)^{\frac{I}{4}}$$

Separation occurs when $\Gamma \approx -0.06$. The method due to von Doenhoff and Tetervin (1943) assumes that the shape of all turbulent boundary layer profiles can be expressed as a function of a single parameter H. Separation occurs for values of H greater than 1.8 and less than 2.6. Garner (1944), Maskel (1951), and Schuh (1954) also employed the parameter H , but with different functional forms. All these methods appear to give some insight into the problem.

2.2.2 Methods based on the momentum and energy integral equations

Using a similar approach, Wieghardt (1948) deduced the energy integral equation by multiplying the boundary layer equation by u and then integrating from $y = 0$ to $y = h > \delta(x)$. In the case of steady two-dimensional incompressible flow the energy integral equation takes the form

$$\frac{d}{dx}(U^3\theta^*) = 2\int_0^\infty \frac{\tau}{\rho}\frac{\partial u}{\partial y}\,dy \qquad (2\text{-}4)$$

where θ^* is the dissipation-energy thickness defined as

$$\theta^* = \int_0^\infty \frac{u}{U}\left(1 - \frac{u^2}{U^2}\right) dy$$

Truckenbrodt (1952) assumed that turbulent velocity profiles formed a one-parameter family of curves, as was done by Doenhoff and Tetervin, and introduced a shape factor L in the form

$$L = \int_{Ho^*}^{H^*} \frac{dH^*}{(H-1)H^*}$$

where H^* is the ratio of dissipation-energy thickness θ^* to momentum thickness θ . He found that $Ho^* \approx 1.73$. Separation occurs at $L \approx -0.13$ to -0.18 . Rotta (1952) made use of the parameter H^* and assumed the logarithmic profile in his calculations. Spence (1956) introduced

$$\gamma = \frac{u|_{y=\theta}}{U}$$

as the characterizing shape parameter and supposed the shear stress distribution to be a function of the shape parameter as well as the non-dimensional pressure gradient. These methods and others are reasonably accurate except near the separation where none of the predictions appear to approach the separation criterion (Sandborn, 1971). In most cases the mathematical development is very complex. For further details concerning the calculations of the turbulent boundary layer and the comparison of the various methods, references can be made to Thompson (1964), Schlichting (1968), Rotta (1962), and Chang (1970). In particular, the recent development of this subject has been summarized in Ref. 17.

2.2.3 Methods based on the inner and outer solutions

The method of inner and outer solutions was first introduced by von Karman and Millikan (1934) for the laminar boundary layer calculation. By a slight modification of von Mises' equation, two solutions were found, one of which was exact at the wall while the other was exact at the outer edge of the boundary layer. By matching these two solutions at the inflection point of the velocity profile, the final solution was obtained. In addition, a relationship for predicting the position of laminar separation was derived, although the resulting form was difficult to apply. Doenhoff (1938) modified Karman and Millikan's solution and derived a form which could be applied to any flow case rapidly. Unfortunately, the accuracy of Doenhoff's method is questionable. Stratford (1957) assumed that in the outer layer the pressure rise mainly produced a lowering of the dynamic head profile; the losses due to the shear stresses being the same as for the flow on a flat plate. In the inner layer, on the other hand, the pressure force was assumed to be balanced entirely by the shear force. The inner solution was matched smoothly with the outer solution at a suitable point. A simple formula for predicting the laminar boundary layer separation was obtained in the form

$$x_s^2 \, C_p \left(\frac{dC_p}{dx}\right)^2 = K_1 \tag{2-5}$$

where C_p is pressure coefficient defined as

$$C_p = 1 - \frac{U^2}{U_o^2}$$

Stratford suggested that a value for $K_1 = 0.0076$ should lead to good prediction of separation. Curle and Skan (1957) pointed out that $K_1 = 0.0104$ would give a better prediction. Liu and Sandborn's (1968) testing of Eq. (2-5) indicated that K_1 lay between 0.0076 and 0.0104.

Similar to the inner and outer solutions for a laminar boundary layer, Stratford (1959A) obtained a relation for the prediction of the turbulent boundary layer separation. Based on the mixing length theory, the formula was derived as

$$(2C_p)^{\frac{n-2}{4}} \left(x_s \frac{dC_p}{dx}\right)^{\frac{1}{2}} = 0.78 \, (10^{-6} \, Re)^{\frac{1}{10}} \tag{2-6}$$

where Re is Reynolds number. Townsend (1962) assumed a logarithmic profile at the initial position instead of a power law profile as was used by Stratford. Liu (1967) obtained similar results by assuming that in the inner layer the eddy viscosity is constant near the separation point. The point of separation was given as

$$C_p^{\frac{1}{4}(2n-1)} \left(x_s \frac{dC_p}{dx}\right)^{\frac{1}{2}} \approx 0.22\ C_2 \qquad (2\text{-}7)$$

C_2 varies from 0.377 for $n = 6$ to 0.24 for $n = 8$.

2.3 Boundary Layer Separation Profiles and Correlations

The prediction of the boundary layer separation depends on the understanding of the velocity distribution in this region. The analyses of Stratford (1959A) and Townsend (1962), which led to the prediction of continuous separating turbulent boundary layer employed a velocity distribution of the form

$$u \propto \left(y \frac{\partial p}{\partial x}\right)^{\frac{1}{2}} \qquad (2\text{-}8)$$

near the wall. Sandborn and Liu (1968) obtained results similar to those of Stratford by using both linear and parabolic velocity distributions in the inner region. Results from these highly approximate velocity distributions suggest that more accurate predictions of separation may be made by using more accurate empirical velocity distribution relations.

Sandborn (1959) developed an empirical velocity profile which can be used in laminar as well as turbulent flow. For laminar boundary layer separation the empirical velocity profile is reduced to the form

$$\frac{u}{U} = 1 + \left(1 - \frac{y}{\delta}\right)^{\sqrt{-\lambda_\delta}} \left[\sqrt{-\lambda_\delta}\ \ell n \left(1 - \frac{y}{\delta}\right) - 1\right] \qquad (2\text{-}9)$$

where

$$\lambda_\delta = - \frac{\delta^2}{\nu} \frac{dU}{dx}$$

For the turbulent boundary layer separation the profile becomes

$$\frac{u}{U} = 1 - (1 - \frac{y}{\delta})^m \tag{2-10}$$

where m is a constant depending on the free stream flow conditions. From the analysis of these empirical velocity profiles, two types of separation, relaxed (steady) and unrelaxed (unsteady), were identified. The words steady and unsteady were used in the original paper. In the model proposed by Sandborn (1971), the transition region was viewed as a region where the velocity distribution relaxed or adjusted to the boundary conditions. Therefore, the words relaxed and unrelaxed have been thought to be a better description of the process. For the relaxed separation case, the relationships between the profile parameters can be expressed parametrically in terms of λ_δ

$$\frac{\delta^*}{\delta} = \frac{2\sqrt{-\lambda_\delta} + 1}{(\sqrt{-\lambda_\delta} + 1)^2} \tag{2-11a}$$

$$\frac{\theta}{\delta} = \frac{(2\sqrt{-\lambda_\delta} + 1)}{(\sqrt{-\lambda_\delta} + 1)^2} - \frac{2\ (\sqrt{-\lambda_\delta}\ )^2}{(2\sqrt{-\lambda_\delta} + 1)^3}$$

$$- \frac{2\sqrt{-\lambda_\delta}}{(2\sqrt{-\lambda_\delta} + 1)^2} - \frac{1}{(2\sqrt{-\lambda_\delta} + 1)} \tag{2-11b}$$

For the unrelaxed case, the empirical relationship between the profile parameters was given as

$$H = 1 + \frac{1}{(1 - \delta^*/\delta)} \tag{2-12}$$

Equations (2-11) and (2-12) are replotted in Fig. 3. The upper curve is called the relaxed separation correlation, while the lower one corresponds to the unrelaxed separation correlation. The unrelaxed separation curve has been found to agree well with most turbulent separation measurements. Both experimental measurements and analytic solutions of laminar separation have been shown to fall approximately on the relaxed separation correlation curve.

In keeping with the observed adjustment concept, Sandborn (1970) recently suggested a more general form of the velocity profile. The model employed a "slip" parameter ζ in the form of

$$\frac{u}{U} = 1 + \zeta \left(1 - \frac{y}{\delta}\right)^{m_1} \left[m_1 \ln \left(1 - \frac{y}{\delta}\right) - 1\right] \qquad (2\text{-}13)$$

where m_1 is a constant depending on the free stream flow conditions. The parameter ζ is equal to 1 for relaxed separation, and $0<\zeta<1$ represents all possible unrelaxed separations. Equation (2-13) is shown in Fig. 3 as dashed curves. The unrelaxed separation curves correspond to values of ζ from 0.80 to 0.85. The experimental data fall in a region between $\zeta = 0.81$ to 0.90 .

Chapter III

THEORETICAL ANALYSIS

Many of the approximate solutions for turbulent boundary layers have already been discussed in Chapter II. The present analysis is based on the inner and outer layer concept developed by Stratford (1959A); in the inner layer the empirical separation velocity profiles proposed by Sandborn and Kline (1961) is employed.

3.1 The Outer Layer

For the flow under consideration a constant pressure exists for a distance x_o , beyond which the pressure begins to rise abruptly. In the outer layer, the shear force is small compared with either the inertia force or the pressure gradient. It may be assumed, following Stratford's Concept, that the losses in the outer layer due to the shear stress in the present flow situation is the same as for a flat plate flow (which has identical conditions as far as $x=x_o$, but which continues at constant static pressure thereafter). By applying Bernoulli's equation along a stream line, the following formula is obtained

$$\frac{1}{2} \rho u^2 (x, \psi) = \frac{1}{2} \rho u'^2 (x, \psi) - (p - p_o) \qquad (\psi \geq \psi_i) \qquad (3\text{-}1)$$

in which the prime denotes the comparison profile of constant pressure for the flat plate case. ψ is stream function defined as

$$\psi = \int_o^y u \, dy$$

and the condition $\psi \geq \psi_i$ denotes the stream line of Eq. (3-1) is in the outer region of the profile. Thus, the dynamic head at any point downstream of x_o is equal to the dynamic head at a corresponding point in the comparison profile of flat plate flow minus the rise in static pressure.

The following power law velocity profile is assumed to exist for the constant pressure flow

$$\frac{u'}{U_o} = (y'/\delta')^{\frac{1}{n}} \tag{3-2a}$$

where

$$\delta' = \frac{(n+1)\ (n+2)}{n}\ \theta' \tag{3-2b}$$

$$\theta' = 0.036\ x\ Re^{-\frac{1}{5}} \tag{3-2c}$$

and n can be approximated by

$$n = \log_{10} Re \tag{3-2d}$$

as suggested by Stratford (1959A).

Differentiating Eq. (3-1) with respect to ψ , and replacing $u \frac{\partial}{\partial \psi}$ by $\frac{\partial}{\partial y}$ yields

$$\left.\frac{\partial u}{\partial y}\right|_{(x,\ \psi)} = \left.\frac{\partial u'}{\partial y'}\right|_{(x,\ \psi')} \qquad (\psi \geq \psi_i) \tag{3-3}$$

where

$$\psi = \psi' \tag{3-4}$$

from the continuity considerations.

3.2 The Inner Layer

In the inner layer, the inertia of the fluid is small. In particular the inertial force at the wall is zero, so the pressure force must be balanced entirely by the shear force, that is

$$\frac{\partial p}{\partial x} = \frac{\partial \tau}{\partial y} \tag{3-5}$$

which follows from the equation of motion by neglecting the inertia forces. This balance at the wall can be achieved only when the shape of the velocity profile is altered. The inner layer starts to grow from the point $x=x_o$, $y=0$, and the slopes of the velocity profiles have to change in the region beyond $x = x_o$.

Several different assumptions have been made for the velocity profile in the inner layer when the flow approaches separation. Coles (1954) assumed that at the point of separation the velocity profile could be described by the wake function alone. By assuming that the mixing length is proportional to the distance from the wall and setting the wall shear stress equal to zero, Stratford (1959A) obtained the velocity distribution near the wall in the form

$$u = \left(\frac{4y}{K^2 \rho} \frac{\partial p}{\partial x}\right)^{\frac{1}{2}} \tag{3-6}$$

Stratford suggested that Eq. (3-6) could be regarded as the first term of the series expansion representing the whole inner layer profile. However, this assumption leads to an infinite shear stress at the wall rather than a zero wall shear. Since the shear stress at the wall

$$\tau_w = \mu \left.\frac{\partial u}{\partial y}\right|_{y=o} = y^{-\frac{1}{2}} \left(\frac{1}{K^2 \rho} \frac{\partial p}{\partial x}\right)^{\frac{1}{2}} \tag{3-7}$$

becomes infinite when y approaches zero. Liu (1967) obtained a linear velocity distribution by using a constant eddy viscosity for the inner layer. Results from these highly approximate velocity distributions suggest that a more realistic empirical velocity distribution relation may improve the prediction of separation.

For the present study, the one-parameter separation velocity profile proposed by Sandborn and Kline (1961)

$$\frac{u}{U} = 1 - (1 - \frac{y}{\delta})^m \tag{3-8}$$

will be analyzed. This empirical profile has been shown to fit most turbulent separation measurements. In addition, the two-parameter separation profile suggested by Snadborn (1970)

$$\frac{u}{U} = 1 + \zeta\ (1 - y/\delta)^{m_1}\ [m_1\ \ell n\ (1 - y/\delta) - 1] \tag{3-9}$$

will be investigated. The comparison of Eqs. (3-6), (3-8), and (3-9) with a set of turbulent separation profiles measured by Stratford is shown in Fig. 4. Linear and parabolic velocity distributions assumed by Sandborn and Liu are also shown in Fig. 4. It is apparent that Eqs. (3-8) and (3-9) are more acceptable than that of Stratford's or Liu's.

3.3 The Equations to Predict Separation

At the join between the inner and outer layers continuity is specified in ψ, u, and $\frac{\partial u}{\partial y}$; that is ψ, u, and $\frac{\partial u}{\partial y}$ for the inner layer are equal to ψ, u, and $\frac{\partial u}{\partial y}$ for the outer layer. From Eqs. (3-3) and (3-4), ψ and $\frac{\partial u}{\partial y}$ for the outer layer are equal to ψ' and $\frac{\partial u'}{\partial y'}$ for the corresponding point on the flat plate comparison profile.

Therefore, ψ and $\frac{\partial u}{\partial y}$ for the inner layer are equal to ψ' and $\frac{\partial u'}{\partial y'}$ for the corresponding point on the comparison profile. Thus, at the join, the following equations are satisfied

$$\psi = \psi' \tag{3-10}$$

$$\frac{\partial u}{\partial y} = \frac{\partial u'}{\partial y'} \tag{3-11}$$

where ψ and $\frac{\partial u}{\partial y}$ are the values obtained from the inner layer.

3.3.1 Prediction of separation by using the one-parameter velocity profile

The one-parameter velocity profile is given by Eq. (3-8). The corresponding values of u , ψ , and $\frac{\partial u}{\partial y}$ for the inner layer at the join as well as u' , ψ' , and $\frac{\partial u'}{\partial y'}$ for the comparison profiles are

$$u = U\,[1 - (1 - \frac{y}{\delta})^{m}] \tag{3-12a}$$

$$\psi = U\,[y + \frac{\delta}{m+1}\,(1 - \frac{y}{\delta})^{m+1} - \frac{1}{m+1}] \tag{3-12b}$$

$$\frac{\partial u}{\partial y} = U\,[\frac{m}{\delta}\,(1 - \frac{y}{\delta})^{m-1}] \tag{3-12c}$$

and

$$u' = U_o\,(y'/\delta')^{\frac{1}{n}} \tag{3-13a}$$

$$\psi' = \frac{U_o n}{n+1}\,(\delta')^{-\frac{1}{n}}\,(y')^{\frac{n+1}{n}} \tag{3-13b}$$

$$\frac{\partial u'}{\partial y'} = \frac{U_o}{n}\,(\delta')^{-\frac{1}{n}}\,(y')^{\frac{1-n}{n}} \tag{3-13c}$$

Substitutions of Eqs. (3-12) and (3-13) into Eqs. (3-10) and (3-11) produce

$$1 - \left[\frac{1}{mn} \frac{U_o}{U} \frac{\delta}{\delta'} \left(\frac{y'}{\delta'}\right)^{\frac{1-n}{n}}\right]^{\frac{1}{m-1}}$$

$$+ \frac{1}{m+1} \left\{ \left[\frac{1}{mn} \frac{U_o}{U} \frac{\delta}{\delta'} \left(\frac{y'}{\delta'} \right)^{\frac{1-n}{n}} \right]^{\frac{m+1}{m-1}} -1 \right\}$$

$$- \frac{n}{n+1} \frac{U_o}{U} \frac{\delta'}{\delta} \left(\frac{y'}{\delta'} \right)^{\frac{n+1}{n}} = 0 \qquad (3\text{-}14)$$

From Eq. (3-1) and the definition of C_p , it can be shown that

$$C_p = 1 - \frac{U^2}{U_o^{\,2}}$$

$$= \left(\frac{y'}{\delta'} \right)^{\frac{2}{n}} \left(1 - \frac{u^2}{u'^2} \right) \qquad (3\text{-}15)$$

Substituting Eq. (3-12) and (3-13) into Eq. (3-15) leads to

$$C_p = \left(\frac{y'}{\delta'} \right)^{\frac{2}{n}}$$

$$- \left(\frac{U}{U_o} \right)^2 \left\{ 1 - \left[\frac{1}{mn} \frac{U_o}{U} \frac{\delta}{\delta'} \left(\frac{y'}{\delta'} \right)^{\frac{1-n}{n}} \right]^{\frac{m}{m-1}} \right\}^2 \qquad (3\text{-}16)$$

where

$$\delta' = \frac{(n+1)\ (n+2)}{n} \theta' \qquad (3\text{-}17)$$

$$\theta' = 0.036 \times R_e^{-\frac{1}{5}} \qquad (3\text{-}18)$$

$$\delta = \frac{(2m+1)\ (m+1)}{m} \theta \qquad (3\text{-}19)$$

and θ can be calculated from Eq. (2-3). For example, Garner (1944) used $n = 6$, $a = 0.0076$, and $b = 3.67$. Eq. (2-3) then reduces to

$$\theta \left(\frac{U\theta}{\nu} \right)^{\frac{1}{6}} = U^{-3.67} \left(C + 0.0076 \int_{x=x_t}^{x} U^{3.67} \, dx \right) \qquad (3\text{-}20)$$

For the quantity n, which pertains to the flat plate comparison profile at $x = x_s$, Stratford (1959A) suggested the following form

$$n = \log_{10} Re \qquad (3\text{-}21)$$

where

$$Re = \frac{U_o x_s}{\nu} \qquad (3\text{-}22)$$

The relation between $\frac{y}{\delta}$ and $\frac{y'}{\delta'}$ can be obtained as

$$\frac{y}{\delta} = 1 - \left[\frac{1}{nm} \frac{U_o}{U} \frac{\delta}{\delta'} \left(\frac{y'}{\delta'} \right)^{\frac{1-n}{n}} \right]^{\frac{1}{m-1}} \qquad (3\text{-}23)$$

Thus, the join at the separation position is determined. Eq. (3-14) can be solved for $\frac{y'}{\delta'}$ if a relation between the profile parameter m and the free stream flow condition is found. The pressure coefficient C_p of the separation condition can be obtained from Eq. (3-16).

In the subsequent chapters the results of the present method will be compared with available published separation data and with data from the CSU separation wind tunnel. In particular, the correlation between the profile parameter m and pressure distribution of the flow field will be determined.

3.3.2 Prediction of separation by using the two-parameter velocity profile

The two-parameter velocity profile is given by Eq. (3-9). The quantities u, ψ, and $\frac{\partial u}{\partial y}$ for the inner layer at the join follow from Eq. (3-9) directly.

$$u = U \left\{ 1 + \zeta \left(1 - \frac{y}{\delta}\right)^{m_1} \left[m_1 \ln \left(1 - \frac{y}{\delta}\right) - 1\right] \right\} \tag{3-24a}$$

$$\psi = U \left\{ y + \frac{\zeta\delta}{m_1+1} \left(1 - \frac{y}{\delta}\right)^{m_1+1} \left[\frac{2m_1+1}{m_1+1} - m_1 \ln \left(1 - \frac{y}{\delta}\right)\right] - \frac{\zeta\,(2m_1+1)}{(m_1+1)^2} \right\} \tag{3-24b}$$

$$\frac{\partial u}{\partial y} = - \frac{U m_1^2 \zeta}{\delta} \left(1 - \frac{y}{\delta}\right)^{m_1-1} \ln \left(1 - \frac{y}{\delta}\right) \tag{3-24c}$$

Following the same procedure as in one-parameter profile case, the equation for the join at the separation position can be obtained as

$$\left[-\zeta n m_1^2 \frac{U}{U_o} \frac{\delta'}{\delta} \left(1 - \frac{y}{\delta}\right)^{m_1-1} \ln \left(1 - \frac{y}{\delta}\right)\right]^{\frac{1+n}{1-n}} - \frac{n+1}{n} \frac{U}{U_o} \frac{\delta}{\delta'} \left\{ \frac{y}{\delta} + \frac{\zeta}{m_1+1} \left(1 - \frac{y}{\delta}\right)^{m_1+1} \left[\frac{2m_1+1}{m_1+1} - m_1 \ln \left(1 - \frac{y}{\delta}\right)\right] - \zeta \frac{2m_1+1}{(m_1+1)^2} \right\} = 0 \tag{3-25}$$

The separation condition for C_p may be derived as

$$C_p = \left(\frac{y'}{\delta'}\right)^{\frac{2}{n}} \left(1 - \frac{u^2}{u'^2}\right) = \left(\frac{y'}{\delta'}\right)^{\frac{2}{n}} - \frac{U^2}{U_o^2} \left\{ 1 + \zeta \left(1 - \frac{y}{\delta}\right)^{m_1} \left[m_1 \ln \left(1 - \frac{y}{\delta}\right) - 1\right] \right\}^2 \tag{3-26}$$

The relation between y/δ and y'/δ' is given in the form

$$\frac{y'}{\delta'} = \left[- \zeta n m_1^2 \frac{U}{U_o} \frac{\delta'}{\delta} \left(1 - \frac{y}{\delta}\right)^{m_1 - 1} \ell n \left(1 - \frac{y}{\delta}\right)\right]^{\frac{n}{1-n}} \tag{3-27}$$

where

$$\delta = \frac{\theta}{\zeta} \frac{1}{\dfrac{2m_1+1}{(m_1+1)^2} - \dfrac{\zeta\,(10m_1^2 + 6m_1+1)}{(2m_1 + 1)^3}} \tag{3-28}$$

θ , n , δ' , and θ' are already given as Eqs. (3-20), (3-21), (3-17), and (3-18) respectively.

In this case there are two parameters to be determined before Eqs. (3-25) and (3-26) can be applied. The parameter m_1 , determines the shape of the profile, and ζ is a measure of the degree of adjustment. At the present time the values of ζ and m_1 cannot be predicted independent of the experimental measurements. The comparison of this method with separation measurements will also be made in Chapter 5.

3.3.3 Flow with favorable pressure gradient or laminar boundary layer over the region up to $x = x_o$

For a boundary layer having a region of favorable pressure gradient up to x_o , Stratford suggested that x_o used in above equations should be replaced by an equivalent value X_o defined as

$$X_o = \int_o^{x_o} \left(\frac{U}{U_o}\right)^3 dx \tag{3-29}$$

where x and X are the actual and the equivalent distances from the leading edge respectively. The criterion for equivalence is for the values of the boundary layer momentum thicknesses at the point of peak velocity to be the same for both the cases of zero pressure gradient and favorable pressure gradient over the first part of the boundary layer. For a flow which has a region of laminar boundary layer up to x_o , the equivalent distance X_o might be calculated from the following equation

$$X_o = 38.2 \left(\frac{\nu}{x_t U_t}\right)^{\frac{3}{8}} \left(\frac{U_o}{U_t}\right)^{\frac{25}{8}} \left[\int_o^{x_t} \left(\frac{U}{U_o}\right)^5 d \left(\frac{x}{x_t}\right) \right]^{\frac{5}{8}} + \int_{x_t}^{x_o} \left(\frac{U}{U_o}\right) dx \tag{3-30}$$

where the suffix t indicates the values at the laminar-turbulent transition position and the suffix o refers to conditions at the position of peak velocity, or at laminar-turbulent transition, whichever is further downstream.

Chapter IV

EXPERIMENTAL EQUIPMENT AND PROCEDURES

The experiment was performed in the separation wind tunnel located in the Fluid Dynamics and Diffusion Laboratory at Colorado State University. The main purposes of this experimental work are to study the flow characteristics in the separation region and to provide data for the prediction of the turbulent boundary layer separation. The mean velocities, turbulent fluctuations, and the shear stresses along the wall of the test model were measured. The experimental equipment and procedures used in this study are described briefly in the following sections.

4.1 Wind Tunnel

Measurements were taken in the boundary layer developed along the floor of the 10-foot test section of the CSU separation wind tunnel shown in Figs. 5 and 6. The wind tunnel is of the open circuit type and the air speed in the tunnel is controlled by means of a variable speed motor. An axial fan is employed to draw the ambient air through a circular inlet, past two transition sections, and then into the test section. In the fiberglass transition section the inside diameters of the wind tunnel vary from 36 to 18 inches and in the sheet metal transition section the cross sectional shape of the tunnel changes from round to square. The front part of the test section is a flat plate with a uniform cross section of 1'-6" by 1'-6", and a length of 3'-5 1/4". The shape of the rear part of the test wall is similar to that of a diffuser (Fig. 7), which was designed to produce separation and to hold the flow in a separating state for some distance downstream.

Static pressure taps of 0.02 inch diameter were embedded along the center line of the curved test wall. Honeycomb screens located in the inlet section produced a free stream turbulent level, $\frac{\sqrt{\overline{u'^2}}}{U}$, of about 3 percent. The measurements were made in a vertical plane along the center of the tunnel. The maximum air speed in the wind tunnel is about 45 fps. Turbulence levels of the order of 40 to 50 percent have been encountered in the separation region. The start of the curvature of the diffuser wall was chosen as origin of the coordinate system in the x-direction.

4.2 Instrumentation

4.2.1 Pitot static tube

During measurements the free stream velocity in the tunnel was checked by a 1/16 inch diameter pitot-static tube located in the uniform test section. The pitot static tube used was calibrated against a 1/4 inch diameter standard pitot static tube, which in turn was calibrated in a whirling-arm apparatus. The outlets of the pressure probe were connected to a pressure transducer by plastic tubing.

4.2.2 Hot-wire probe and anemometer

Mean velocities and turbulent fluctuations were measured by means of the hot-wire technique. The hot wire, made of 80 percent platinum and 20 percent iridium with a diameter of 0.0004 inch, was operated by a constant-temperature anemometer designed at Colorado State University. By using a constant-temperature hot-wire anemometer the electric resistance of the wire and its temperature are kept constant. A slight variation in velocity will result in a variation in heat loss from the hot wire, which in turn produces an unbalance of a Wheatstone bridge. Any unbalance in the bridge is compensated for by means of an electronic feedback system. The feedback system senses the unbalance in the bridge and alters the current to the bridge to rebalance it. Such a feedback system operates almost instantaneously, and it can follow and balance the bridge for frequencies up to 50,000 cps or greater. Mean voltages of the output signal of the anemometer were determined with an integrating circuit and a digital voltmeter. The integrator was employed to obtain long time period averages. The periods of averaging used was about 30 seconds for the present measurements. The integrator could easily be calibrated by introducing a non-fluctuating voltage from a power supply for the required time of integration. The root mean square of the output was measured by a true rms voltmeter.

The wire was aligned so that the axis of the sensing element was parallel to the floor and perpendicular to the flow direction. Typical wire lengths of the order of 0.04 inch were soldered to supports protruding from a 3/32 inch diameter ceramic probe. The ceramic probe was held by the sliding bearings of the probe holder, which in turn was held by a horizontal bar mounted on the axis of the probe actuator. Thus, the hot-wire probe could be moved through the boundary layer to measure the mean velocity profiles and turbulent fluctuations. The probe was calibrated against a standard hot wire probe in the wind tunnel in the free stream outside the boundary layer. The standard wire in turn was calibrated in an open circuit type small calibration wind tunnel. A typical calibration curve of voltage output versus flow velocity for the boundary layer hot wire is shown in Fig. 8.

4.2.3 Probe actuator

The hot wire probe was moved vertically through the boundary layer by means of a precision actuator. The movement of the actuator was controlled by an actuator controller. The position of the probe could be read at one thousandth of one inch intervals by means of a dial indicator which was connected to the actuator movement. The position of the probe with respect to the tunnel floor was determined from the dial indicator readings when the probe was touching the floor. The total travel distance of the actuator was approximately 6 inches. The actuator was fastened to the tunnel floor outside the tunnel, so that only the moving axis of the actuator was allowed to protrude into the boundary layer to minimize the disturbance to the flow.

4.2.4 Surface gage

The wall shear stresses were measured by means of a surface gage. A Ludwieg type (1950) heat transfer-shear stress gage was employed. A thin film platinum gage was mounted on a 0.003 inch mica sheet and glued to the surface of the test section. The surface gage was calibrated in the flat plate region of the test section. The calibrated gage was then moved to the downstream stations.

4.2.5 Microtector manometer

In the calibration of the pitot-static tube and the standard hot-wire probe, a microtector manometer (Fig. 9) was used. The microtector combines the principles of the Hook Gage type manometer and solid state integrated circuit electronics. The accuracy and repeatability of the gage is within ±0.00025 inch of water throughout its 0 to 2 inches water column range. A pressure to be measured is applied to the manometer fluid which is displaced in each leg of the manometer by an amount equal to one half the applied pressure. The hook is then lowered until it contacts the manometer gage fluid. The instant of contact is detected by completion of a low power A.C. circuit operating at a frequency of approximately 2000 cps. Completion of the A.C. circuit activates a bridge rectifier which provides the signal for indication on a sensitive D.C. microammeter.

4.3 Experimental Procedures and Data Reduction

4.3.1 Flow visualization technique

The start of the turbulent boundary layer separation was identified as the forward-most point where smoke was seen to reverse when released downstream. Smoke was produced by burning cigars with service air. The rate of smoke production and injection into the airstream were carefully controlled by means of settling bottles and pressure regulators. The area of separation was also alternatively identified by tufts indicating the forward-most point of flow reversal and by observing the evaporation rates of chemical tracer sprayed on the surface. A mixture of Methyl Salictlate, Glycerin, and fine Kaolin powder was used as the tracer. Results of these visual observations indicated that separation of the turbulent boundary layer occurred at approximately the 9 inches station. Separation was also observed to occur in the corners soon after the start of the curvature of the wall. Thus, the region of separation was not two dimensional across the diffuser. The observed separation appeared to be similar to many actual cases encountered in real applications.

4.3.2 Measurements of the mean velocities and the turbulent fluctuations

In the preliminary measurements, the mean velocity profiles were measured by means of total and static pressure tubes. The high turbulent level and low mean velocity encountered in the separation region making measurements of mean velocity with the Pitot-static tube difficult. Moreover, the directions of mean velocity vectors might be appreciably different from point to point in this region. Consequently, the hot wire technique of measurements was considered preferable over that of Pitot-static tube in the measurements of mean velocities for the present case. In transient measurements, the hot-wire anemometer has been accepted as a standard instrument for experimental studies of fluctuating velocities of the air flow.

In the hot-wire annemometer applications (Sandborn, 1972), it has been found that the heat loss from a specific hot wire is a function of velocity, temperature, fluid properties, and flow direction. For the present experiment, the temperature and the fluid properties of the flow were reasonably constant, and the mean flow direction along the vertical plane of the center line was approximately in the x-y plane. Thus, for a hot wire with its axis parallel to the floor and perpendicular to the flow direction, the heat loss might be assumed to be a function of the total velocity only. The relation between the mean heat loss and the mean velocity could be expressed by the modified King's Law

$$\frac{I^2R}{R-R_a} = A + Bu^r \qquad (4\text{-}1)$$

where r varies with Reynolds number. The dirivative of Eq. (4-1) with respect to u yields an expression from which the velocity sensitivity can be obtained. However, for this study a straight-forward method was used. The mean velocity was obtained directly from the calibration curve of the hot-wire voltage output versus flow velocity. The sensitivity of the hot wire was evaluated from the slope of the calibration curve. The rms values of the turbulent fluctuation $\sqrt{\overline{u'^2}}$, was obtained with a rms voltmeter.

4.3.3 Effect due to large turbulence

In the measurements of the mean velocities and the turbulent intensities, it was assumed that the fluctuating part of the velocity was small compared to the mean velocity. For a wire, as shown in Fig. 10, the total velocity which affects the convective heat transfer around the hot wire is

$$u_t = [(u+u')^2 + v'^2 + w'^2]^{\frac{1}{2}} \tag{4-2}$$

If it is assumed that

$$2\frac{u'}{u} >> \left(\frac{u'}{u}\right)^2 \text{ or } \left(\frac{v'}{u}\right)^2 \text{ or } \left(\frac{w'}{u}\right)^2$$

Eq. (4-2) then can be written approximately as

$$\left(\frac{u_t}{u}\right)^2 = 1 + 2\,\frac{u'}{u} \tag{4-3}$$

This shows that if the wire is aligned as shown in Fig. 10, the fluctuating part of the signal is predominately due to u' component of the velocity. However, in the separation region very near the surface the mean velocity is nearly zero, and the total velocity is approximately

$$u_t = (u'^2 + v'^2)^{\frac{1}{2}} \tag{4-4}$$

where w' was omitted in Eq. (4-2) because it is in the same direction as the axis of the wire and it has a negligible effect on the heat transfer rates of the wire. Thus, the heat loss is equally affected by both the u' and v' components. The upper limit on the error in assuming the wire normal to the mean flow for measuring $\sqrt{\overline{u'^2}}$ is 41 percent, as shown by Sandborn and Liu (1968). This maximum error could occur only in the region very near the surface. Since, in this region the boundary has a more restrictive effect on the magnitude of v' than on u', it is expected that the error in u' is much less than 41 percent.

4.3.4 Effect due to the solid boundary

When a hot wire is close to a solid boundary, errors may be introduced if the effect of the boundary on the rate of heat loss from the wire is ignored. The hot wire loses heat to the surface due to conduction, as well as to the air due to forced convection. Wills (1962) showed the effect of the solid boundary on the heat loss of the wire for laminar flow. Due to turbulent mixing, it is expected that correction for the wall effect would be smaller in the turbulent flow case than in the laminar flow case. The effect of the boundary on the heat transfer from the hot wire used in the present experiments for the no-flow condition is shown in Fig. 11. It can be seen that the effect of the surface becomes negligible when the wire is more than

0.04 inch away from the surface. When the wire is at a distance, y_o say, less than 0.04 inch from the wall, a correction for the molecular heat conduction of the hot wire to the wall can be made such that the ratio of the heat transfer at position y_o under a given flow condition to the heat transfer at position y_o under no-flow condition is the same as the ratio obtained by interpolation from the curves of Wills.

4.3.5 Shear stresses along the wall

The heat transfer from the surface gage to the flow is a function of the wall shear stress. It has been found that the relation between the heat transfer and the wall shear stress can be expressed approximately as

$$Q \approx \tau_w^{\frac{1}{3}} \tag{4-5}$$

where Q is the heat transfer from the gage. The wall shear for the flat plate region of the test section is determined from the measured mean velocity profiles. From the velocity profiles the skin-friction coefficient is computed by using the Ludwieg-Tillman formula (1950).

$$C_f = \frac{0.246}{10^{0.678H} R_\theta^{0.268}} \tag{4-6}$$

where R_θ is Reynolds number based on the momentum thickness and C_f is skin-friction coefficient defined as

$$C_f = \frac{\tau_w}{\frac{1}{2}\rho U^2} \tag{4-7}$$

The calibrated surface gage is then moved to the downstream stations to measure the shear stresses along the center line of the wall.

Chapter V

NUMERICAL PROCEDURES

Data were taken from the measurements of von Doenhoff and Tetervin (1943), Hewson (1949), Schubauer and Klebanoff (1951), Sandborn and Liu (1968), and Stratford (1959B) as well as from the present measurements in the CSU separation wind tunnel. In these measurements, the velocity profiles near or in the separation region have been reported. For the prediction of the turbulent separation position, the experimental data for the variations of free stream velocity and momentum thickness along the x-direction are needed, although the latter can also be calculated directly from Eq. (3-20).

5.1 Velocity Profile Parameters

Velocity profiles of the form expressed by Eqs. (3-8) and (3-9) were fitted by the least square method to the available mean velocity profiles in the separation region.

Velocity profiles of the one-parameter family (Eq. (3-8)) were fitted to the data for values of m varying in the range of 1.01 to 15.00 at equal increments of 0.01. The value of m giving the smallest computed variance would henceforth be substituted into Eq. (3-8) for subsequent computations.

Similarly, for the case of the two-parameter family of velocity profiles expressed by Eq. (3-9), the parameter ζ was first set equal to a fixed value in the range 0.70 to 1.00. For this fixed value of $\zeta = \zeta_j$, say, the value of m_{1j} which gave the smallest variance, σ_j^2 was determined just as in the one-parameter case. ζ was then allowed to take on values at equal increments of 0.01. Consequently, for each ζ_j , there corresponded a m_{1j} , giving the smallest variance σ_j^2 . The combination of the parameters ζ and m_1 resulting in the smallest σ^2 were used in Eq. (3-9).

The reason for the choice of the ranges for m In Eq. (3-8) and for m_1 and ζ in Eq. (3-9) was that all available separation velocity profiles appeared to fall well within this region. The fitting procedures were carried out with the aid of Colorado State University's CDC 6400 computer.

5.2 Free Stream Velocity and Momentum Thickness

For systemic calculations, the experimental values of the free stream velocity distributions, U(x), were first fitted to a suitable degree of polynomial by the least square method.

In applying Eq. (3-14) or eq. (3-25) to predict the turbulent separation position for the actual applications, the variations of the momentum thickness along the x-direction should be calculated directly from Eq. (3-20). However, since the purpose of the present study was to test the accuracy of the derived prediction formulae, the experimentally determined momentum thickness was used. To expedite calculations the experimental values of $\theta(x)$, were also smoothed out by a polynomial of the same degree as that used in the free velocity distribution case.

5.3 Prediction of Separation

With the velocity profile parameter m from section 5-1 and the data of free stream velocity U and momentum thickness θ from section 5-2, Eq. (3-14) can now be solved for y'/δ' for any point along the x-direction. The values of δ', θ', δ , and n , which are needed in solving Eq. (3-14), can be obtained from Eqs. (3-17), (3-18), (3-19), and (3-20), respectively. The pressure coefficient C_f is then obtained by substituting y'/δ' into Eq. (3-16). The calculations proceeded point by point in the downstream direction. If the computed pressure coefficient C_f agrees with the experimental results, the separation point is then determined.

In solving Eq. (3-14), Newton's iteration scheme was used in the form

$$x_{i+1} = x_i - \frac{f(x_i)}{f'(x_i)} \qquad (i = 1,2,3,\ldots)$$

where $f(x) = 0$ corresponds to Eq. (3-14), the prime denotes differentation. This scheme refines the initial guess x_i of a root of the general nonlinear equation $f(x) = 0$. Each iteration step requires one evaluation of $f(x)$ and one evaluation of $f'(x)$. The iterative procedure is terminated if the following conditions are satisfied

$$\delta \leq 0.0001 \quad \text{and} \quad |f\,(x_{i+1})| \leq 0.01$$

where

$$\delta = \begin{cases} \left|\dfrac{x_{i+1}-x_i}{x_{i+1}}\right| , & |x_{i+1}| > 1 \\ \\ |x_{i+1}-x_i| , & |x_{i+1}| \leq 1 \end{cases}$$

If no solution can be obtained for the specified initial guess and iteration steps, the procedure would also stop.

A similar procedure would also be applied to the case of the two-parameter family of velocity profiles. For a point on the surface, Eq. (3-25) is solved for y/δ with the velocity profile parameters, ζ and m_1 , from section 5-1 and boundary layer thickness δ from Eq. (3-28). The other data can be obtained in the same way as in the case of one-parameter family of velocity profiles. The join y'/δ' can be determined by substituting y/δ into Eq. (3-27). The pressure coefficient C_f follows from Eq. (3-26). The separation position is then determined by comparing the pressure coefficient C_f computed from Eq. (3-26) with the experimental results.

Equation (3-25) is also solved by the Newton's iteration scheme as described in the one-parameter case. Numerical computations were again performed on the Colorado State University's CDC 6400 computer.

Chapter VI

RESULTS AND DISCUSSION

6.1 Prediction of Turbulent Boundary Layer Separation and Comparison with Experimental Results

Figures 12 through 26 show the fitting of one-parameter velocity profiles (Eq. (3-8)) and two-parameter velocity profiles (Eq. (3-9)) to the measured separation velocity profile data. The calculated velocity profile parameters, m in the one-parameter parameter profiles and m_1 and ζ in the two-parameter profiles are also shown in Table 1. For the present measurements (Figs. 12-16), at the 9 inch station the one-parameter profiles could be fitted to the separation profile closely except near the surface. Downstream of the 9 inch station the discrepancy between the one-parameter profiles and measured separation profiles increased in the x-direction. The measured velocity profiles in the separation region were found to be well represented by the two-parameter profiles. For the data obtained by other investigators (Figs. 17-26) the separation velocity profiles were also found to be consistently well represented by the two-parameter velocity profiles. In fact, excluding very near the wall the neasured separation velocity profiles were in reasonable agreement with the one-parameter profiles, with the possible exception of the measurements of Sandborn and Liu at station 3.5. The correlation of this velocity profile parameter was shown by Sandborn and Liu (1968) to fall near the relaxed separation correlation curves. All the other separation profile correlations appear to approach the unrelaxed separation curve.

For any point along the x-direction, the join y'/δ' (or y/δ) can be evaluated as described in section 5.3. The pressure coefficient C_p is obtained from Eq. (3-16) or Eq. (3-26) respectively. If C_p computed by Eq. (3-16) or Eq. (3-26) agrees with experimental value, the separation point is then determined.

The positions of flow separation and pressure coefficient at separation as computed from the prediction equations, using (a) the one-parameter profiles and (b) the two-parameter velocity profiles were shown in Table 2 and in Figs. 27 through 41. The computed results using Stratford's method and the measured results in the present series of experiments as well as those from other sources were also presented in the table and in the figures for comparison.

The points of separation calculated by both the one-parameter and two-parameter methods were found generally to be closer to the actual separation point than that computed form Stratford's method. The percentage difference of the predicted pressure coefficient from the measured values for the one-parameter and two-parameter methods were also found to be generally smaller than that calculated by Stratford's method. In most cases the difference between the predicted and experimental pressure coefficients was less than 10 percent by using both the one-parameter and two-parameter methods. Since the predicted separation points computed by the two-parameter method were about the same as those by the one-parameter case; (and difficulties might be encountered in solving the two-parameter equation having logarithmic velocity profile in the inner layer) the simpler one-parameter method is suggested for prediction purposes. From the present results it appears that very accurate representation of the velocity profile in the inner layer is not critical in the prediction of the separation position.

Although the one-parameter method requires the solution of a non-linear algebraic equation, it is still preferable over the more cumbersome step-by-step and other numerical methods which involve a lengthy iteration procedure of solving the differential or difference equations. The equation for the join in Stratford's method can be solved directly. However, it involves a term expressing the gradient of the pressure coefficient which is not presented in the present method. Near the separation, the degree of accuracy of this gradient term calculated from experimental data is sometimes questionable. Due to its simplicity and reasonable degree of accuracy, the present one-parameter method may be employed in actual applications.

6.2 Correlation between the Profile Parameter and Free Stream Flow Condition

To apply the one-parameter equation in predicting the separation position, a correlation between the profile parameter and the free stream flow condition should be developed. Stratford's prediction formula indicates that the separation position depends only on the local pressure coefficient and pressure coefficient gradient. Sandborn (1969) suggested that the separation velocity profiles should depend on both the past history and local conditions of the flow. A nondimensional quantity, σ , which is defined as

$$\sigma = \frac{1}{x_s - x_o} \left[\int_{x_o}^{x_s} x \, C_p \, \frac{dCp}{dx} \right]^{1.2} \Big/ \frac{1}{x_s - x_o} \int_{x_o}^{x_s} C_p \, dx$$

was chosen as the free stream flow parameter. This parameter takes into account the effects of the pressure coefficient, the pressure gradient, and the past history of the flow on the separation velocity profiles. The variations of the profile parameter m versus the free stream flow parameter σ for the separation velocity profiles which fell approximately on the unrelaxed separation curve are shown in Fig. 42. Although the points show some degree of scatter, a definite trend for the variations of m with respect to σ was observed. It may be pointed out that Fig. 42 was an experimental determined criterion, the accuracy of the criterion depends on the accuracy of the measurements. It is possible that the scatter in the points represents second order effects. Thus, it appears that at the start of separation the turbulent separation profiles can be represented approximately by the one-parameter family of velocity profiles.

6.3 Flow Characteristics in the Turbulent Boundary Layer Separation Region

Very little information on the development of the flow downstream of the turbulent separation point has been reported. Stratford (1959A) was able to produce a continuous turbulent separation flow throughout a region of pressure rise. Sandborn and Liu (1968) reported some measurements in the separation region, which showed the turbulent separation profile developing to a laminar-like separation profile.

The geometry of the present test section was determined from considerations of the "continuous turbulent separation" flow of Stratford and the "relaxed separation" flow of Sandborn and Liu. It was desirable to obtain a flow which would develop beyond the usual turbulent separation point, with the transition region being maintained for some distance downstream of this point before becoming fully separated flow. The actual flow obtained was somewhat different than originally expected. A region was observed in which the flow appeared to approach the desired condition; however, further downstream of this region the boundary layer appeared to return to an unseparated state. Visual observations and measurements do not indicate a complete reversal of flow anywhere in the separation region. Instead, a rather large degree of intermittent type flow was observed near the surface in this region. The return of the flow to an unseparated condition was also noted as an increase in pressure along the wall downstream of the separation point as shown in Fig. 43. In the separation region the pressure along the wall is nearly constant.

6.3.1 Mean velocity profiles and separation correlations

The mean velocity profiles along the center line of the test section measured by the hot wire technique are shown in Fig. 44. For clarity, the velocity profiles are drawn on two separate sheets. The velocity profiles at stations of 0, 3, 6.25, 8.10, 9, 11, and 13 inches are shown in Fig. 44 a and the profiles at other stations are shown in Fig. 44 b. When the hot wire is at a distance less than 0.04 inches from the wall the correction of the conduction heat loss of the wire to the surface was made as described in Section 4.3.4 Downstream of the zero station, the boundary layer velocity profiles are of a typical turbulent shape and the boundary layer thickness increases stably. At the 9-inch station a typical turbulent boundary layer separation velocity profile was observed. In the separation region, downstream of the 9 inches station, the velocity distributions near the surface all appeared to be nearly the same. This observation was consistent with the similarity analysis of turbulent separation given by Sandborn (1970).

Figure 45 and Fig. 46 show the free stream velocity distributions and the growth of the boundary layer thickness along the test section. The boundary layer thickened from approximately 1.95 inches at the 0 station to 3.95 inches at the separation point (9 inch station). The integral parameters of the velocity profiles; displacement thickness δ^* , momentum thickness θ , and form factor H were computed from the measured velocity profiles. In calculating these parameters, 40 mesh points were taken across each velocity profile and Simpson's rule of integration was employed. Figures 47 to Fig. 49 show the variations of these parameters along the x-direction. The values of δ^*, θ, and H were found to increase gradually for some distance downstream of the 0 station, then increase more rapidly to separation. After the separation point, the values of δ^* and θ increased at about the same rates, thus the form factor H remained almost the same. The integral parameters and the wall shear stresses are also shown in Table 3. It is supposed that the energy required to create and maintain the large scale turbulence within the boundary layer, as it approaches separation, must be supplied from the boundary layer itself, resulting in a loss of momentum and an increased momentum thickness.

The relationship between the form factor H and ratio δ^*/δ for the present measurements is compared with Sandborn and Kline's relaxed and unrelaxed separation correlation as shown in Fig. 50. At the 0 station the values of δ^*/δ and H are 0.089 and 1.329 respectively. Both δ^*/δ and H increased systematically in the downstream direction and appeared to approach the unrelaxed separation curve. At the 9 inch station the velocity profile correlation falls on the unrelaxed separation correlation curve. Downstream of this point, the correlations of the profile parameters appeared to stay between the relaxed and unrelaxed correlation curves. The two-parameter correlation curves proposed by Sandborn (1970) are shown as dash curves in Fig. 50. The two-parameter velocity profiles was suggested by Sandborn to represent the velocity distributions throughout the whole separation region. The present experimental data fall in a region between ζ = 0.84 to 0.89. The present results confirm that at least a two-parameter velocity profile is required to completely specify the turbulent separate region. For engineering calculations it may be reasonable to employ the one-parameter relation of Eq. (3-8).

6.3.2 Turbulent intensity

Figure 51 shows the turbulent intensity distributions along the center line of the test section near and in the separation region. Near the surface, these measurements can only be considered as first-order approximations. Since in this region the mean velocity is small and the assumption of $u \gg u'$ or v' is not valid. As separation is approached, local high turbulent levels as great as ten times the mean velocity were observed. In the separation region the turbulent signal from the hot wire anemometer showed a definite skewing and a definite intermittent character near the wall. The position of the maximum intensity in the profile is found to move out away from the surface when flow approaches the separation region. The measurements at 6.25 inch station shows a maximum intensity at approximately 0.01 inch from the surface. For zero pressure gradient turbulent boundary layers, maximum intensity appears to approach the surface. The shift of the maximum intensity position from near the surface to the outer edge of the boundary layer is associated with adverse pressure gradient and turbulent separation, as reported by Sandborn and Slogar (1955) and Sandborn and Liu (1968).

6.3.3 Shear stresses along the wall

Figure 52 shows how the wall shear stresses vary along the center line of the diffuser. The wall shear stresses evaluated by the local heat transfer measurements were obtained by the technique developed by Ludwieg (1950). The heat transfer measurements are compared with values of the wall shear stress calculated from velocity profile measurements, using Ludwieg and Tillman's shear stress-profile parameter relationship Eqs. (4-6) and (4-7). The heat transfer measurements and the Ludwieg-Tillman relation are in good agreement at most stations. It is apparent that the wall shear stress in the separation region is not equal to zero as implied by Prandtl's separation definition. The wall shear stress decreases rapidly when the flow approaches separation and becomes negligible in the separation region.

6.3.4 Momentum balance in x-direction

From the preliminary mean velocity measurements an approximate balance of the x-direction momentum equation was made. Crude estimates of the velocity gradients and the vertical velocity were obtained from contour plots such as shown in Fig. 53. Figure 54 shows typical plots of the terms in the equation of motion as a function of the normal distance from the wall. These balances indicate that the shear stress term in the momentum equation is small compared to the inertial and pressure gradient terms except very near the surface where the shear stress is balanced by the pressure force. These results suggest that shear stress in the separation region is not important, as proposed by Sandborn and Liu (1968).

Chapter VII

CONCLUSIONS

A method to predict the position of the turbulent boundary layer separation and pressure coefficient at separation is derived. The method is based on the inner and outer velocity distributions technique developed by Stratford, the separation criterion can be applied directly to the separation position.

For the outer region the equivalent velocity distribution for the flow on a flat plate is used. For the inner region, both the empirical one-parameter and two-parameter families of separation profiles proposed by Sandborn are employed. The results are compared with experimental separation measurements as well as with the computed results using Stratford's method.

The points of separation calculated by both the one-parameter and two-parameter methods are found generally to be closer to the separation point than those computed from Stratford's method. The percentage differences of the predicted pressure coefficients from the measured values for the one-parameter and two-parameter methods are also found to be generally smaller than those calculated by Stratford's method. In most cases the differences between the predicted and experimental pressure coefficients are less than 10 percent by using both the one-parameter and two-parameter methods. The degree of accuracy for the one-parameter and two-parameter methods is about the same. From the present results it appears that very accurate representation of the velocity profile in the inner layer is not critical in the prediction of the separation position.

In solving the two-parameter equation difficulties were encountered in some flow cases due to the logarithmic velocity profile expression in the inner layer. Furthermore, the profiles parameters of the two-parameter profiles cannot be determined independent of experimental measurements. Therefore, the simpler one-parameter method is suggested to be employed in separation prediction.

A free stream flow parameter is introduced to correlate the one-parameter profiles to the free stream velocity distributions. The results show that the separation profile parameter can be expressed as a unique function of nondimensional pressure coefficient of the flow field.

Experimental measurements for a turbulent boundary layer up to and through the separation region have been made to further investigate the characteristics of the turbulent boundary layer separation. The measurements are taken along the test wall of a diffuser. Mean velocity profiles, turbulent fluctuations, shear stresses along the wall are measured in detail. The integral parameters are evaluated from the measured velocity profiles.

At the start of the separation, the one-parameter velocity profiles are seen to fit the separation profile well except near the surface. Downstream of the separation point, the discrepancy between the one-parameter profiles and measured separation profiles increases in the x-direction. The velocity profiles in the separation region are found to be well represented by the two-parameter profiles.

The relationship of the integral parameters for a new set measured velocity profiles are compared to Sandborn and Kline's relaxed and unrelaxed separation correlation. At the start of separation, the velocity profile falls on the unrelaxed separation correlation curve. Downstream of this point, the profile parameters stay between the relaxed and unrelaxed correlation curves. The present results thus add strength that at least a two-parameter velocity profile is required to completely specify the turbulent separation region.

The measured wall shear stresses in the separation region are not equal to zero as implied by Prandtl's separation model. Instead, the wall shear stresses decrease rapidly when separation is approached and become negligible in the separation region. From the approximate calculation of the momentum balance in x-direction, the turbulent shear stress is found to be small near the separation region comparing to the inertial forces. These results are consistant with the measurements reported by Sandborn and Liu.

BIBLIOGRAPHY

BIBLIOGRAPHY

1. Buri, A., Eine Berechnungsgrundlage fur die turbulente Grenzschicht bei beschleunigter und verzogerter Stromung. Diss. Zurich, 1931.

2. Chang, P. K., Separation of flow. Pergamon Press Inc., 1970.

3. Coles, D., The problem of the turbulent boundary layer. ZAMP 5, p. 181, 1954.

4. Curle, N., and Skan, S. W., Approximate methods for predicting separation properties of laminar boundary layers. Aeronautical Quarterly, Vol. VIII, p. 257, 1957.

5. von Doenhoff, A. E., and Tetervin, N., Determination of general relations for the behavior of turbulent boundary layers. NACA Report 772, 1943.

6. von Doenhoff, A. E., A method of rapidly estimating the position of the laminar separation point. NACA TN 671, 1938.

7. Garner, H. C., The development of turbulent boundary layers. ARC R&M 2133, 1944.

8. Gruschwitz, E., Die turbulente reibungsschicht in ebener stronmung bei Druckabfall and Druckanstieg. Ing.-Arch. 2, p. 321, 1931. Summary in ZFM 23, p. 308, 1932.

9. Hewson, C. T. Growth and separation of a turbulent boundary layer. ASME Symposium on Stall, 1958. (Part of Ph.D. Thesis, Univ. of Cambridge, England), 1949.

10. von Karman, T., and Millikan, C. B., On the theory of laminar boundary layers involving separation, NACA Report 504, 1934.

11. Kline, S. J., Some new concepts of the mechanism of stall in turbulent boundary layer. Journal of the Aeronautical Sciences, Vol. 24, p. 470, 1957.

12. Liu, C. Y., and Sandborn, V. A., Evaluation of the separation properties of laminar boundary layers. Aeronautical Quarterly, Vol. XIX, p. 235, 1968.

13. Liu, C. Y., Boundary layer separation, PhD. Dissertation, Colorado State University, Fort Collins, Colorado, 1967.

14. Ludwieg, H., Instrument for measuring the wall shearing stress of turbulent boundary layers. NACA TN 1289, 1950.

15. Ludwieg, H., and Tillman, W., Investigation of the wall shearing stress in turbulent boundary layers. NACA TN 1285, 1950.

16. Maskell, E. C., Approximate calculation of the turbulent boundary layer in two dimensional incompressible flow.. RAE Report AERO 2443, 1951.

17. Proceedings; Computation of turbulent boundary layers - AFOSR-IFP - Stanford Conference, Vol. 1. Editors: Kline, S. J., Morkovin, M. V., Sovran, G., and Cockrell, D. J. Stanford University, 1968.

18. Rotta, J. C., Turbulent boundary layers in incompressible flow. Progress in Aeronautical Sciences, Vol. 2, Pergamon Press, Oxford, 1962.

19. Rotta, J. C., Schubspannungsverteilung und energie dissipation bei turbulenten grenzschichten, Ing. - Arch. 20, p. 195, 1952.

20. Sandborn, V. A., Resistance temperature tranducers. Metrology Press, 1972.

21. Sandborn, V. A., Boundary layer separation and reattachment. International Symposium on Fluid Mechanics and Design of Turbomachinery, to be published as a NASA Special Report, 1971.

22. Sandborn, V. A., Note on the turbulent boundary layer velocity distribution at turbulent separation. Department of Civil Engineering, Colorado State University, Fort Collins, Colorado, 1970.

23. Sandborn, V. A., Characteristics of boundary layers at separation and reattachment. Research Memorandum No. 14, Department of Civil Engineering, Colorado State University, Fort Collins, Colorado, 1969.

24. Sandborn, V. A. and Liu, C. Y., On turbulent boundary layer separation. Journal of Fluid Mechanics, Vol. 23, p. 293, 1968.

25. Sandborn, V. A. and Kline, S. J., Flow models in boundary layer stall inception. Journal of Basic Engineering, Trans. ASME, Series D, Vol. 83, p. 317, 1961.

26. Sandborn, V. A., An equation for the mean velocity distribution of boundary layers. NASA RM 2-5-59E, 1959.

27. Sandborn, V. A. and Slogar, R. J., Longitudinal turbulent spectrum survey of boundary layers in adverse pressure gradients. NACA TN 3264, 1955.

28. Schlichting, H., Boundary layer theory. Sixth edition, McGraw-Hill Publishing Co., New York, New York, 1968.

29. Schubauer, B. S. and Klebanoff, P. S., Investigation of separation of the turbulent boundary layer. NACA Report 1030, 1951.

30. Schuh, H., On calculating imcompressible turbulent boundary layers with arbitrary pressure distribution. KTH AERO TN 41, 1954.

31. Spence, D. A., The development of turbulent boundary layers. Journal of the Aeronautical Sciences, Vol. 23, p. 3, 1956.

32. Stratford, B. S., The prediction of separation of the turbulent boundary layer. Journal of Fluid Mechanics, Vol. 5, p. 1, 1959A.

33. Stratford, B. S., An experimental flow with zero skin friction throughout its region of pressure rise. Journal of Fluid Mechanics, Vol. 5, p. 17, 1959B.

34. Stratford, B. S., Flow in the laminar boundary layer near separation. ARC R&M 3002, 1957.

35. Thompson, B. G. J., A critical review of existing methods of calculating the turbulent boundary layer. ARC - Report 26109, 1964.

36. Townsend, A. A., The behavior of a turbulent boundary layer near separation. Journal of Fluid Mechanics, Vol. 12, p. 143, 1962.

37. Truckenbrodt, E., Ein quadraturverfahren zur berechnung der laminaren und turbulenten reibungsschicht bei ebner und rotationssymmetrischev Stromung. Ing.-Arch. 20, p. 211, 1952.

38. Wieghardt, K., Uber einen energiesatz zur berechnung laminar Grenschichten. Ing.-Arch. 16, p. 231, 1948.

39. Wills, J. A. B., The correction of hot wire readings for proximity to a solid boundary. Journal of Fluid Mechanics, Vol. 12, p. 388, 1962.

TABLES

Table 1. Profile parameters for experimental separation profiles.

m	ζ	m_1	Reference
2.82	.84	5.29	Present measurements Station 9.00"
2.10	.89	4.07	Present measurements Station 10.25"
1.94	.89	3.78	Present measurements Station 11.00"
1.66	.88	3.20	Present measurements Station 12.00"
1.49	.87	2.83	Present measurements Station 13.00"
1.64	.87	3.18	Doenhoff and Teteroin α=8.1°, Re= 0.91×10^6
1.69	.86	3.24	Doenhoff and Teteroin α=8.1°, Re= 2.67×10^6
2.07	.80	3.48	Doenhoff and Teteroin α=10.1°, Re= 2.64×10^6
1.64	.84	3.04	Hewson, Test 3 Moderate pressure gradient
3.68	.88	7.21	Sandborn and Liu Station 2
3.15	.92	6.63	Sandborn and Liu Station 3
2.75	.99	6.25	Sandborn and Liu Station 3.5
1.24	.90	2.55	Schubauer and Klebanoff, X = 25.77'
1.36	.83	2.39	Stratford, Experiment 6, Station 6
1.46	.85	2.66	Stratford, Experiment 6, Station 7

Table 2. Predicted separation positions and pressure coefficients at separation

Experiment		One-parameter method			Two-parameter method			Stratford's theory			
x_s (feet)	Cps	x_s (feet)	Cps	Difference in Cps (%)	x_s (feet)	Cps	Difference in Cps (%)	x_s (feet)	Cps	Difference in Cps (%)	Reference and figure
0.750*	.401	0.721	.378	5.7	**	**	**	0.415	.227	43.4	Figure 27 Present measurements
0.854*	.432	0.833	.426	1.4	.907	.455	5.3	--	--	--	Figure 28 Present measurements
0.917*	.468	0.884	.447	4.5	.923	.463	0.6	--	--	--	Figure 29 Present measurements
1.000*	.488	0.975	.491	0.6	.983	.479	1.8	--	--	--	Figure 30 Present measurements
1.083*	.494	1.186	.533	7.9	1.038	.499	1.0	--	--	--	Figure 31 Present measurements
1.200	.439	1.048	.358	18.4	1.139	.415	5.5	1.074	.374	14.8	Figure 32, Doenhoff and Teteroin (1943) $\alpha=8.1°$, $Re=0.91x10^6$
1.200	.456	1.197	.458	0.4	1.232	.494	8.3	1.129	.397	12.9	Figure 33, Doenhoff and Teteroin (1943) $\alpha=8.1°$, $Re=2.67x10^6$
1.100	.472	1.200	.493	4.4	1.040	.421	10.8	1.024	.414	12.3	Figure 34, Doenhoff and Teteroin (1943) $\alpha=10.1°$, $Re=2.64x10^6$
2.333	.581	2.244	.579	0.3	**	**	**	1.983	.544	6.4	Figure 35, Hewson (1949) Test 3, Moderate pressure gradient
4.104	.177	4.113	.183	3.4	**	**	**	4.165	.224	27.6	Figure 36 Sandborn and Liu (1968)
4.146	.203	4.169	.227	11.8	**	**	**	--	--	--	Figure 37 Sandborn and Liu (1968)
4.167	.228	4.176	.236	3.5	**	**	**	--	--	--	Figure 38 Sandborn and Liu (1968)
25.77	.512	24.76	.492	3.9	24.09	.460	10.2	24.00	.442	13.7	Figure 39 Schubauer and Klebanoff (1951)
5.322	.624	4.792	.588	5.8	**	**	**	--	--	--	Figure 40, Stratford (1959B) Experiment 6
6.236	.682	5.320	.635	6.9	**	**	**	--	--	--	Figure 41, Stratford (1959B) Experiment 6

* The distance from the position of maximum velocity
**No solution could be obtained

Table 3. Variations of the profile integral parameters and the wall shear stresses along the center line of the diffuser.

X (inches)	U (fps)	δ (inches)	δ^* (inches)	θ (inches)	H	δ^*/δ	θ/δ	τ_w (lb/ft^2) (using Ludwieg-Tillman formula)
0.000	44.300	1.950	.174	.131	1.329	.089	.067	.00683
2.000	43.300	2.000	.188	.138	1.359	.094	.069	.00617
3.000	40.200	2.000	.228	.159	1.435	.114	.080	.00464
5.000	38.400	2.900	.399	.252	1.582	.138	.087	.00301
6.250	37.800	3.647	.584	.345	1.692	.160	.095	.00227
7.050	37.300	3.680	.734	.387	1.896	.199	.105	.00156
8.100	35.800	3.845	.890	.409	2.174	.231	.106	.00093
9.000	34.300	3.945	1.036	.451	2.297	.263	.114	.00069
10.250	33.400	4.017	1.283	.484	2.652	.320	.121	.00037
11.000	32.300	4.300	1.444	.534	2.707	.336	.124	.00032
12.000	31.700	4.563	1.686	.607	2.780	.369	.133	.00026
13.000	31.500	4.685	1.865	.667	2.795	.398	.142	.00025

FIGURES

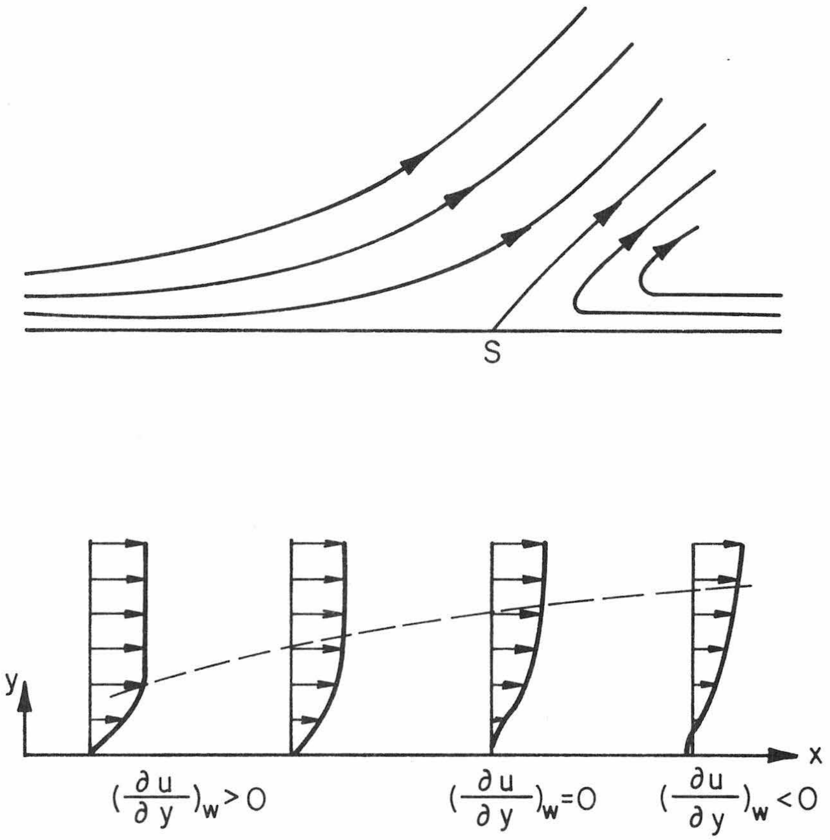

Fig. 1. Two-dimensional separation

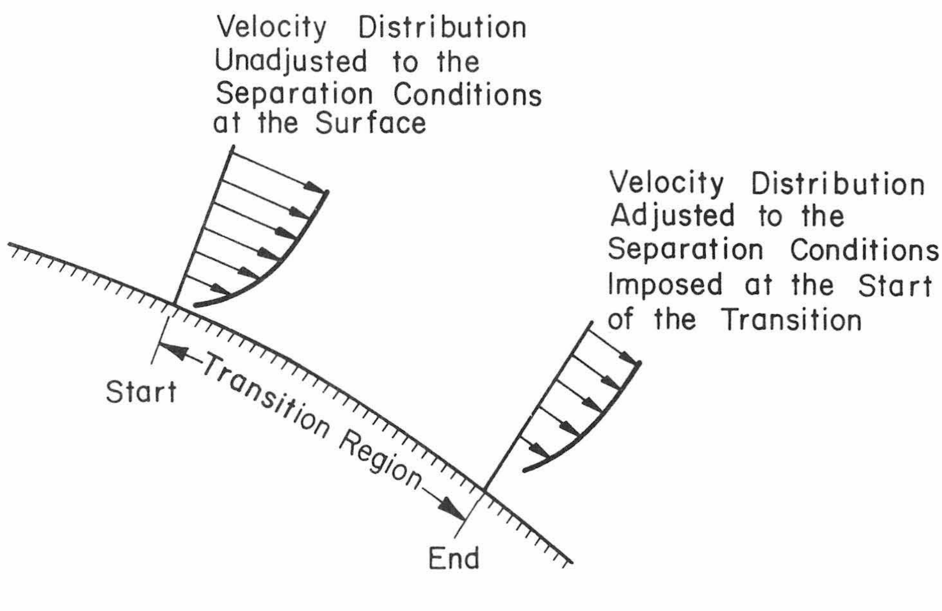

Fig. 2. Sketch of Sandborn's separation model

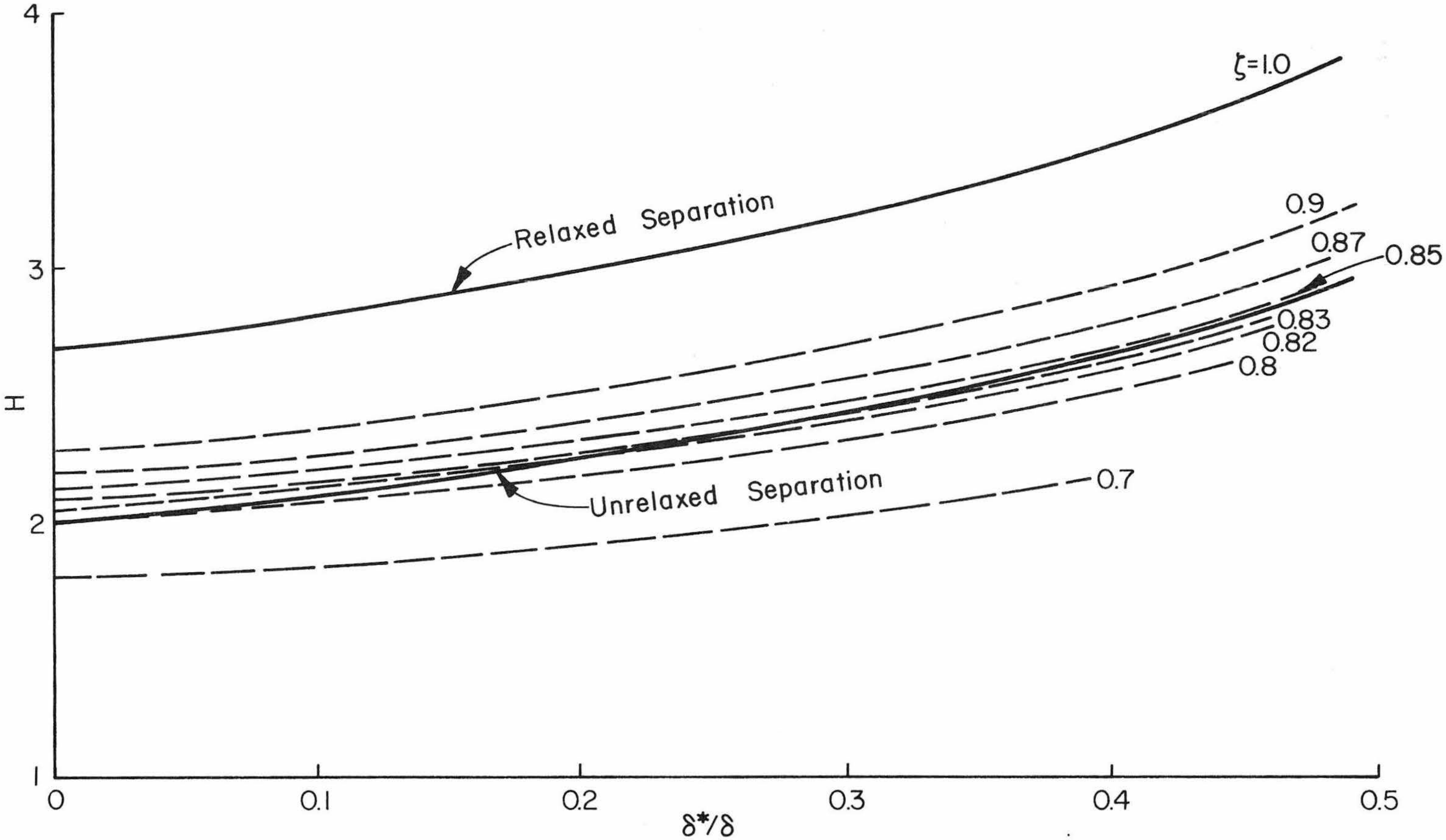

Fig. 3. Correlation of relaxed and unrelaxed separation parameters

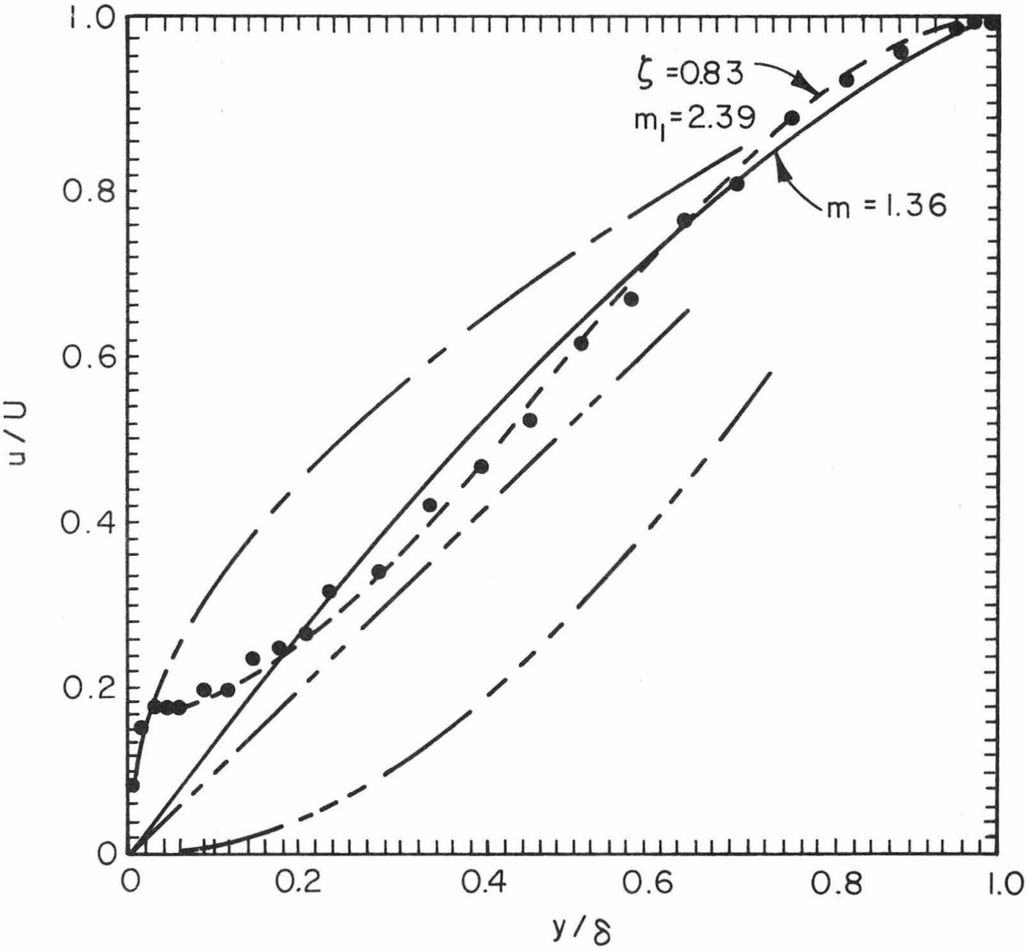

a) measured by Stratford, Station 6

Fig. 4. Separation velocity profile

——————— One-parameter separation profile,
$\frac{u}{U} = 1 - (1 - \frac{y}{\delta})^m$

— — — — Two-parameter separation profile,
$\frac{u}{U} = 1 + \zeta (1 - \frac{y}{\delta})^{m_1} [m_1 \ell_n (1 - \frac{y}{\delta}) - 1]$

—— – —— Stratford's separation profile,
$\frac{u}{U} \propto (y \frac{\partial p}{\partial x})^{\frac{1}{2}}$

— – – — Sandborn and Liu's linear profile,
$u \propto y$

— – – – — Sandborn and Liu's parabolic profile,
$u \propto y^2$

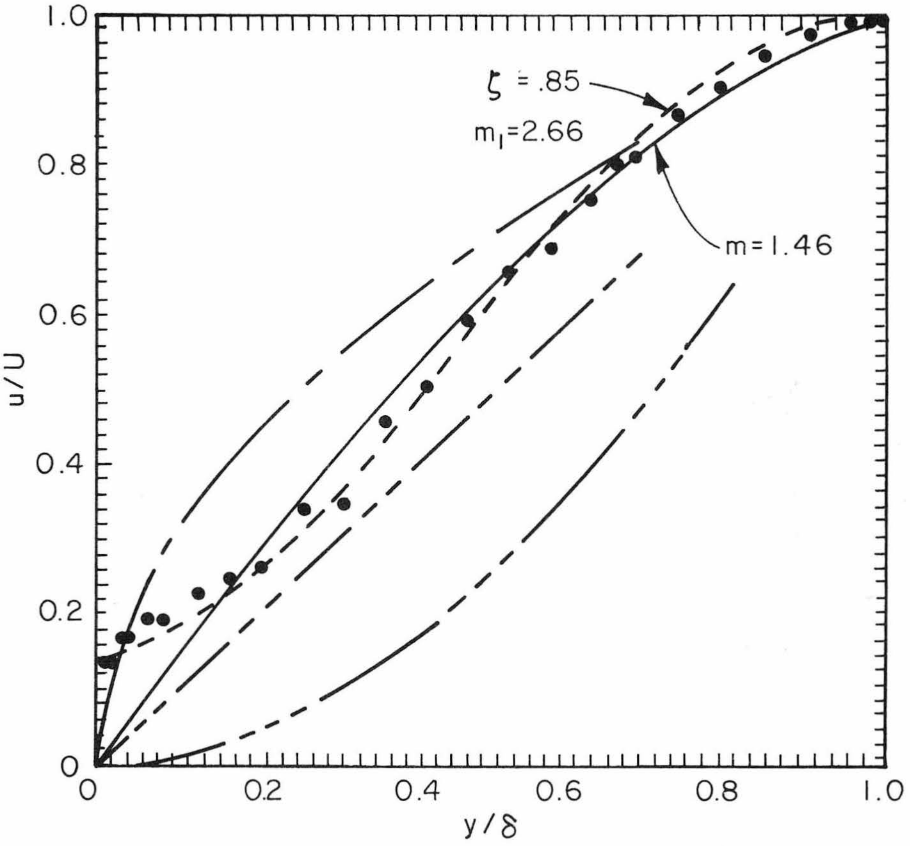

b) measured by Stratford, Station 7

Fig. 4. Separation velocity profile

——————— One-parameter separation profile, Eq. (3-8), $\frac{u}{U} = 1 - (1-\frac{y}{\delta})^m$

— — — — Two-parameter separation profile, Eq. (3-9), $\frac{u}{U} = 1 + \zeta\,(1 - \frac{y}{\delta})^{m_1}\,[m_1 \ell_n (1-\frac{y}{\delta}) - 1]$

—— – —— Stratford's separation profile, Eq. (3-6), $\frac{u}{U} \propto (y\,\frac{\partial p}{\partial x})^{\frac{1}{2}}$

— – – — Sandborn and Liu's linear profile, $u \propto y$

— – – – — Sandborn and Liu's parabolic profile, $u \propto y^2$

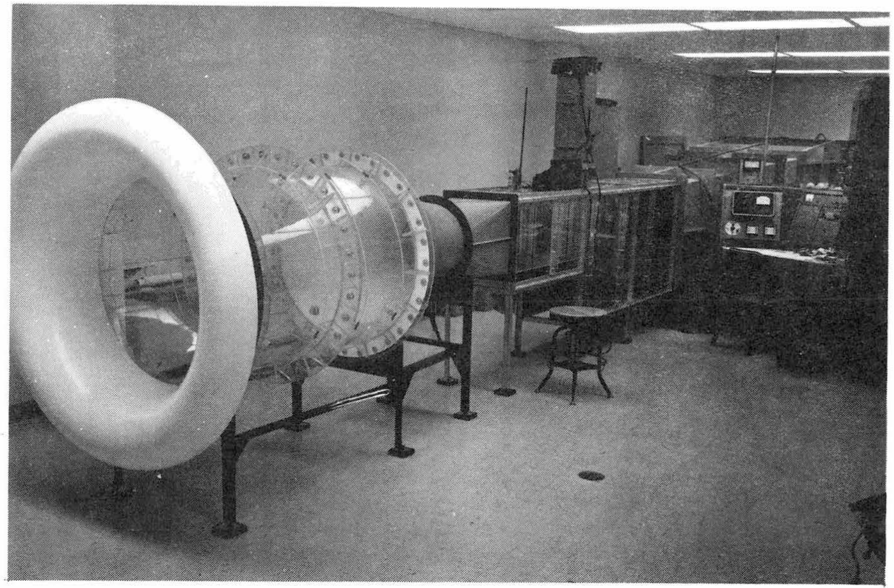

Fig. 5. Overall view of the CSU separation wind tunnel

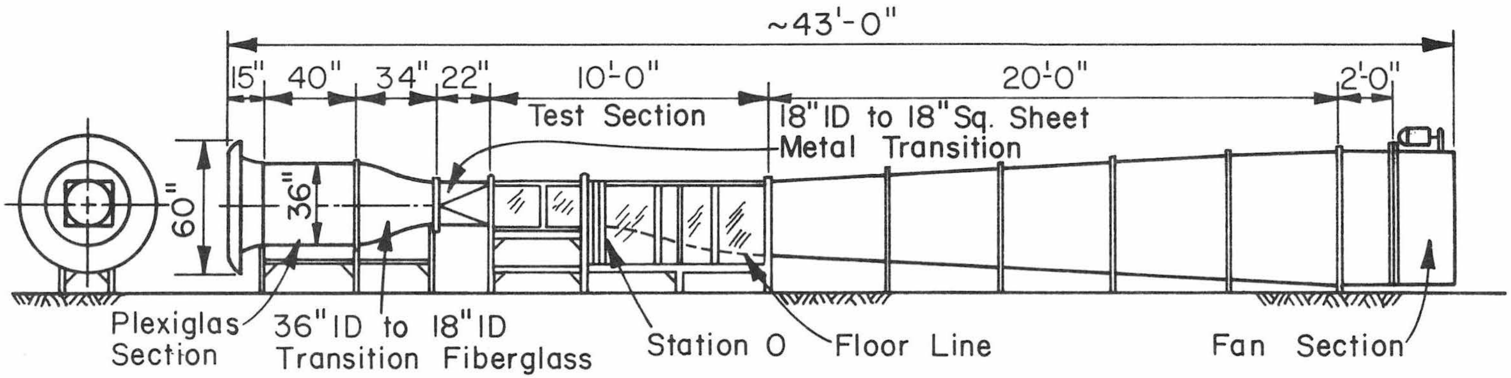

Fig. 6. Schematic of the separation wind tunnel

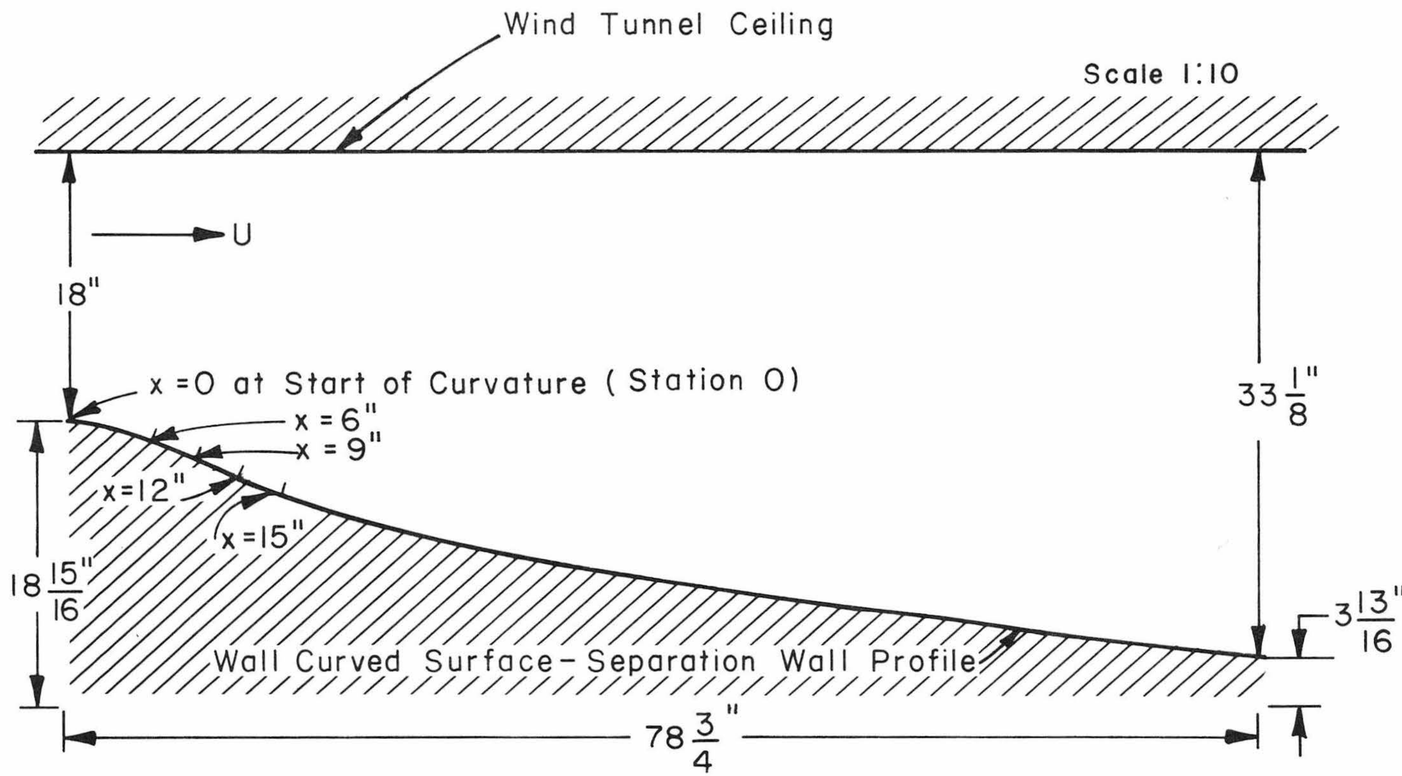

Figure 7. Schematic of the separation wind tunnel test section

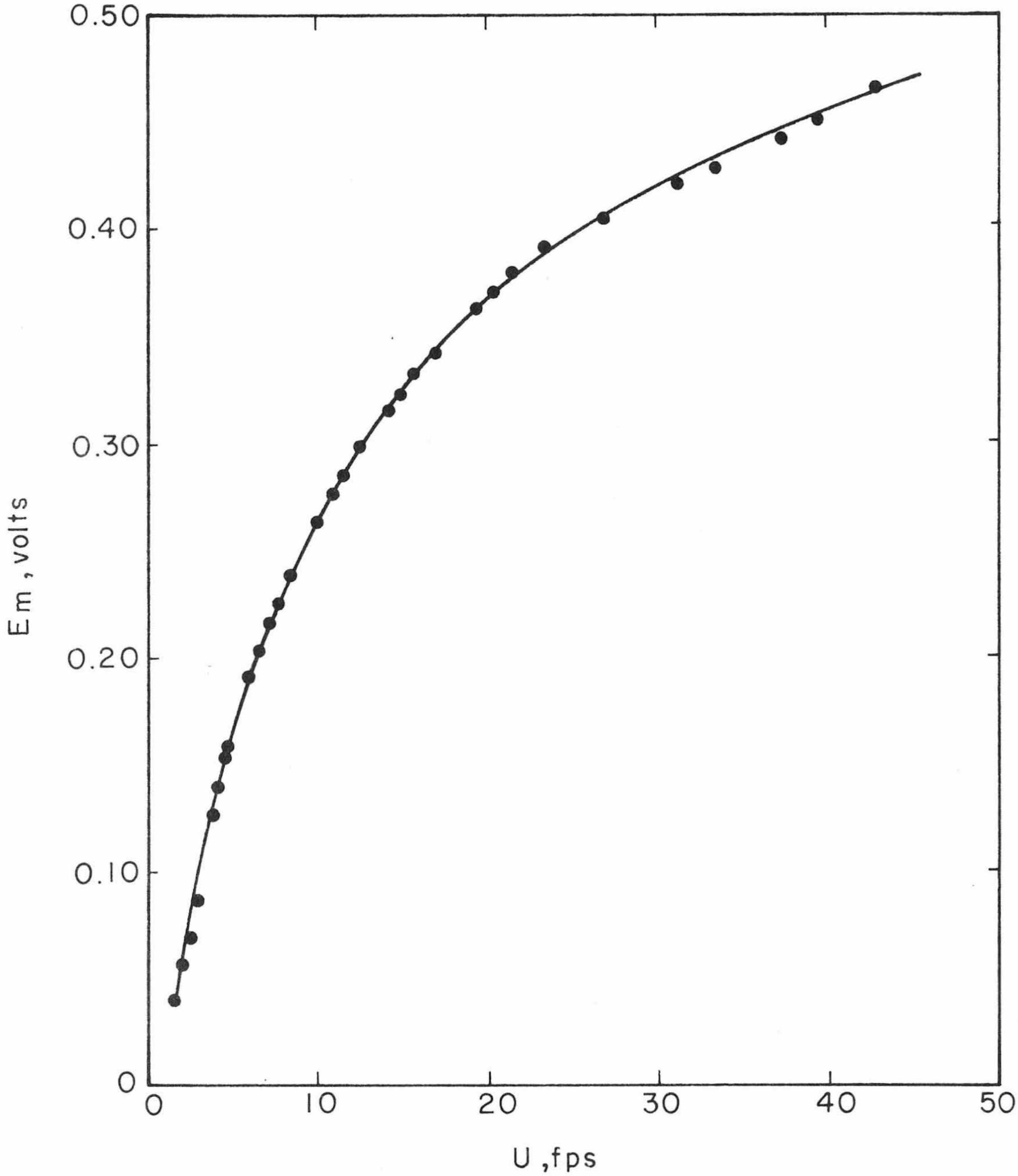

Fig. 8. Typical boundary layer hot-wire calibration

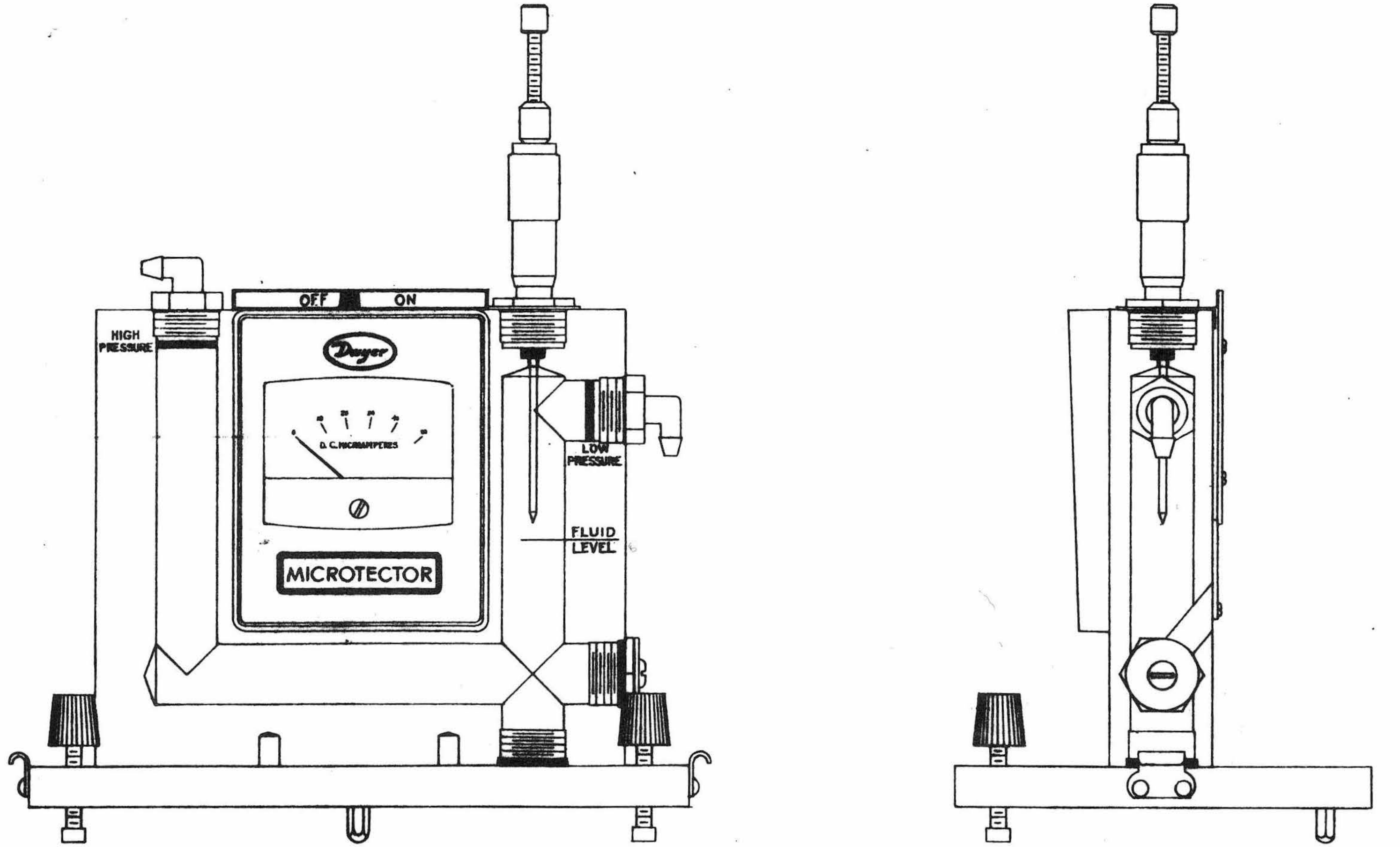

Fig. 9. Microtector manometer gage

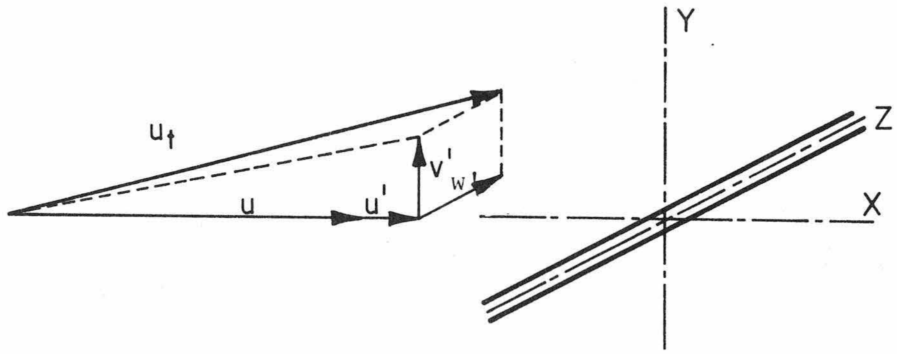

Fig. 10. Hot-wire normal to mean flow

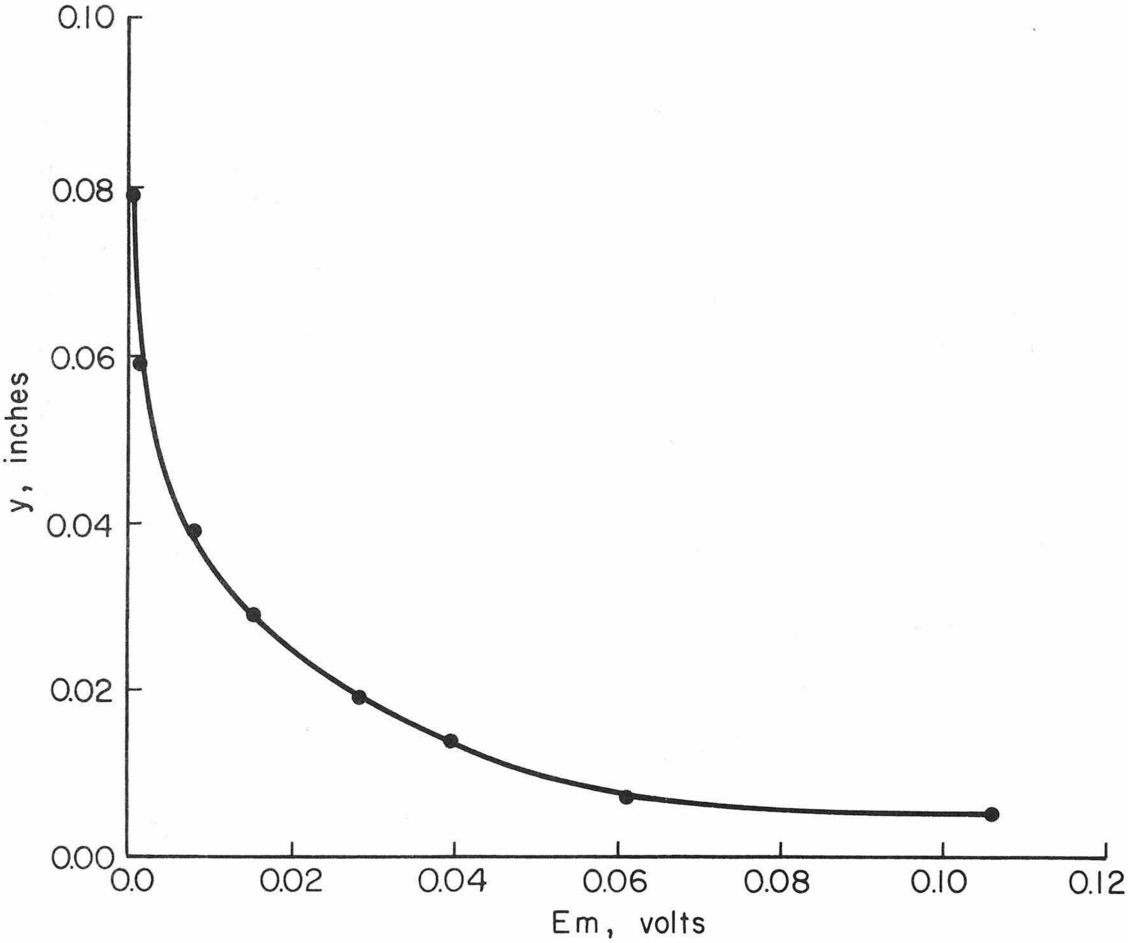

Fig. 11. Evaluation of wall effect on hot-wire heat loss for no-flow

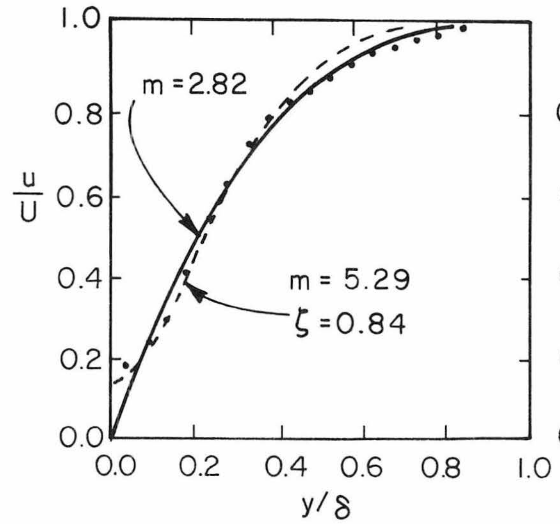

Fig. 12. Velocity profile at separation Present measurements, X=9.00 inches

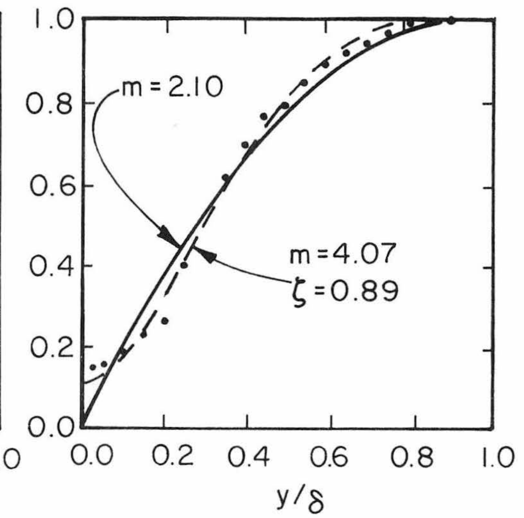

Fig. 13. Velocity profile at separation Present measurements, X=10.25 inches

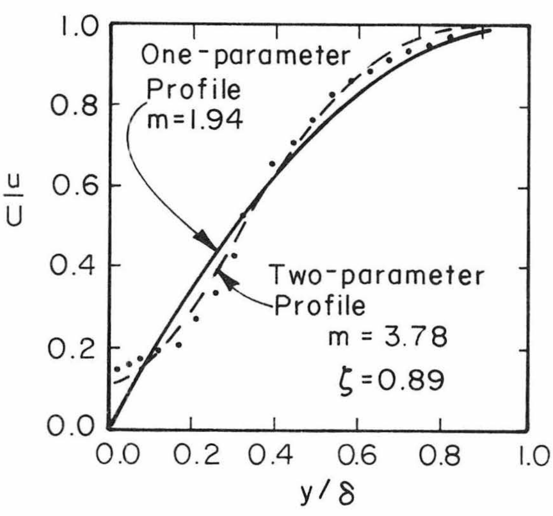

Fig. 14. Velocity profile at separation Present measurements, X=11.00 inches

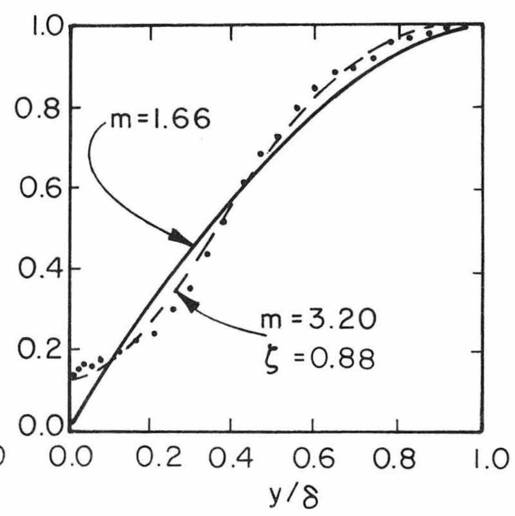

Fig. 15. Velocity profile at separation Present measurements, X=12.00 inches

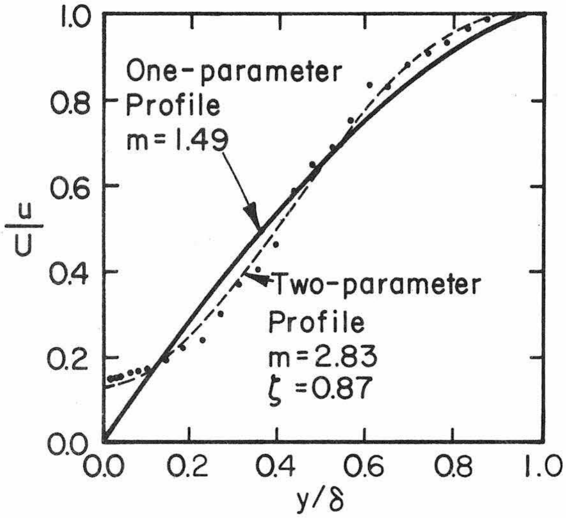

Fig. 16. Velocity profile at separation
Present measurements, X=13.00 inches

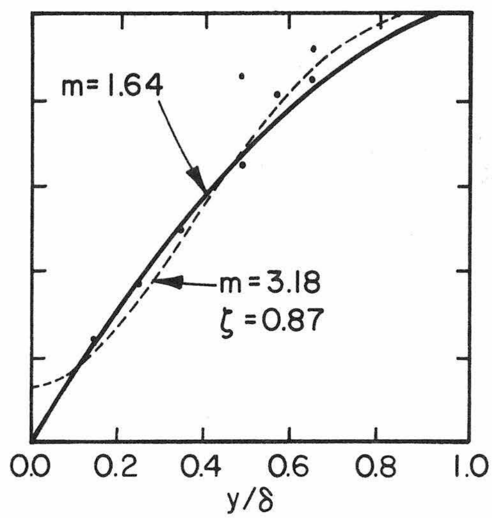

Fig. 17. Velocity profile at separation
Doenhoff and Tetervin, R_e=0.92E6, α=8.1°

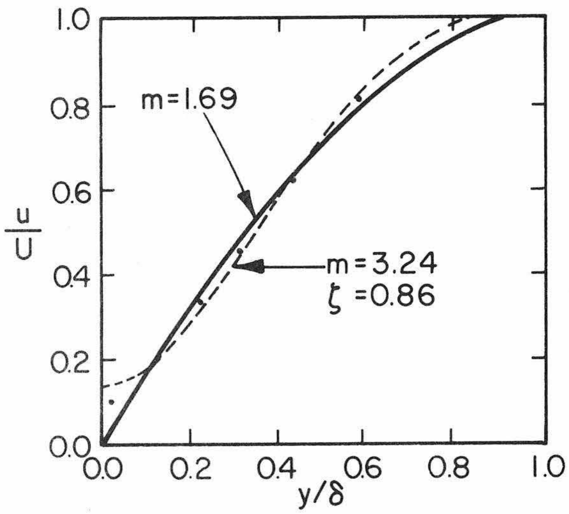

Fig. 18. Velocity profile at separation
Doenhoff and tetervin, R_e=2.67E6, α=8.1°

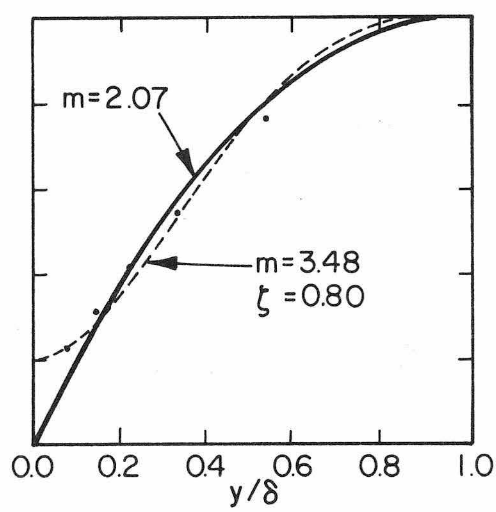

Fig. 19. Velocity profile at separation
Doenhoff and Tetervin, R_e=2.64E6, α=10.1°

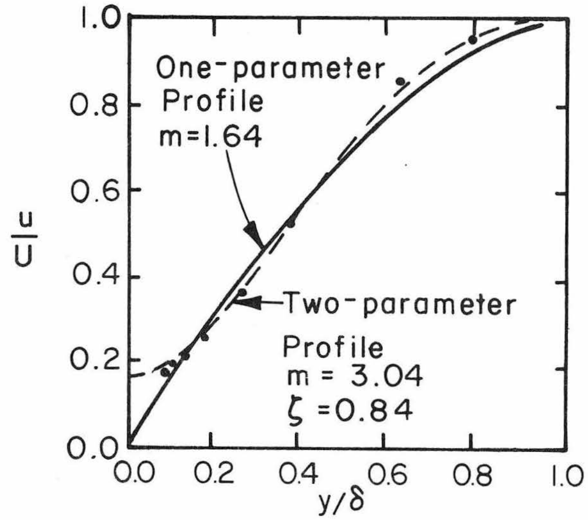

Fig. 20. Velocity profile at separation
Hewson, Test 3, moderate pressure gradient

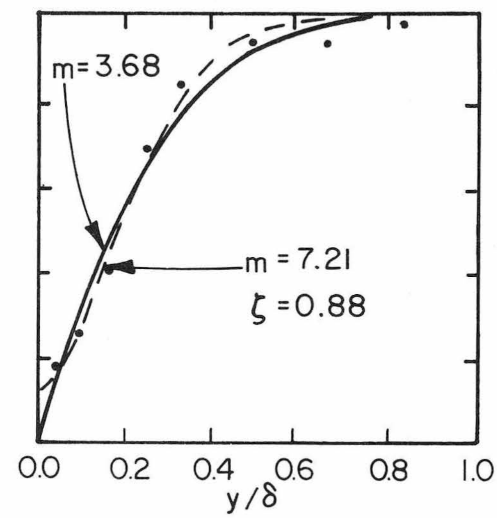

Fig. 21. Velocity profile at separation
Sandborn and Liu, Station 2

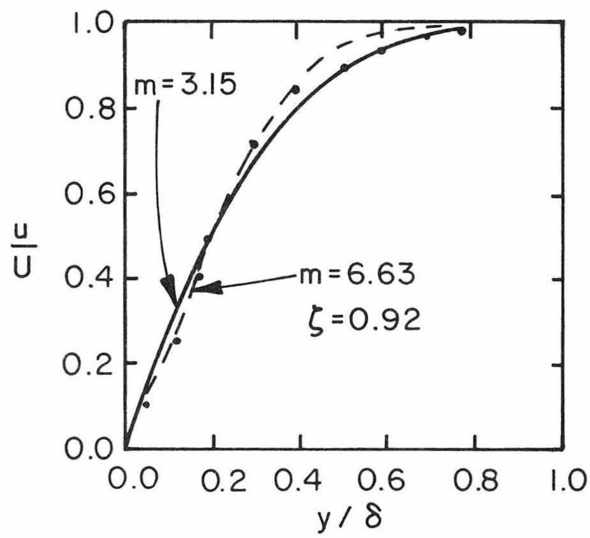

Fig. 22. Velocity profile at separation
Sandborn and Liu, Station 3

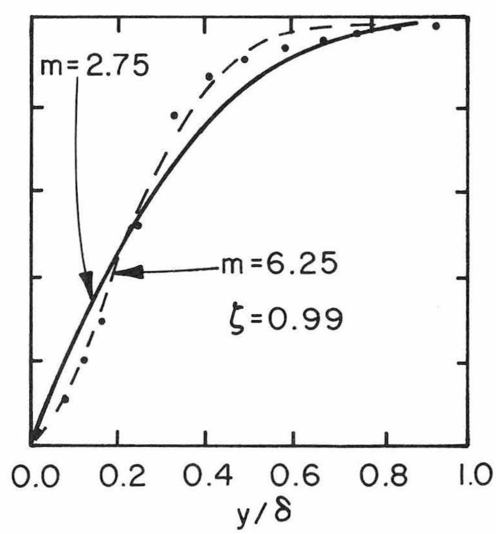

Fig. 23. Velocity profile at separation
Sandborn and Liu, Station 3.5

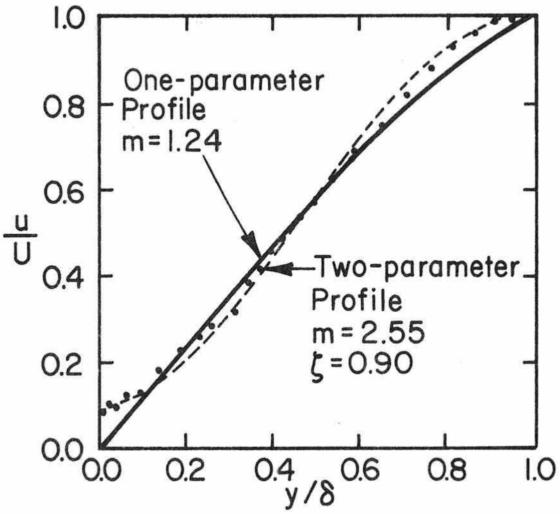

Fig. 24. Velocity profile at separation
Schubauer and Klebanoff

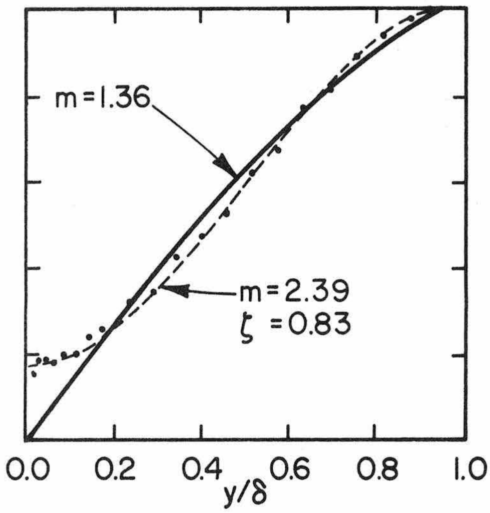

Fig. 25. Velocity profile at separation
Stratford, Experiment 6, Station 6

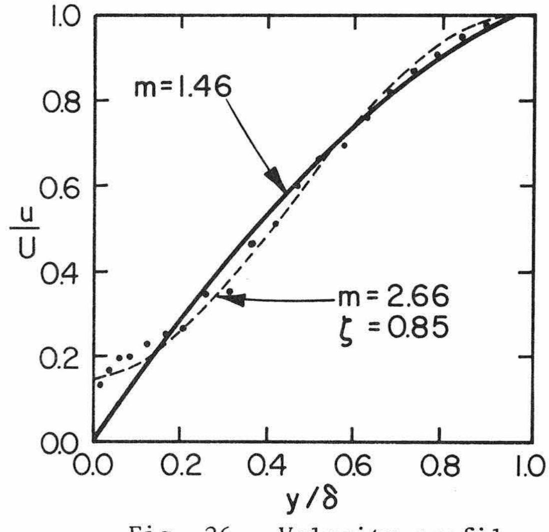

Fig. 26. Velocity profile at separation
Stratford, Experiment 6, Station 7

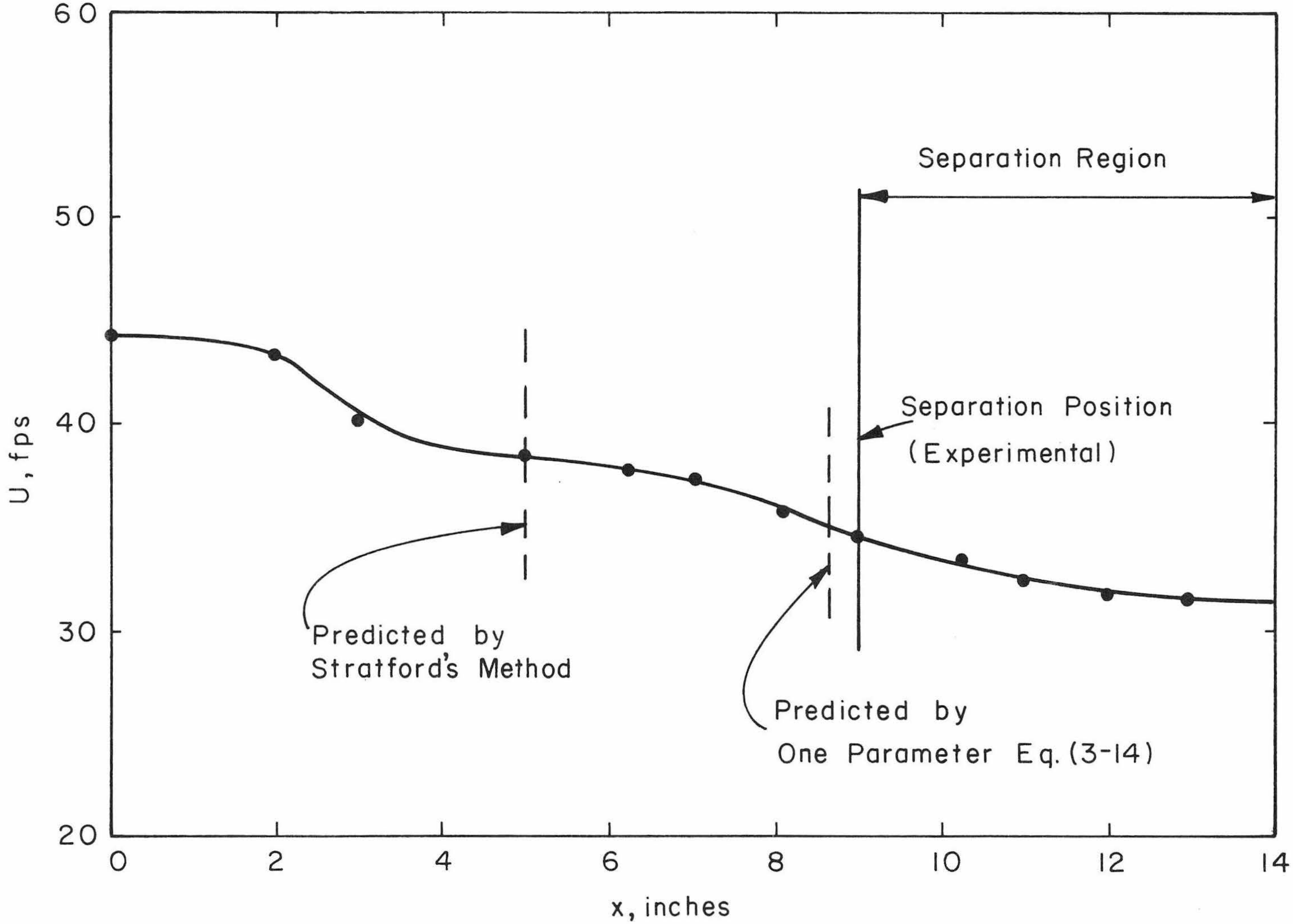

Fig. 27. Comparison of present separation prediction and experimental results (Present measurements, 9" Station)

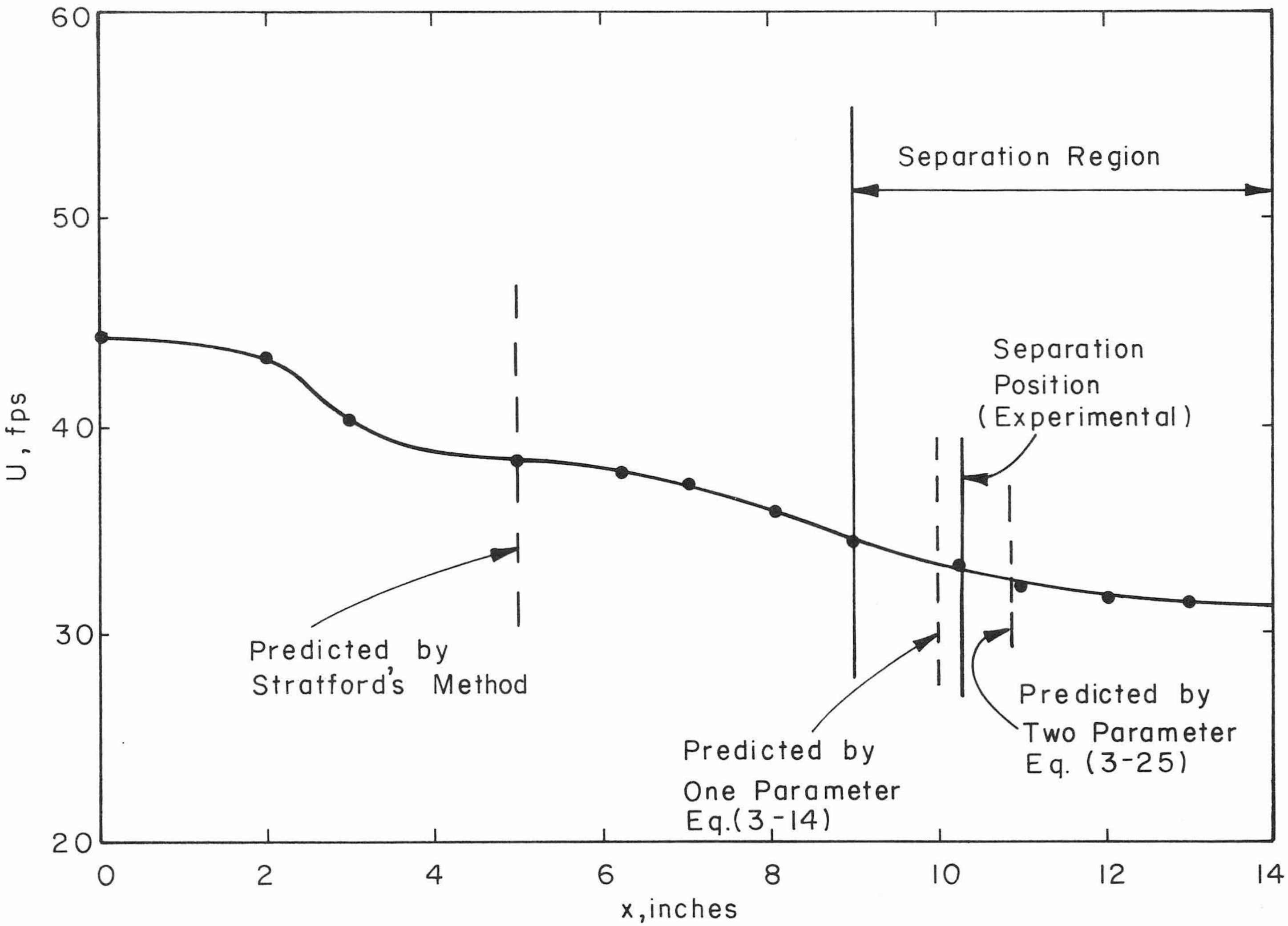

Fig. 28. Comparison of present separation prediction and experimental results (Present measurements, 10.25 Station)

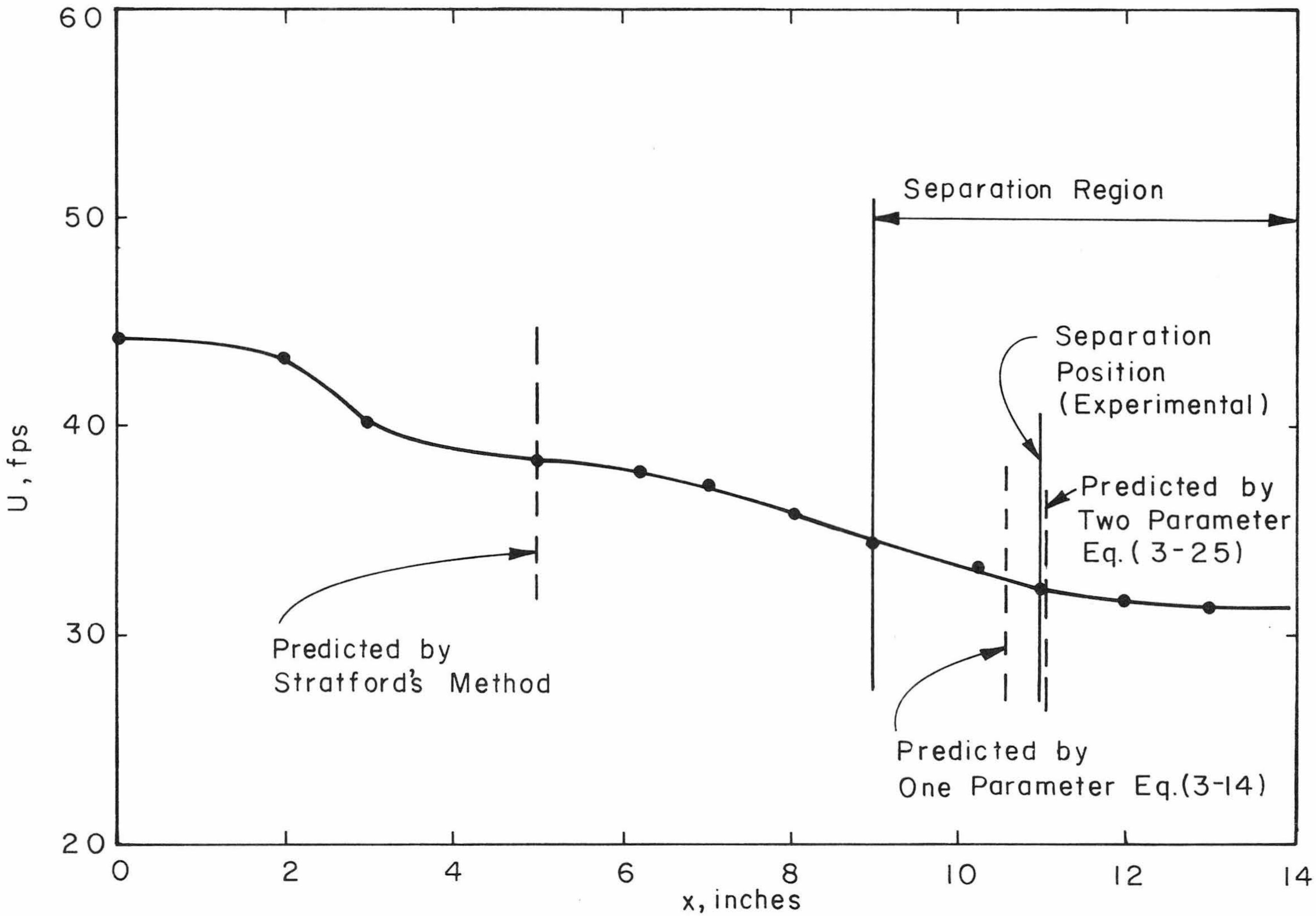

Fig. 29. Comparison of present separation prediction and experimental results (Present measurements, 11" station)

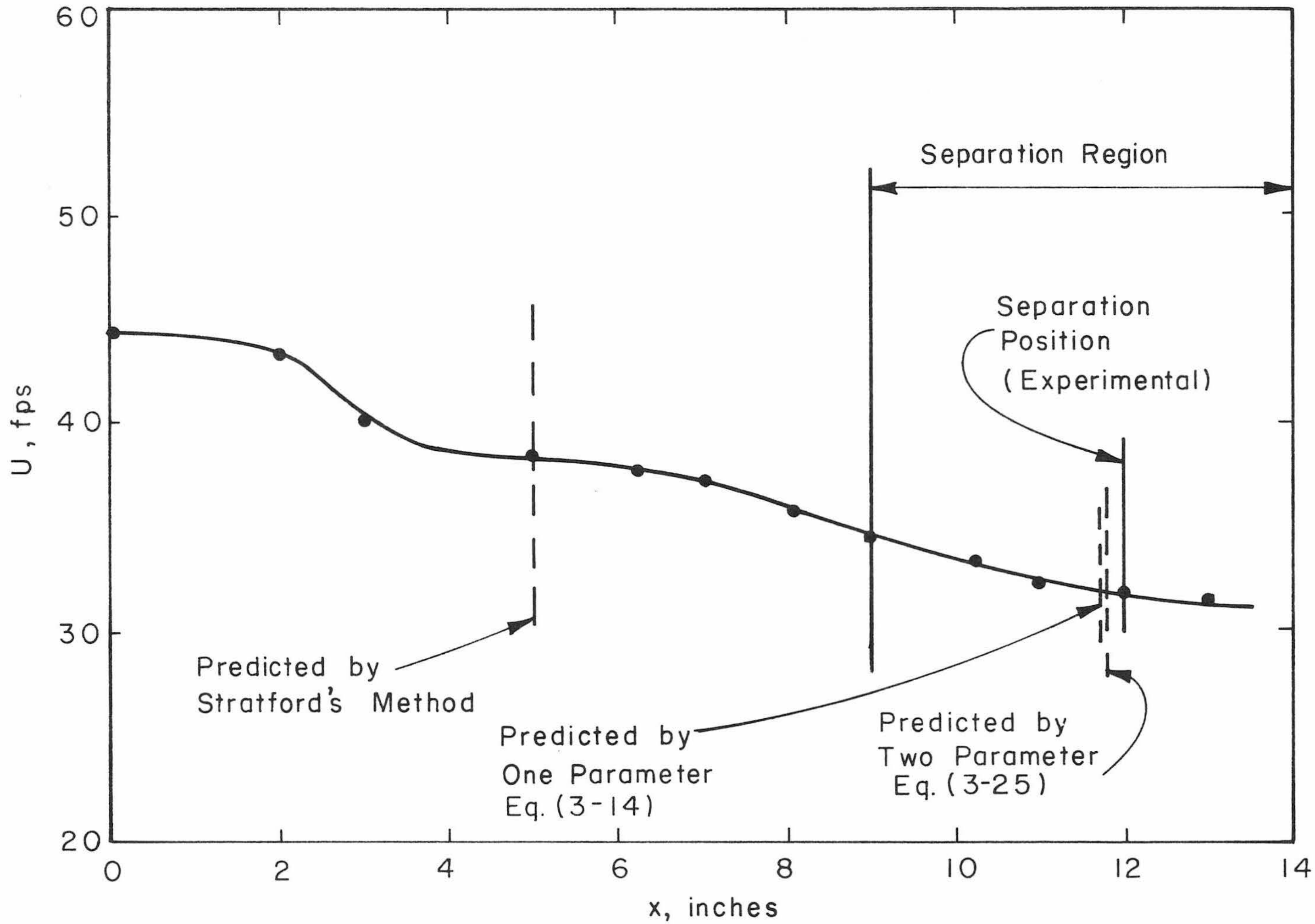

Fig. 30. Comparison of present separation prediction and experimental results (Present measurements, 12" station)

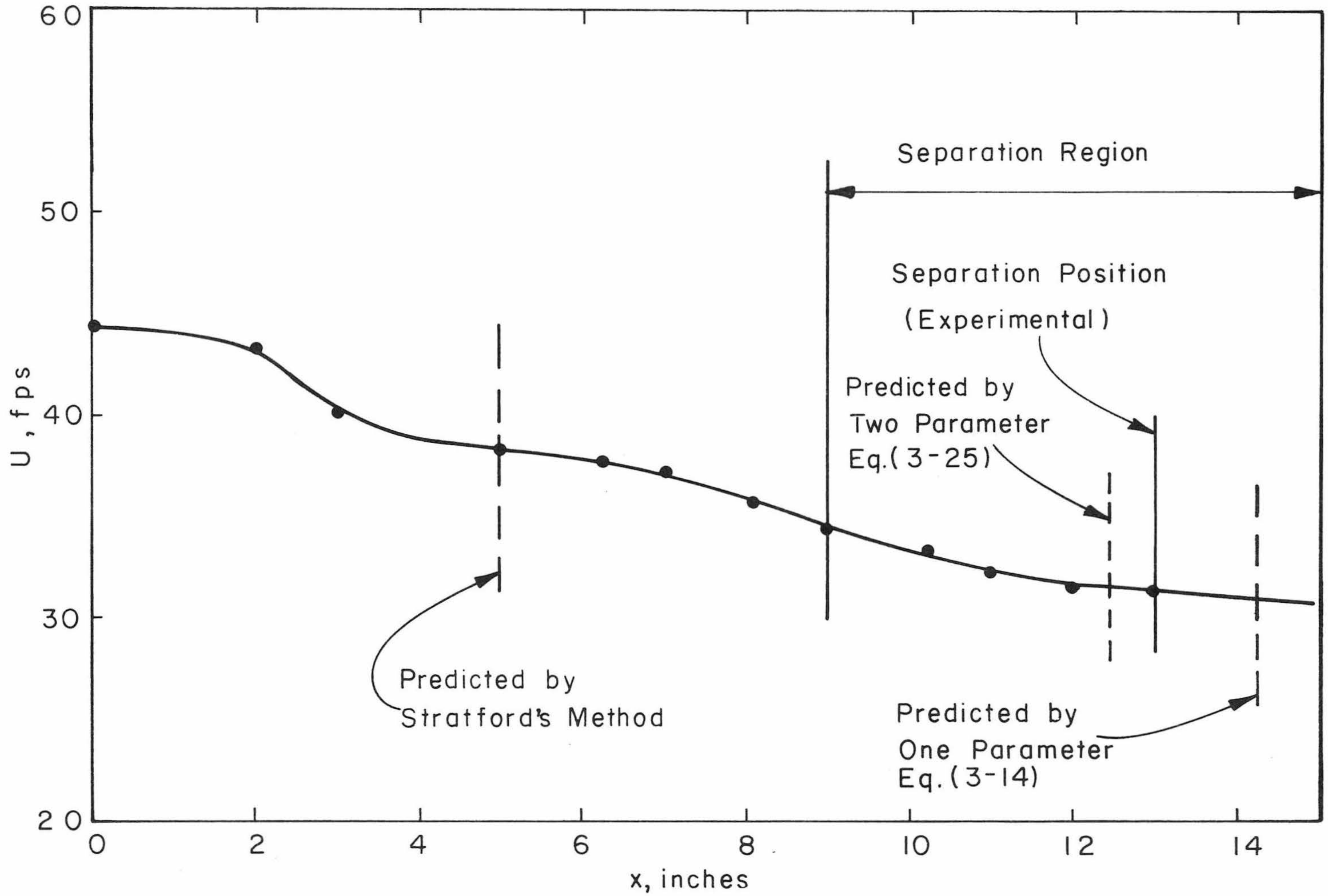

Fig. 31. Comparison of present separation prediction and experimental results (Present measurements, 13" station)

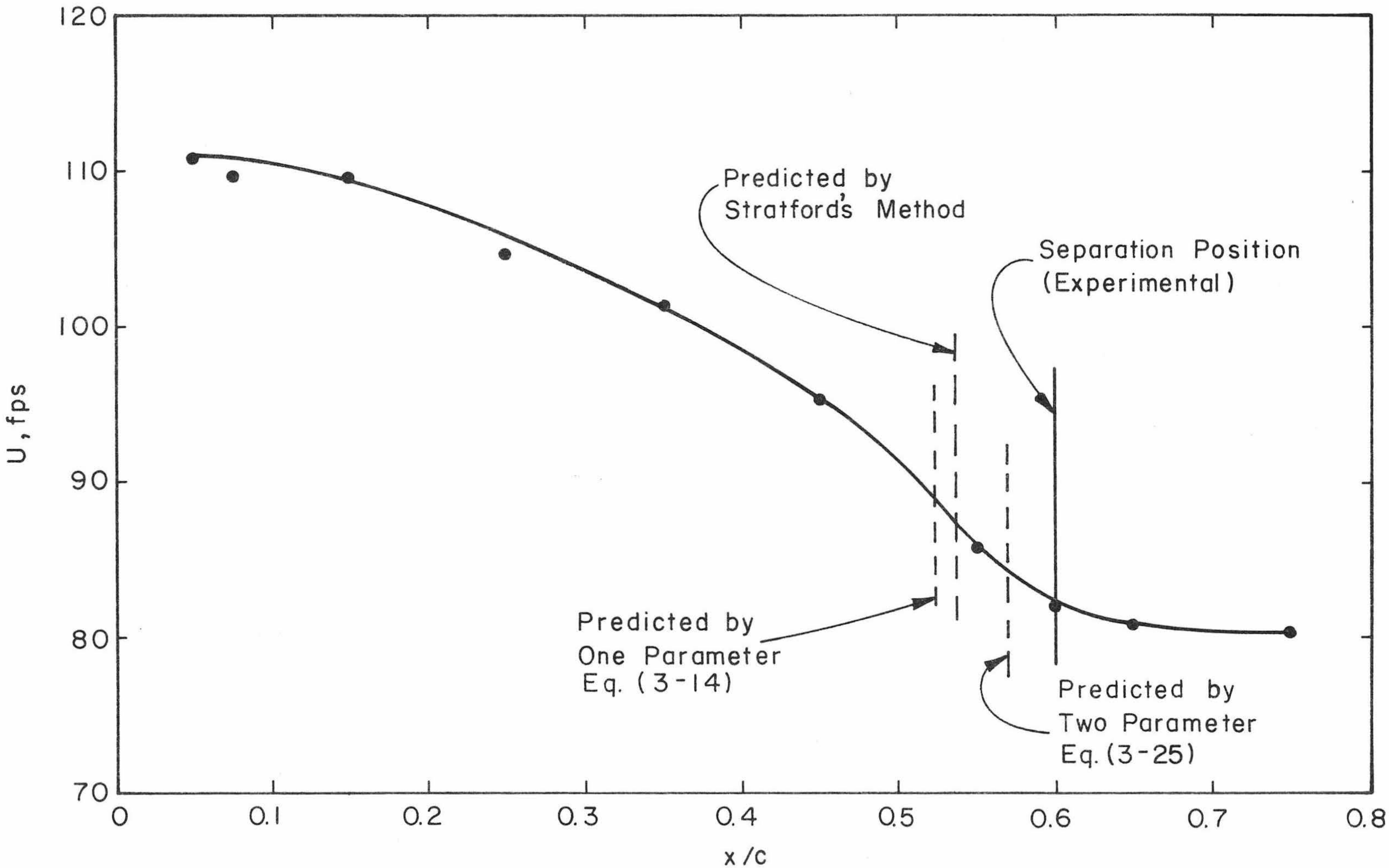

Fig. 32. Comparison of present separation prediction and experimental results (Von Doenhoff and Tetervin; $\alpha = 8.1°$, $R_e = .91 \times 10^6$)

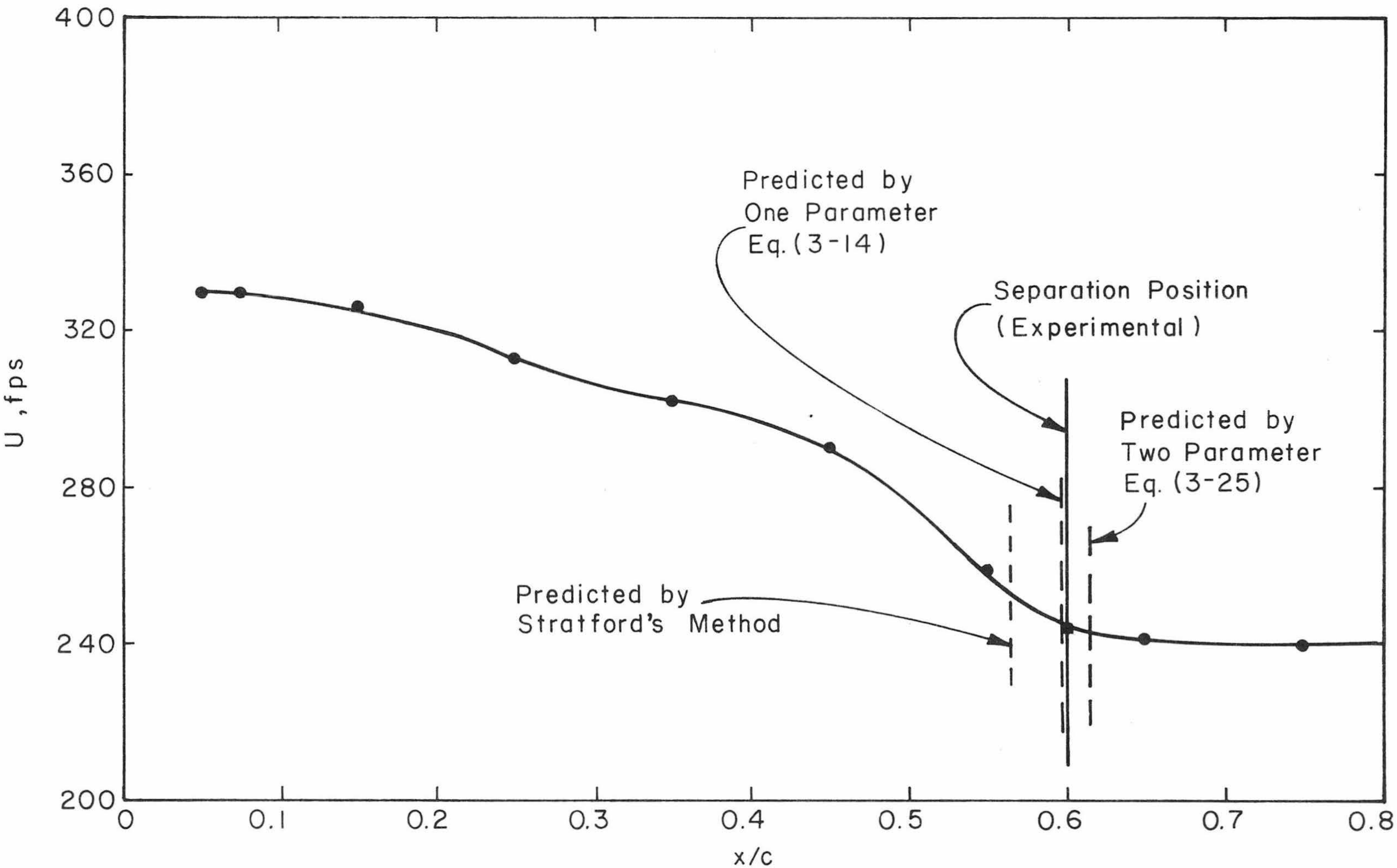

Fig. 33. Comparison of present separation prediction and experimental results (Von Doenhoff and Tetervin; $\alpha = 8.1$, $R_e = 2.67 \times 10^6$)

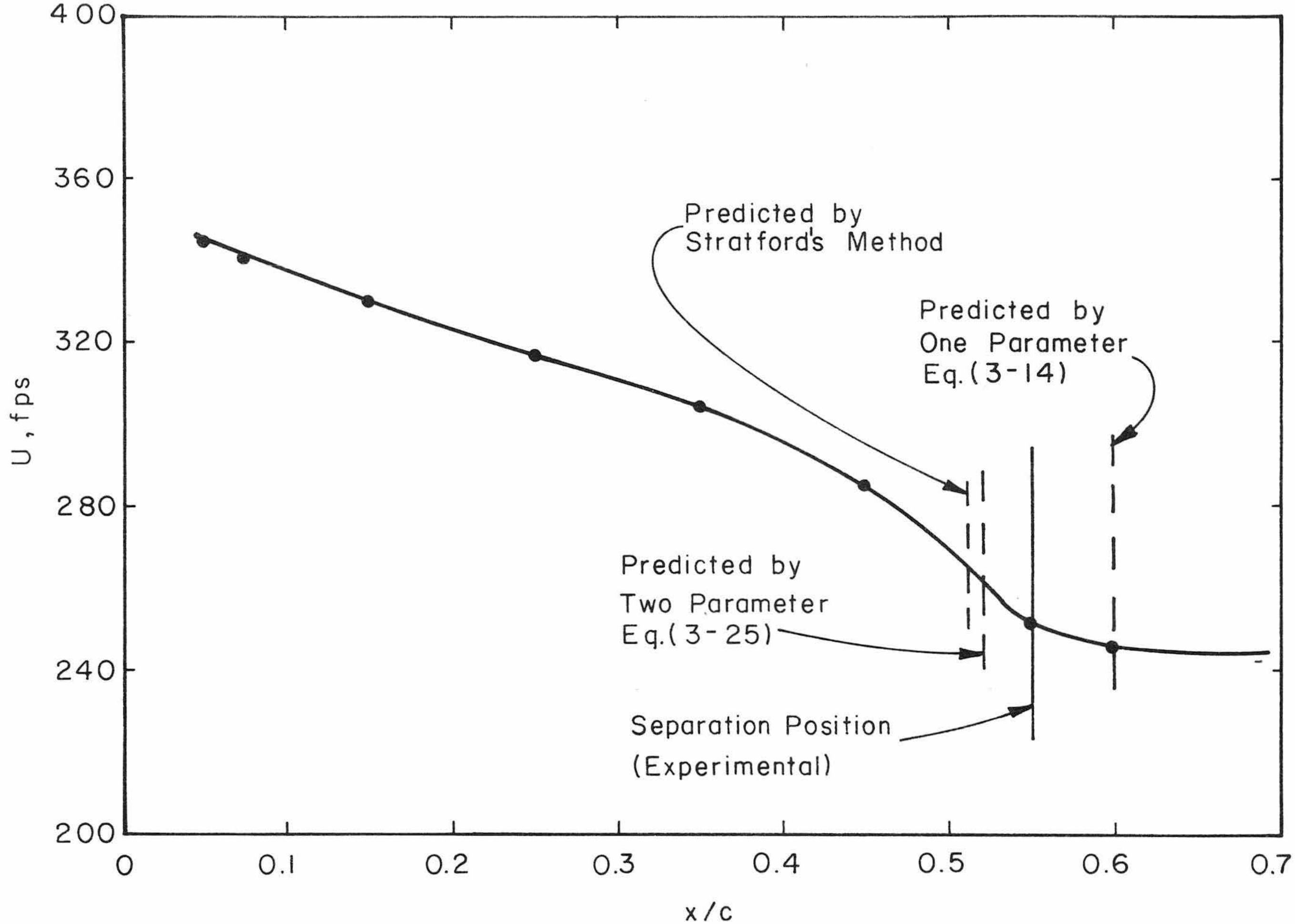

Fig. 34. Comparison of present separation prediction and experimental results (Von Doenhoff and Tetervin; α = 10.1 , R = 2.64 x 10^6)

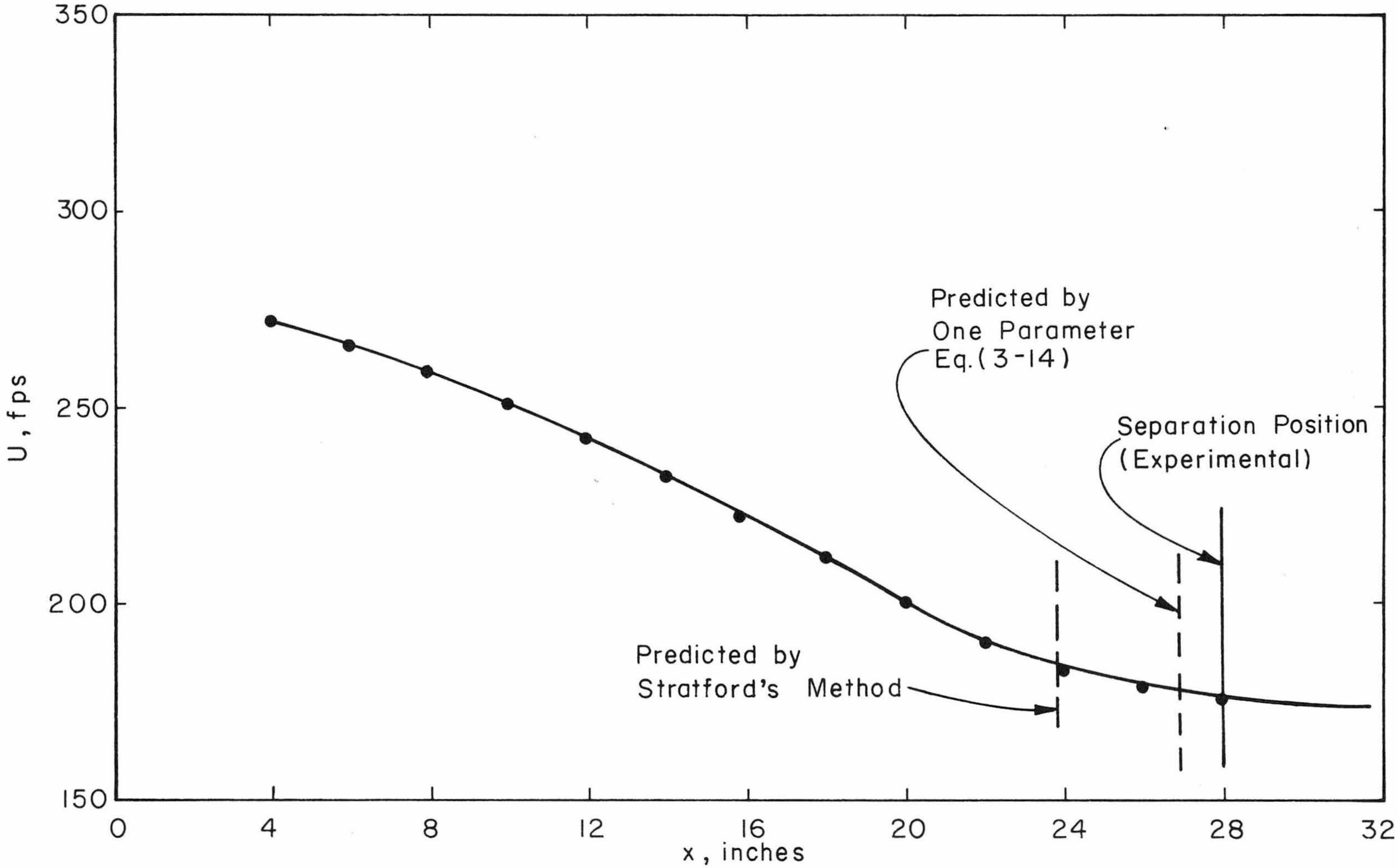

Fig. 35. Comparison of present separation prediction and experimental results (Hewson, Test 3, moderate pressure gradient)

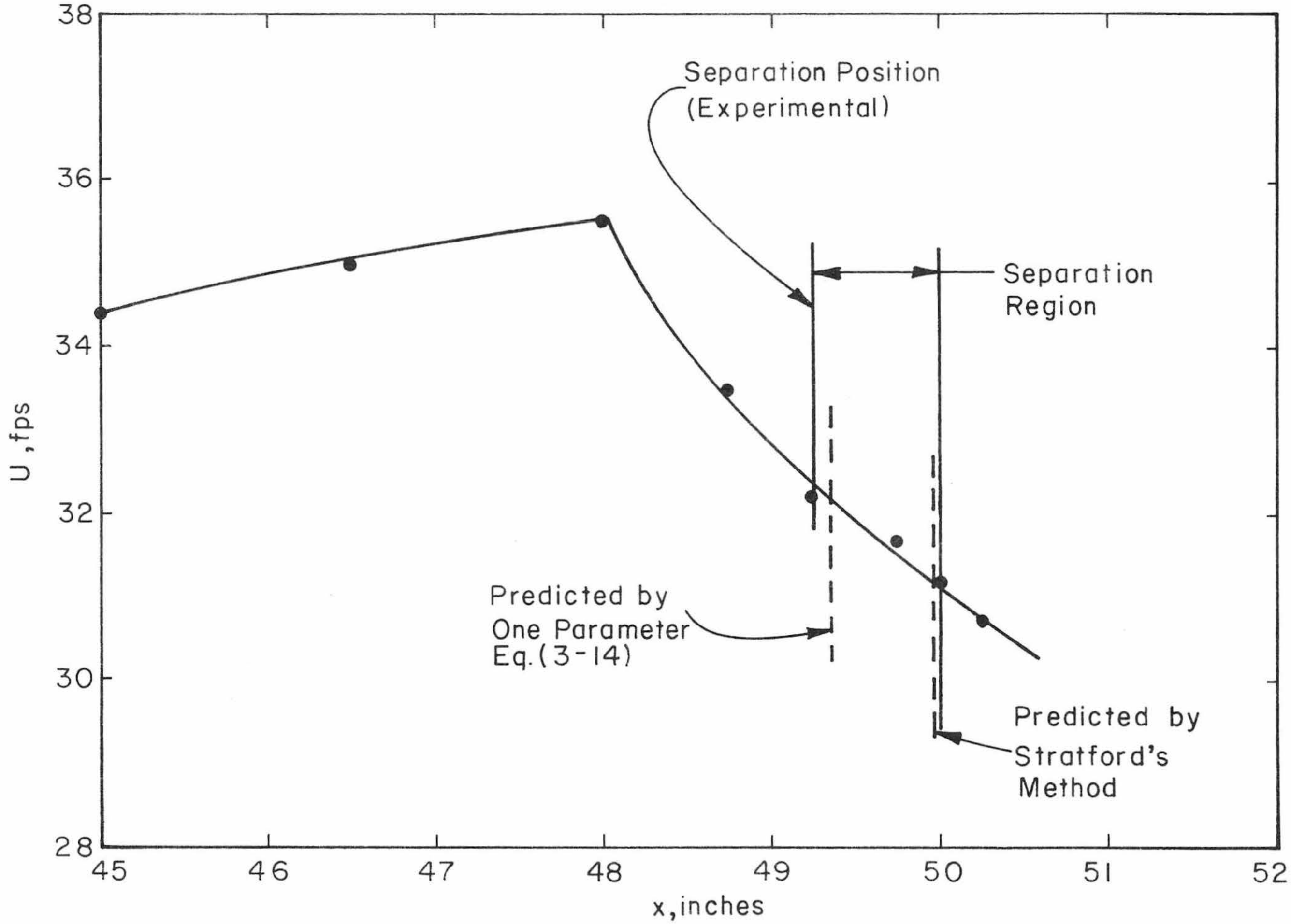

Fig. 36. Comparison of present separation prediction and experimental results (Sandborn and Liu, Station 2)

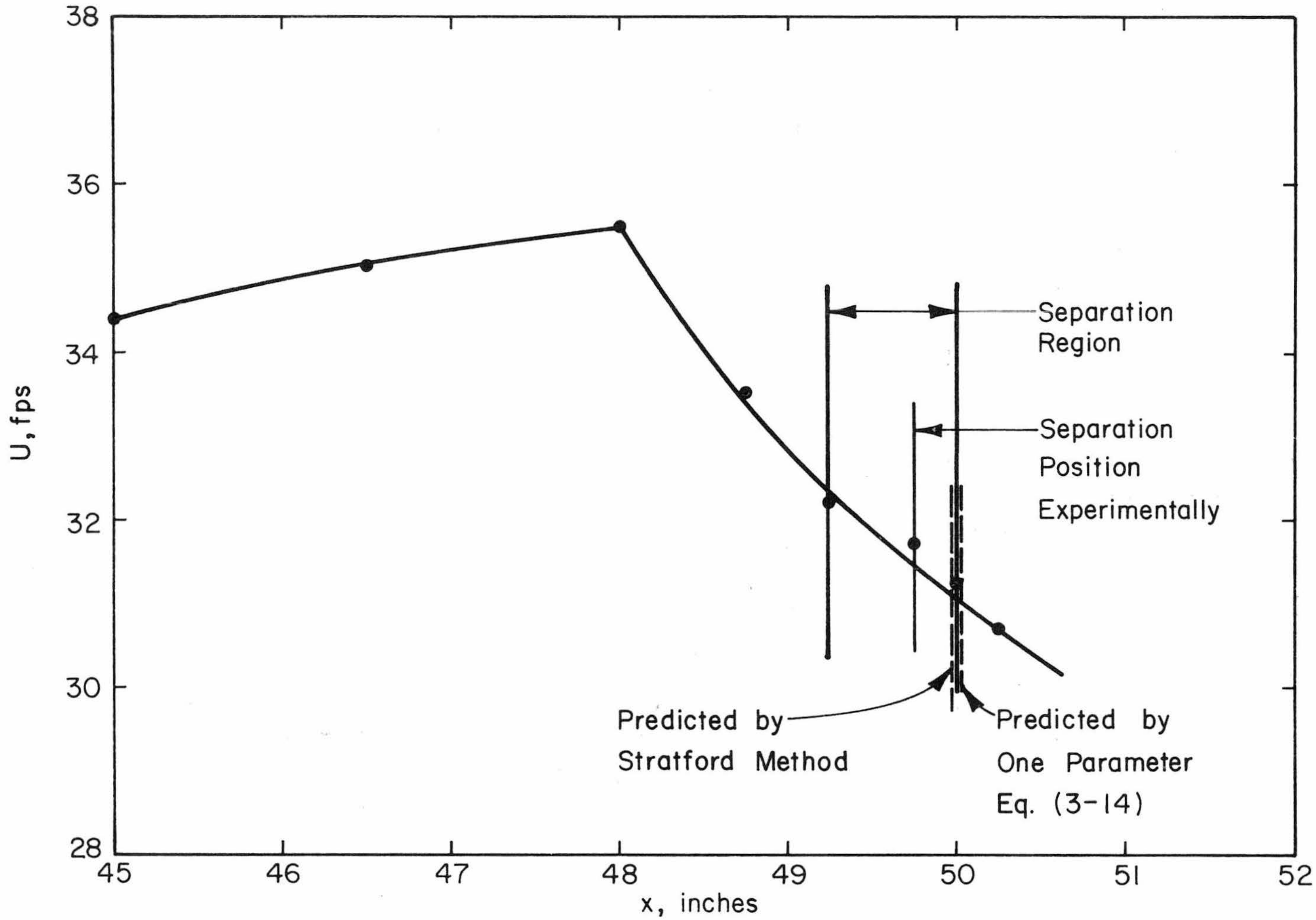

Fig. 37. Comparison of present separation prediction and experimental results (Sandborn and Liu, Station 3)

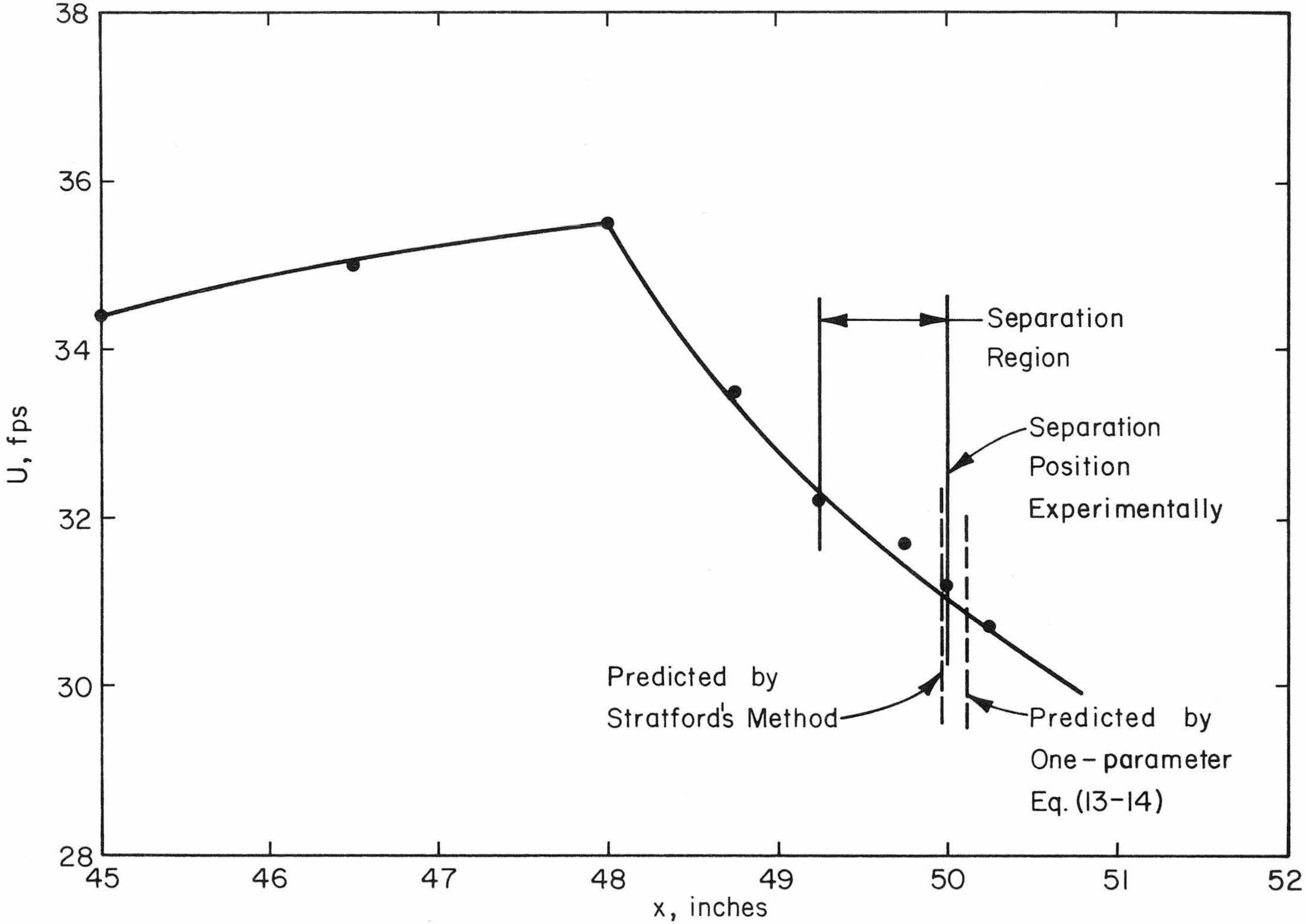

Fig. 38. Comparison of present separation prediction and experimental results (Sandborn and Liu, station 3½)

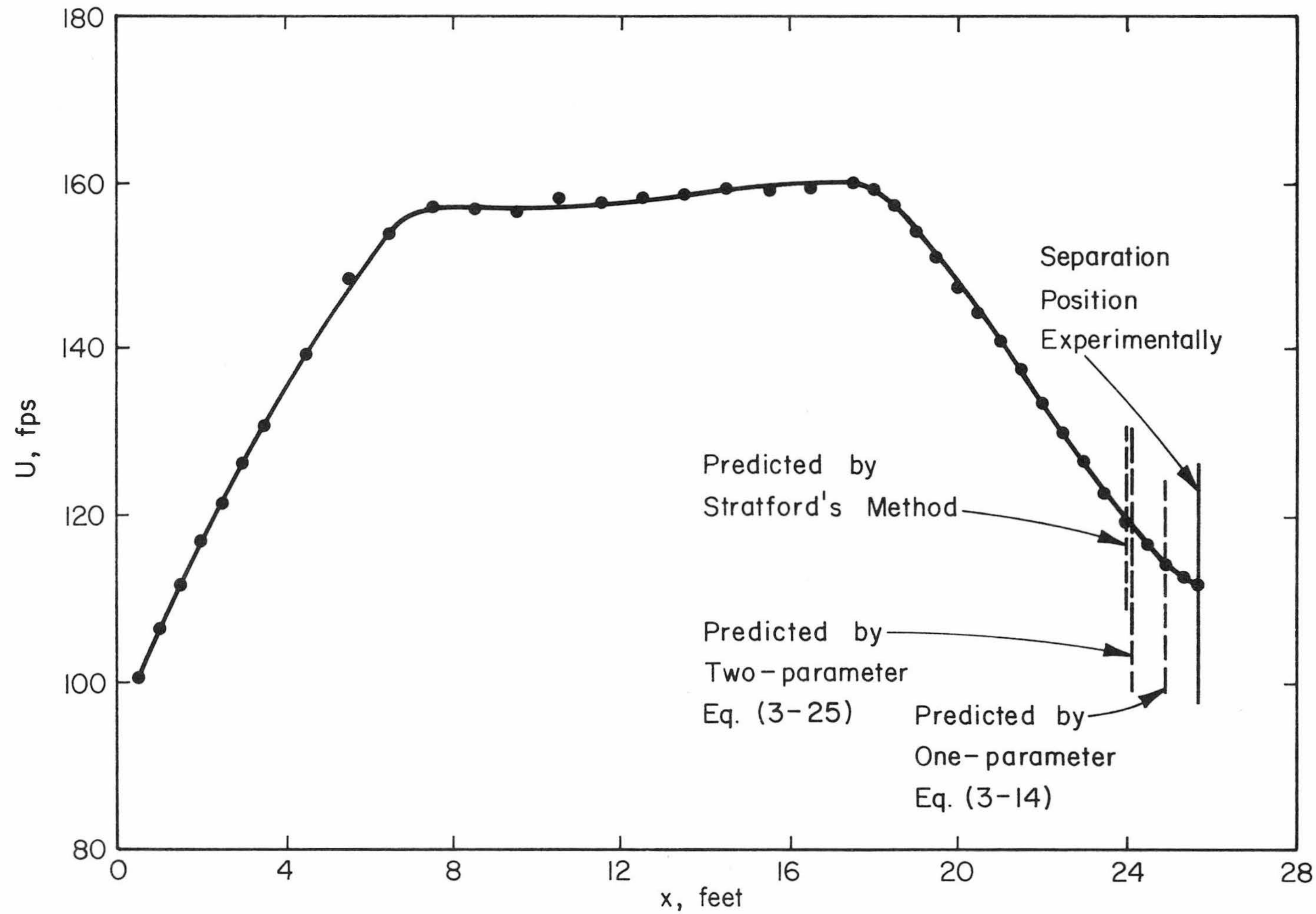

Fig. 39. Comparison of present separation prediction and experimental results (Schubauer and Klebanoff)

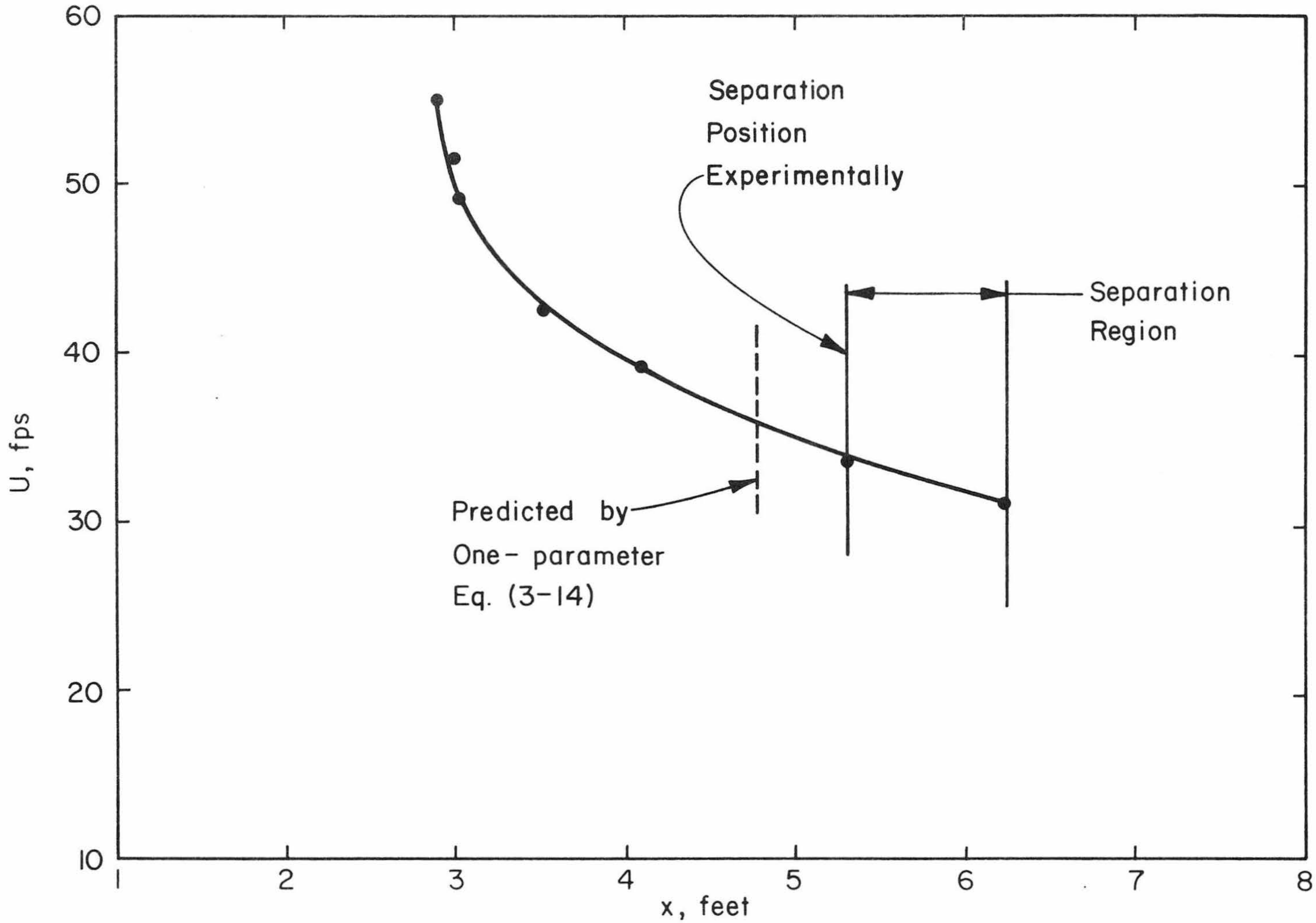

Fig. 40. Comparison of present separation prediction and experimental results (Stratford; Experiment 6)

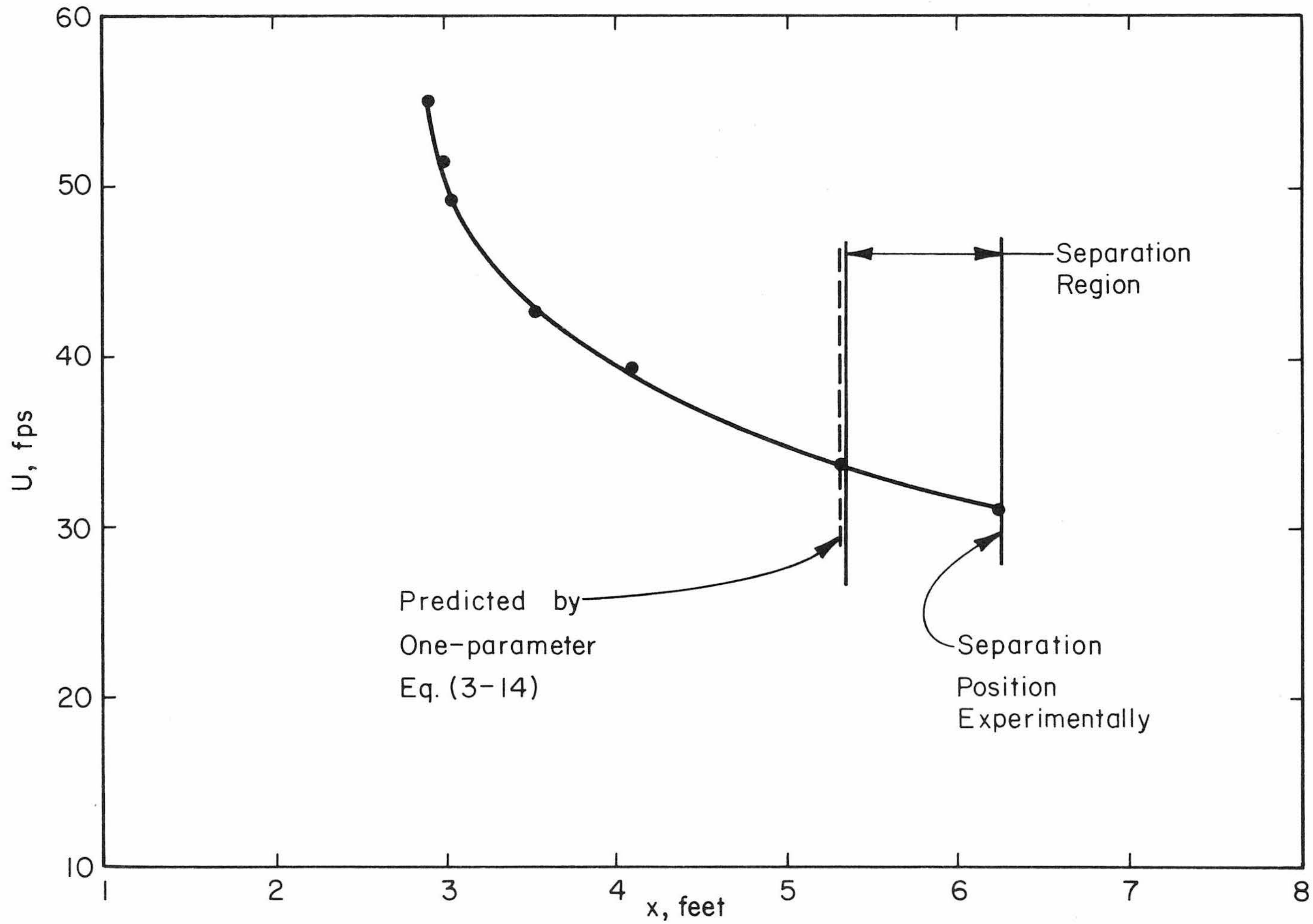

Fig. 41. Comparison of present separation prediction and experimental results (Stratford; Experiment 6)

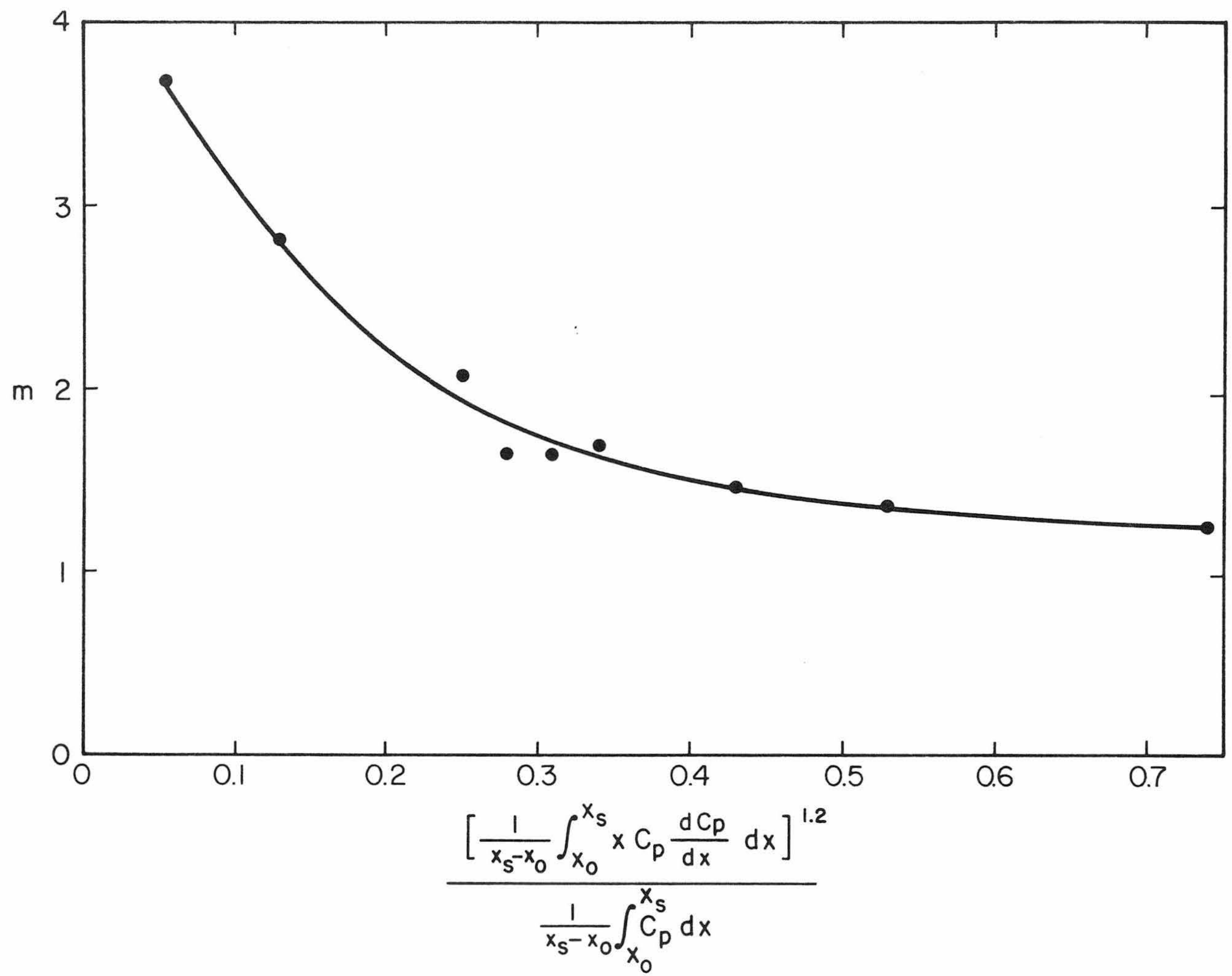

Fig. 42. Variations of the separation profile parameter m with the free stream flow condition

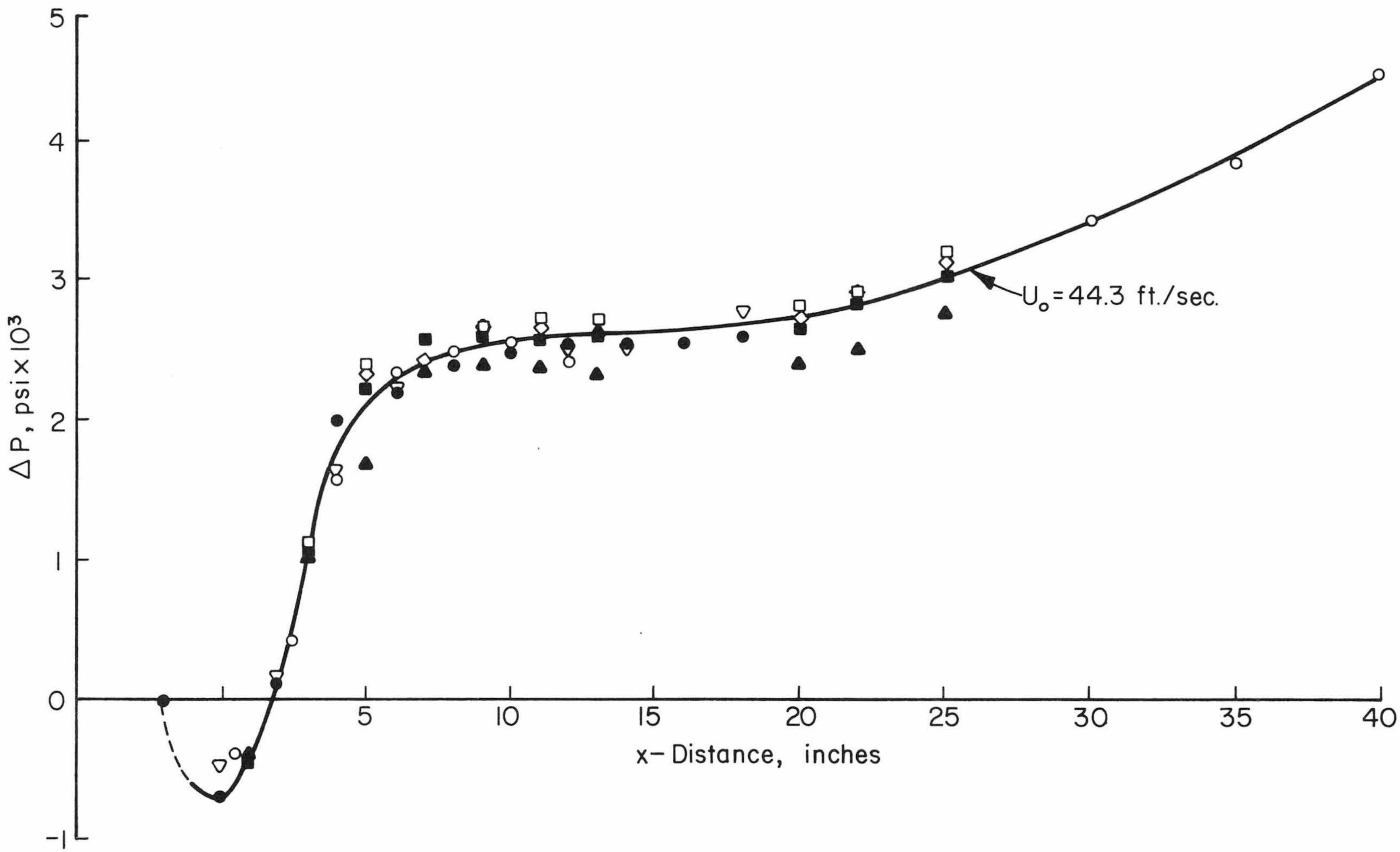

Fig. 43. Static pressure variations along the surface

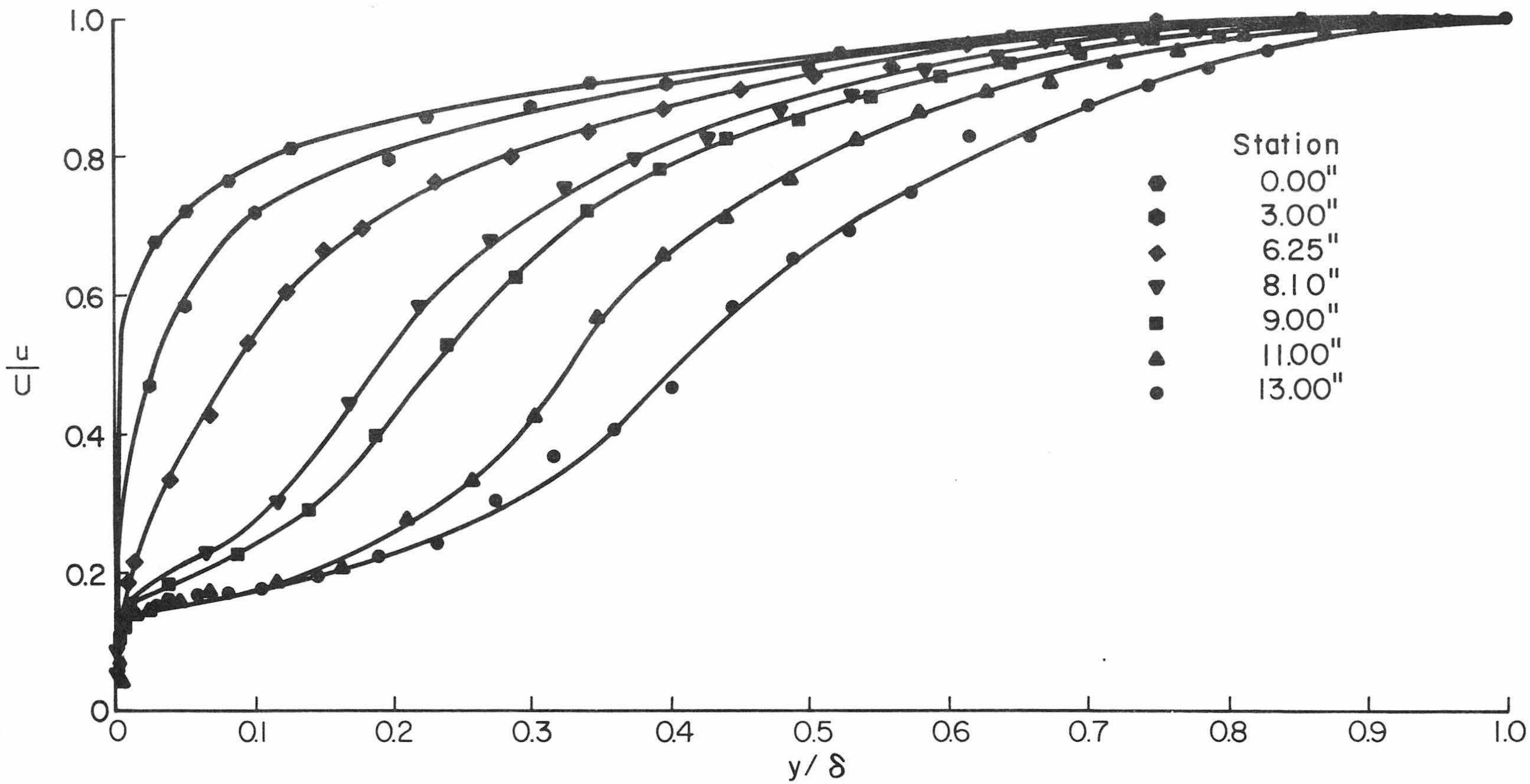

Fig. 44a. Mean velocity profiles along the center line of the diffuser

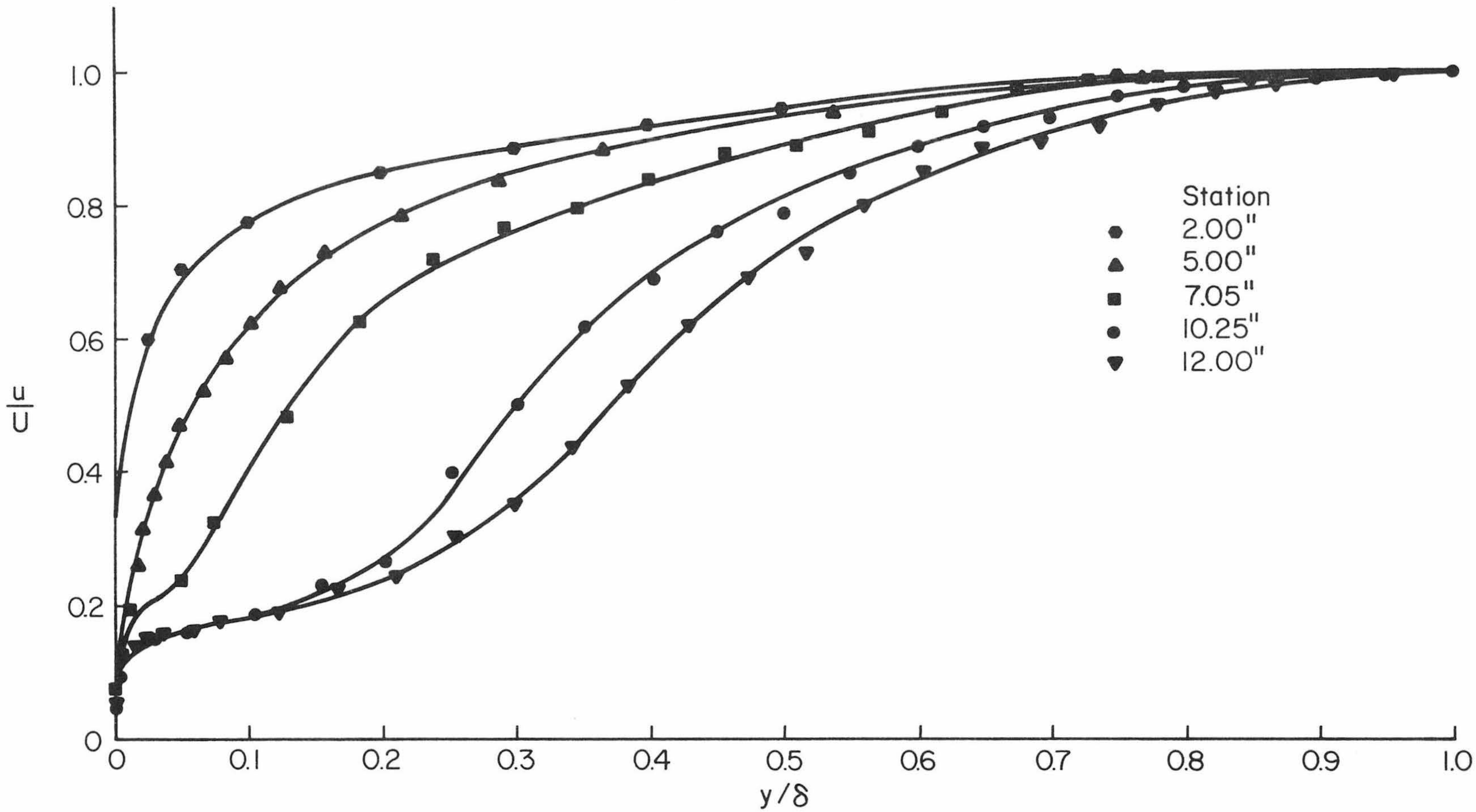

Fig. 44b. Mean velocity profiles along the center line of the diffuser

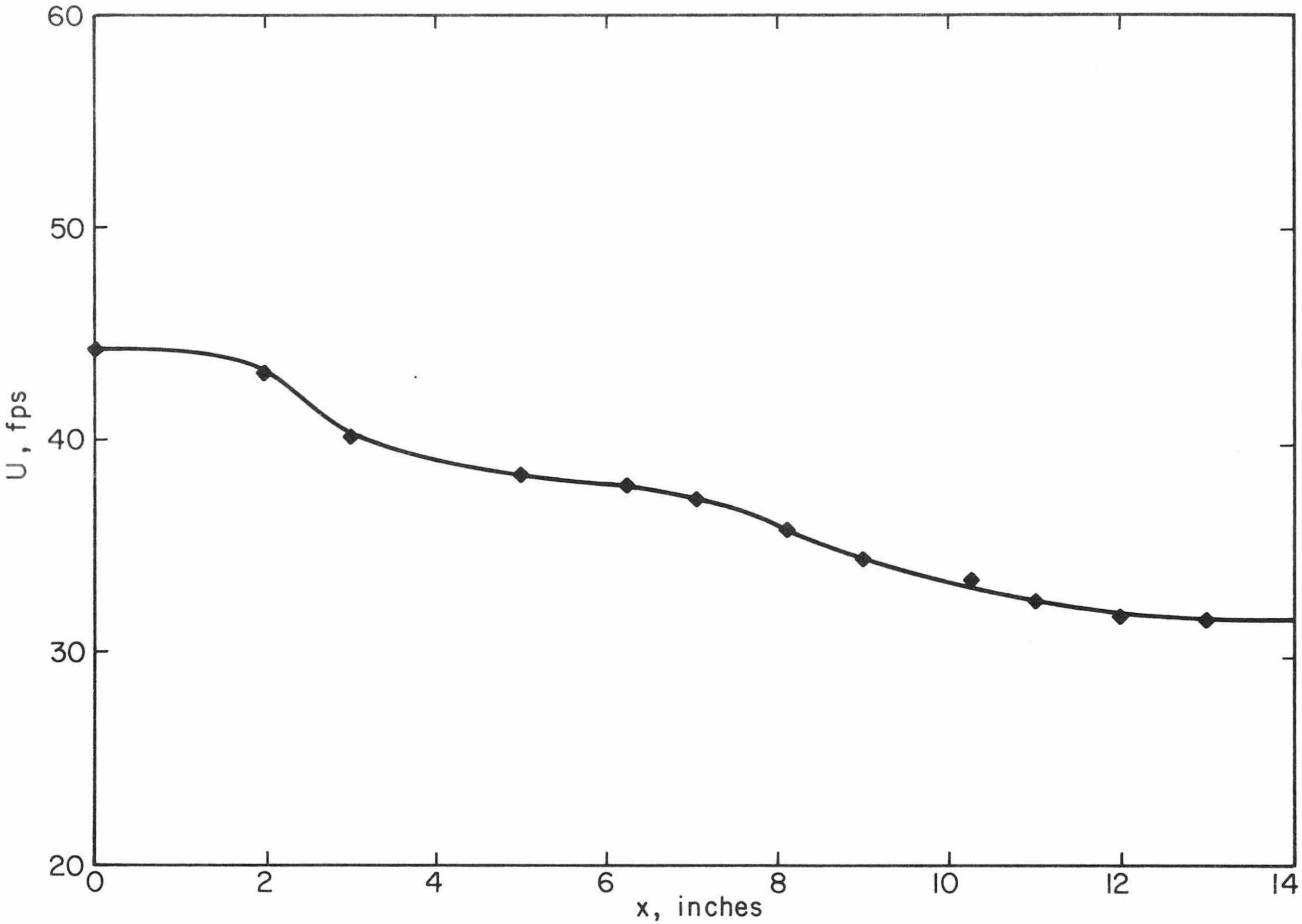

Fig. 45. Free stream velocity distribution

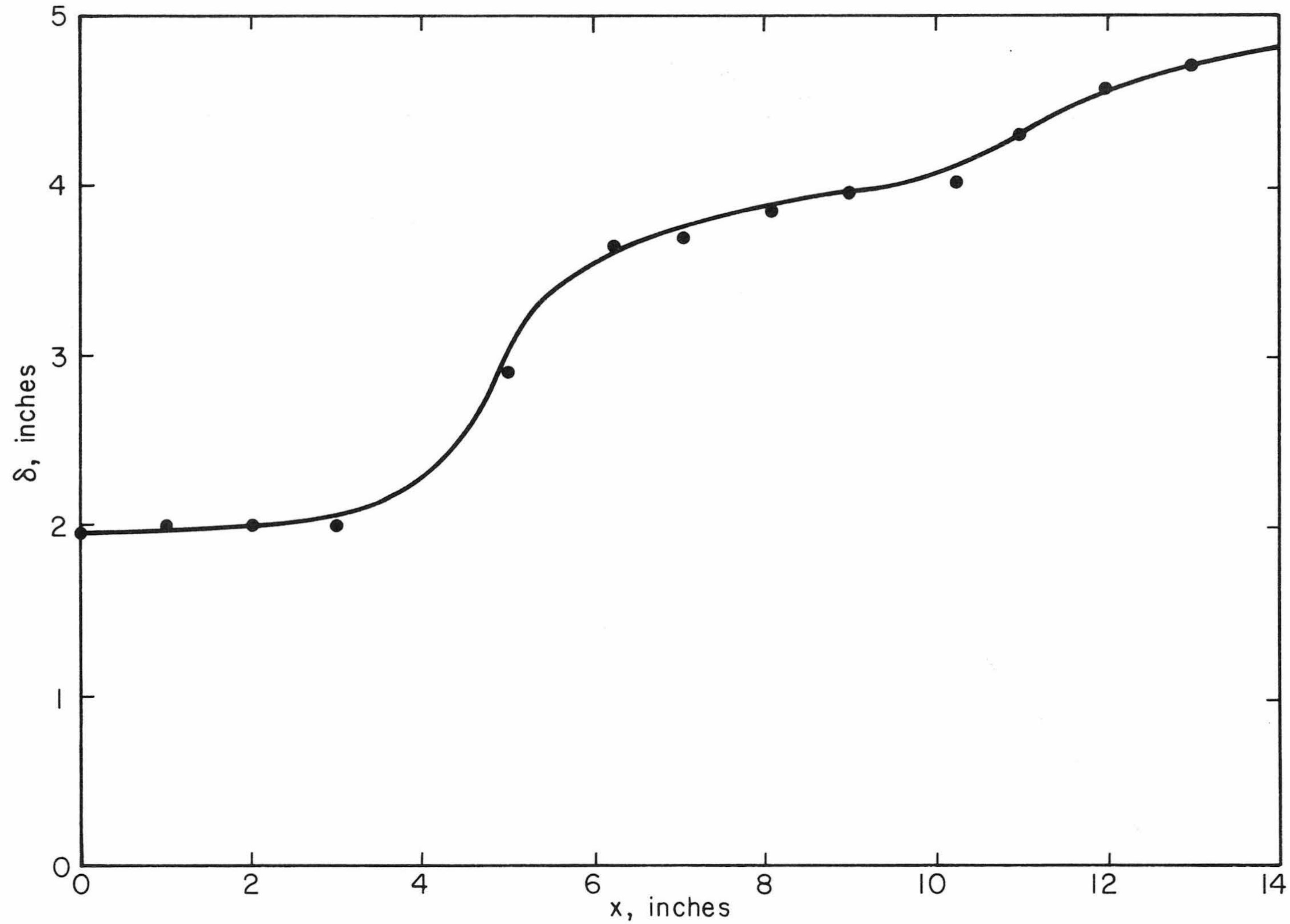

Fig. 46. Variations of boundary layer thickness

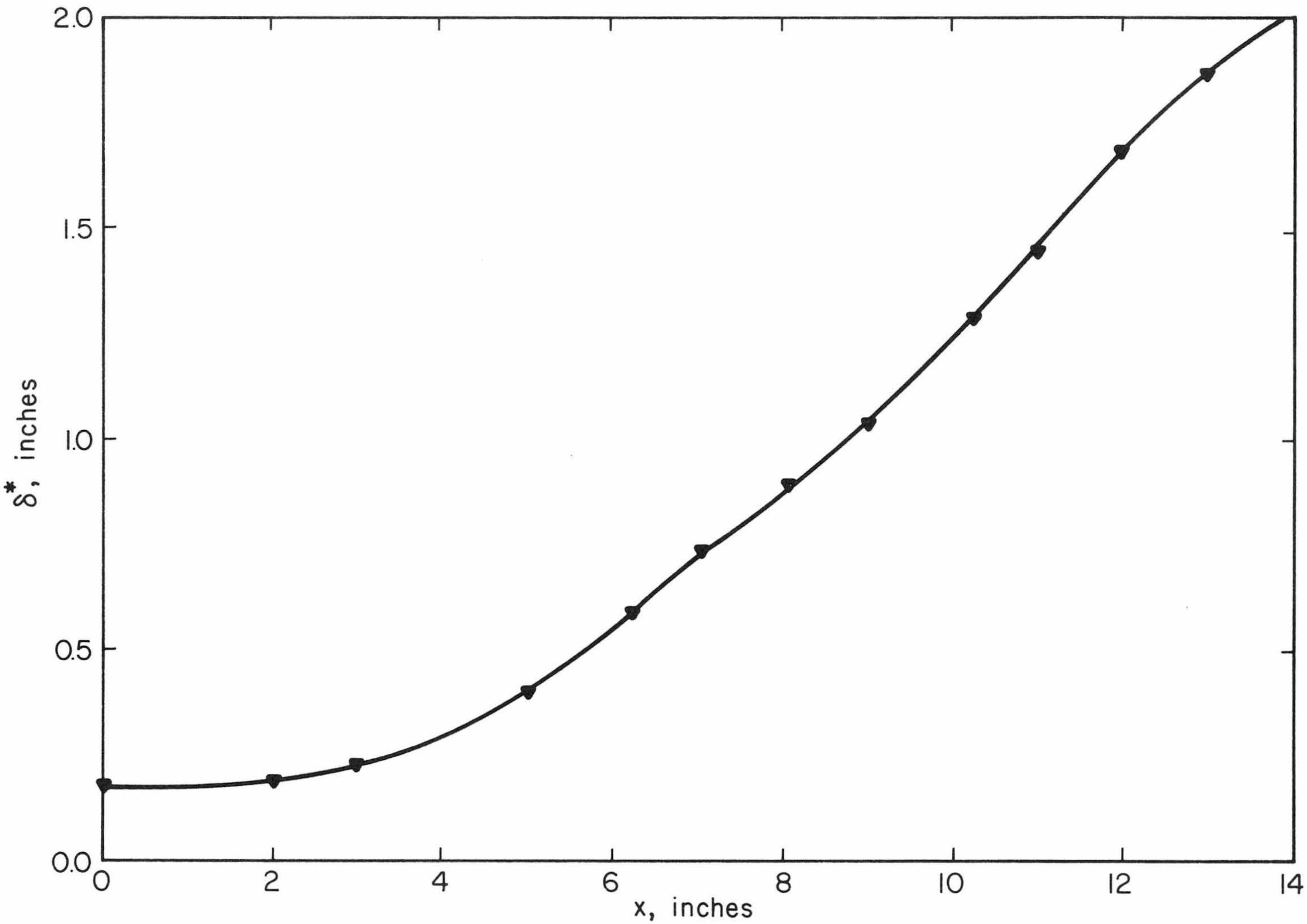

Fig. 47. Variations of displacement thickness

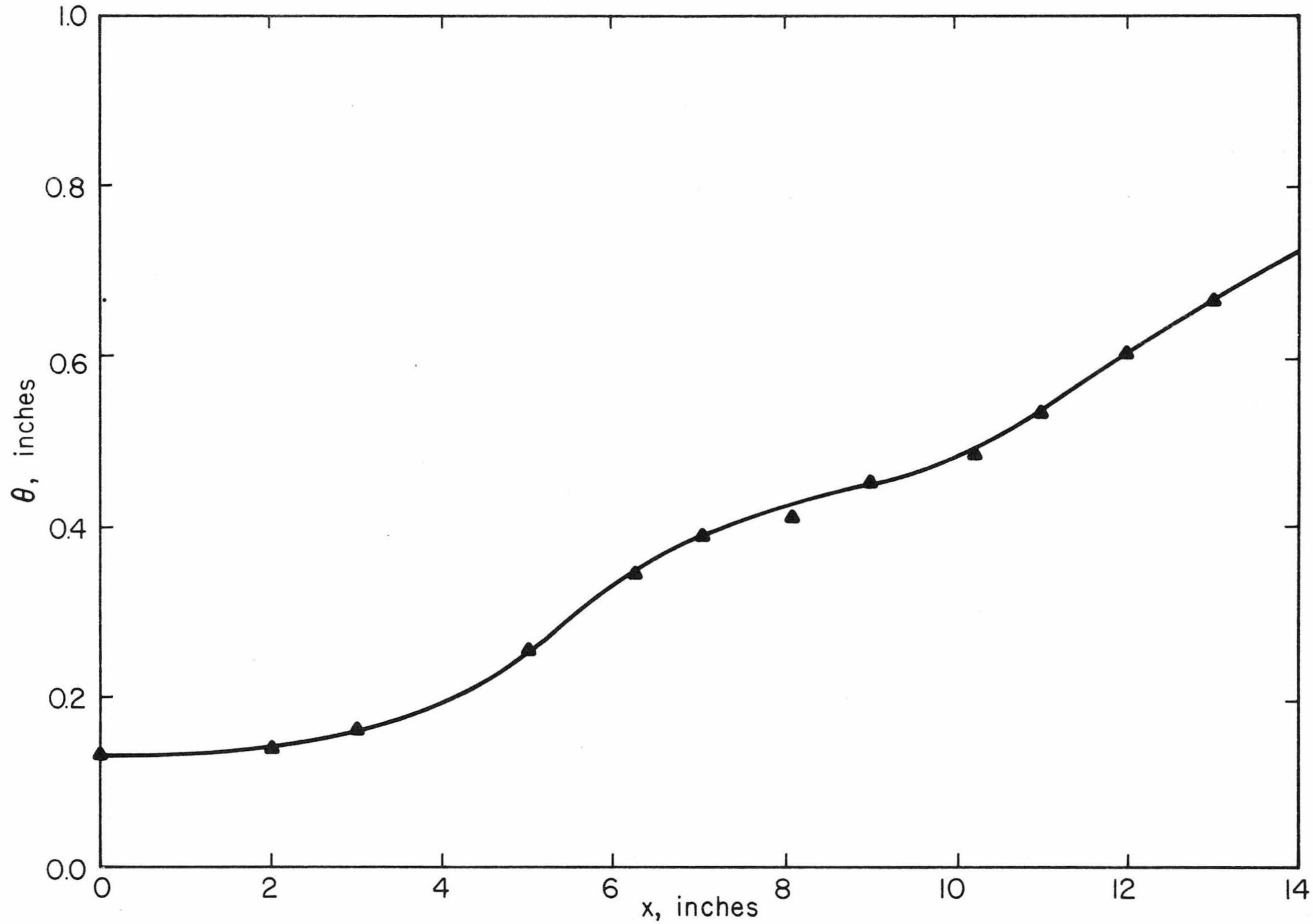

Fig. 48. Variations of momentum thickness

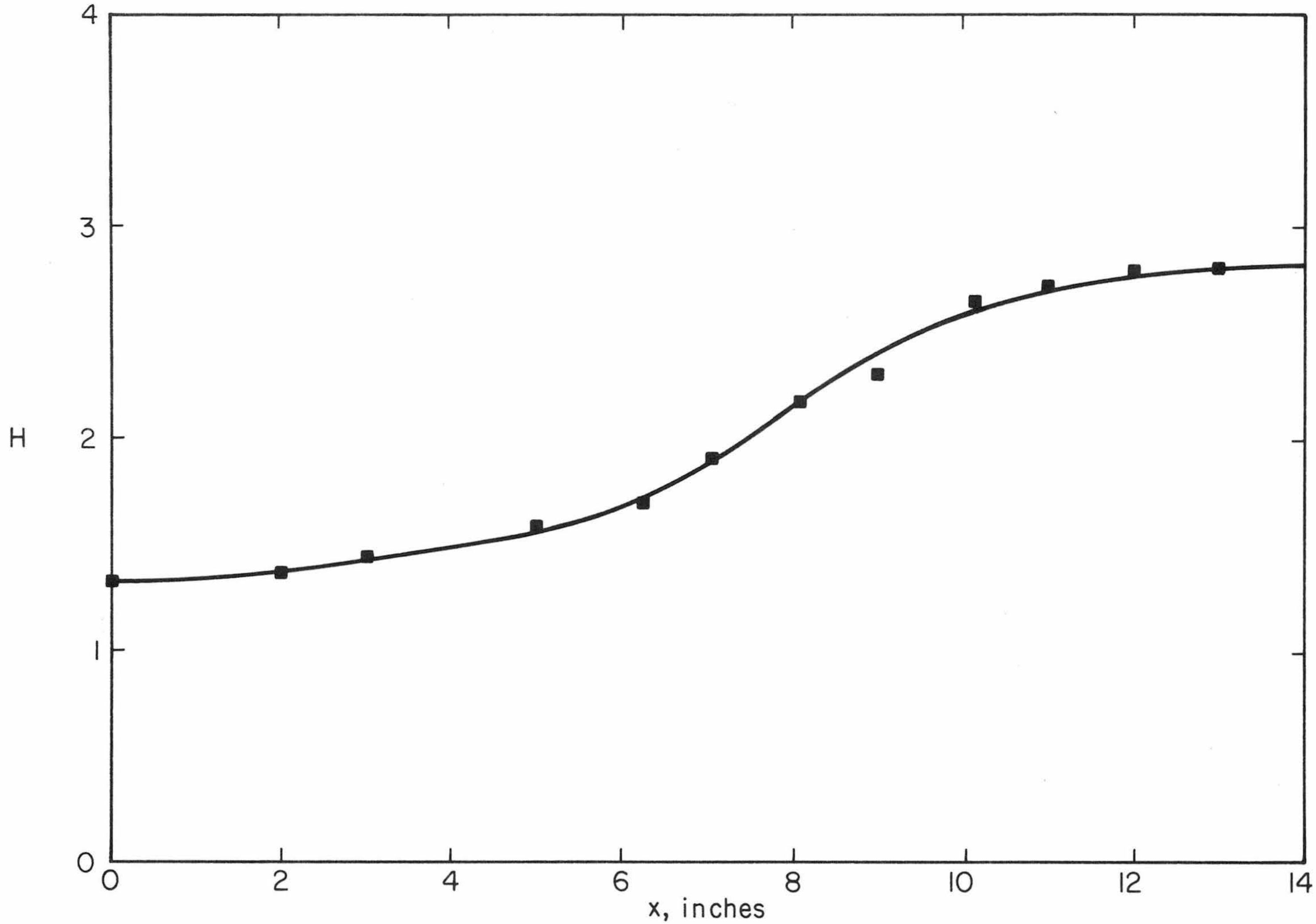

Fig. 49. Variations of form factor

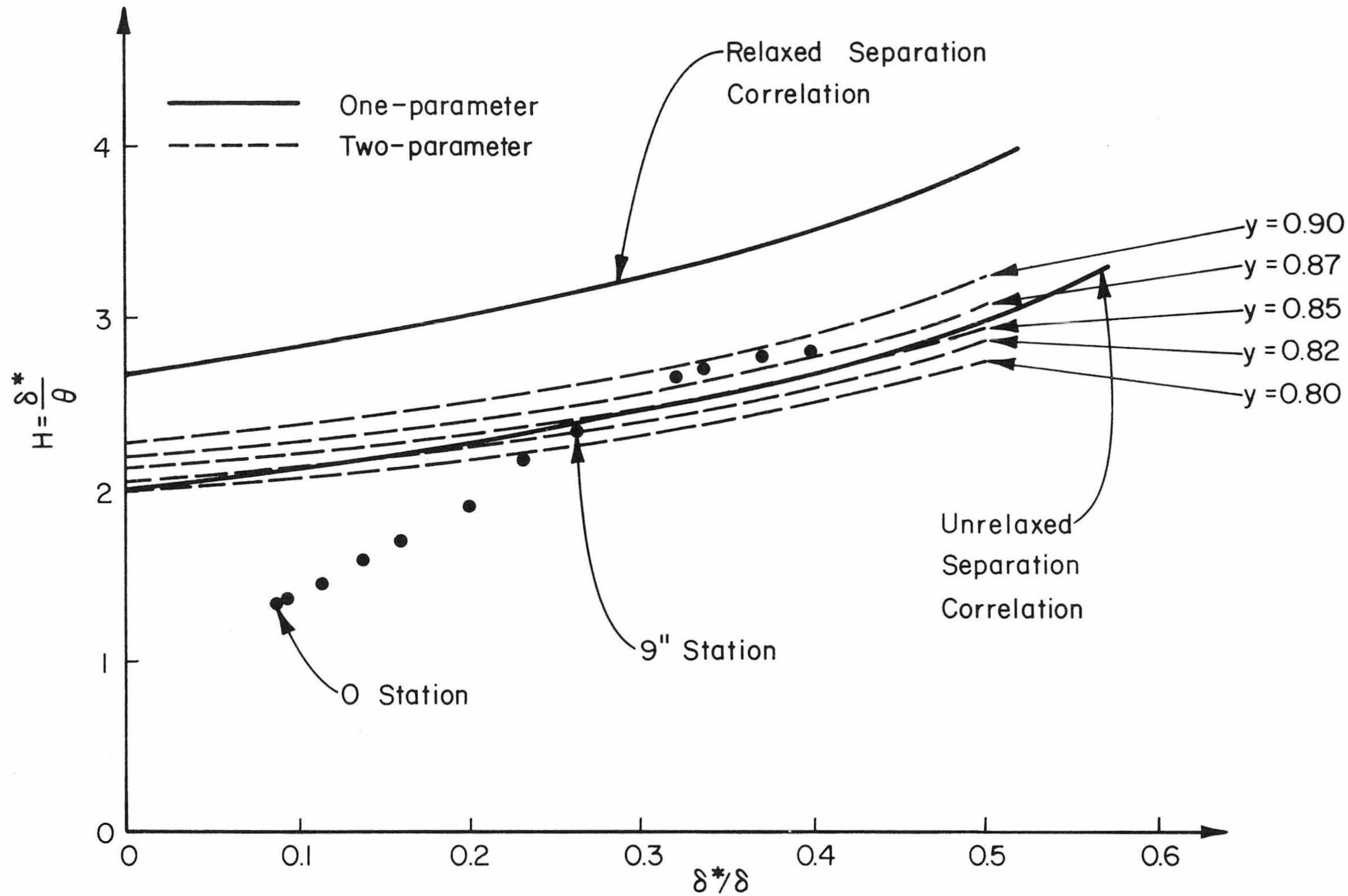

Fig. 50. Comparison of measurements with Sandborn and Kline's relaxed and unrelaxed spearation criterions.

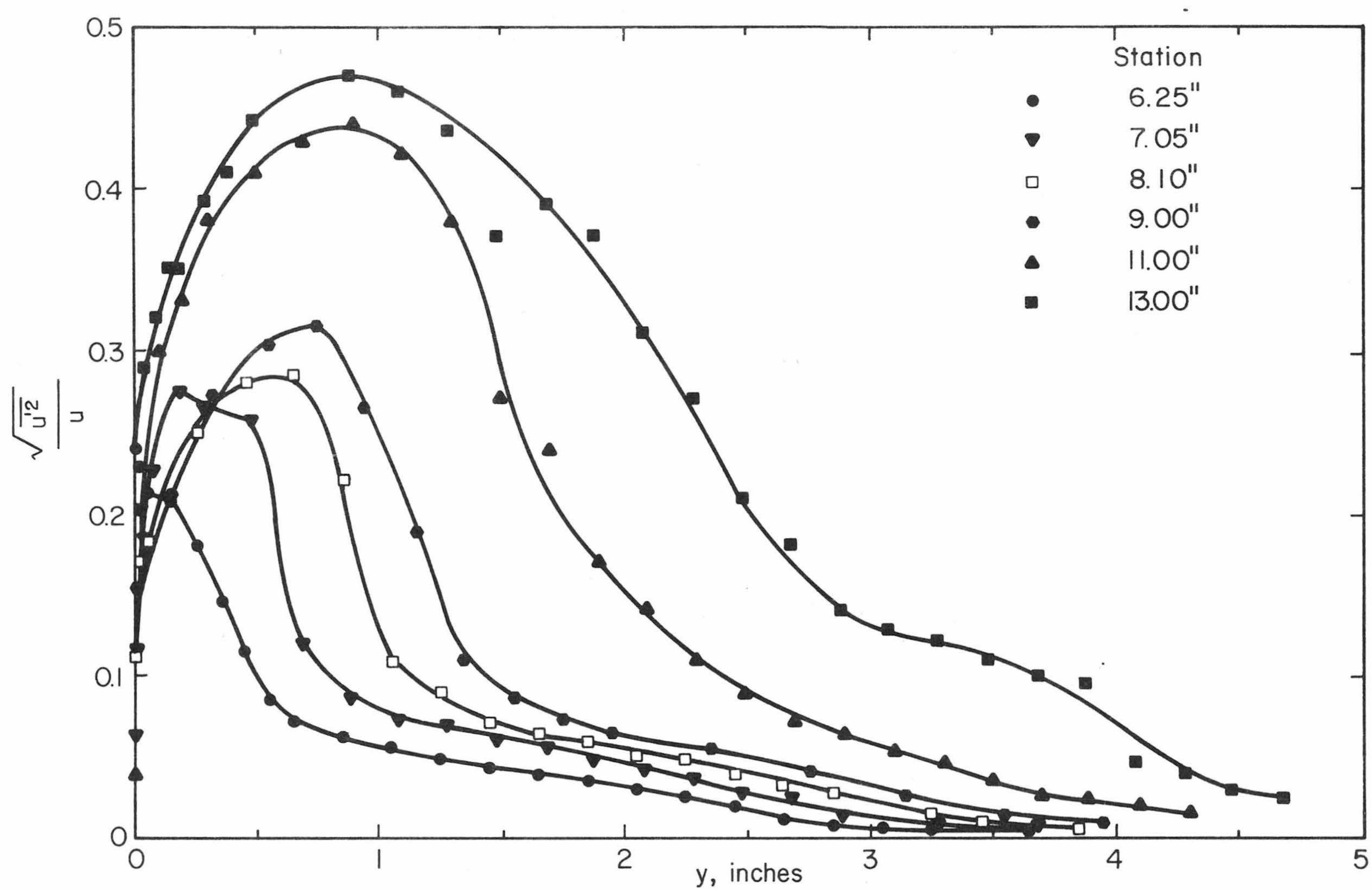

Fig. 51. Turbulent intensity along the center line of the diffuser

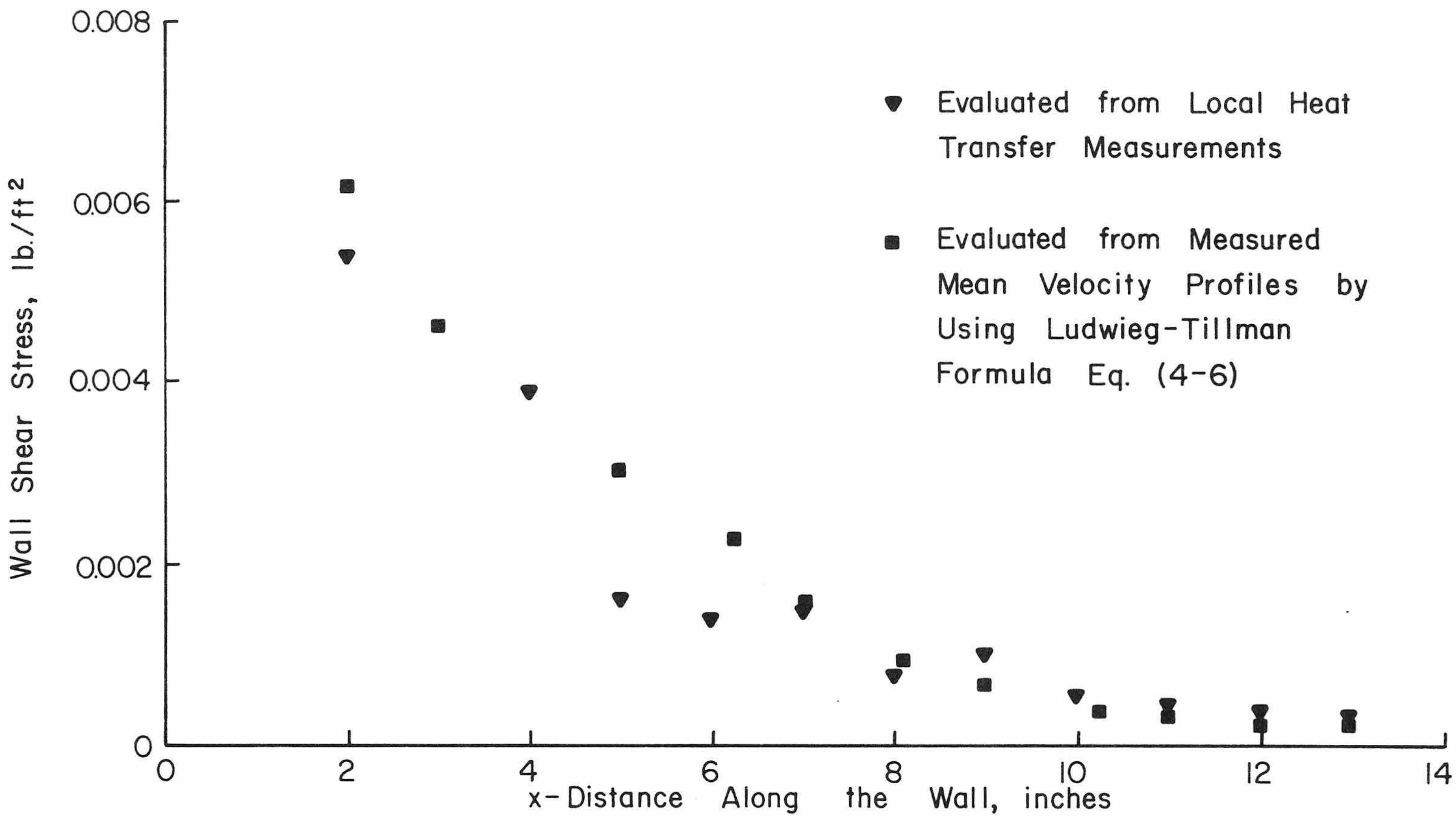

Fig. 52. Variations of the wall shear stresses along the test wall

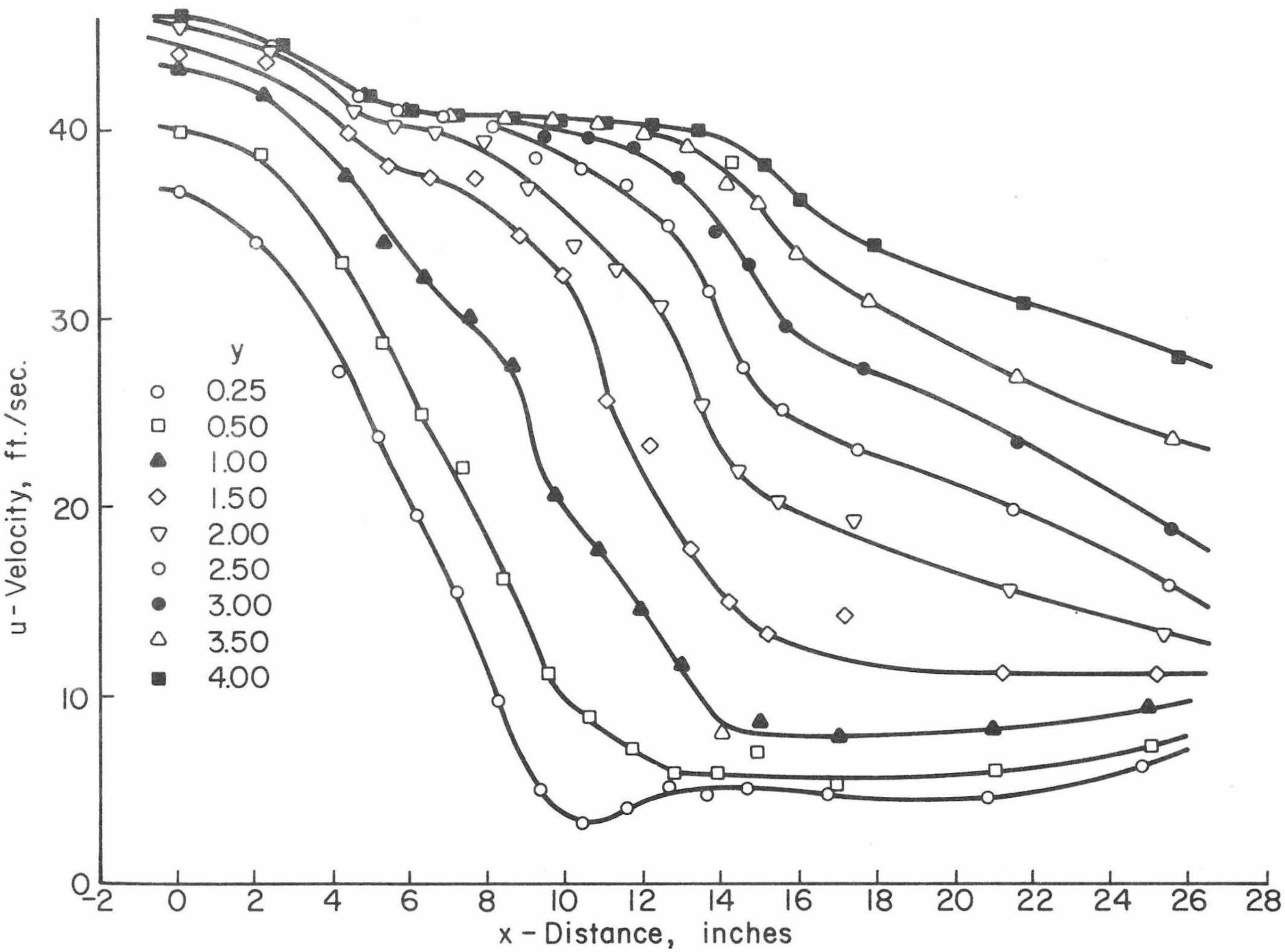

Fig. 53. Contour plot of velocity along test wall

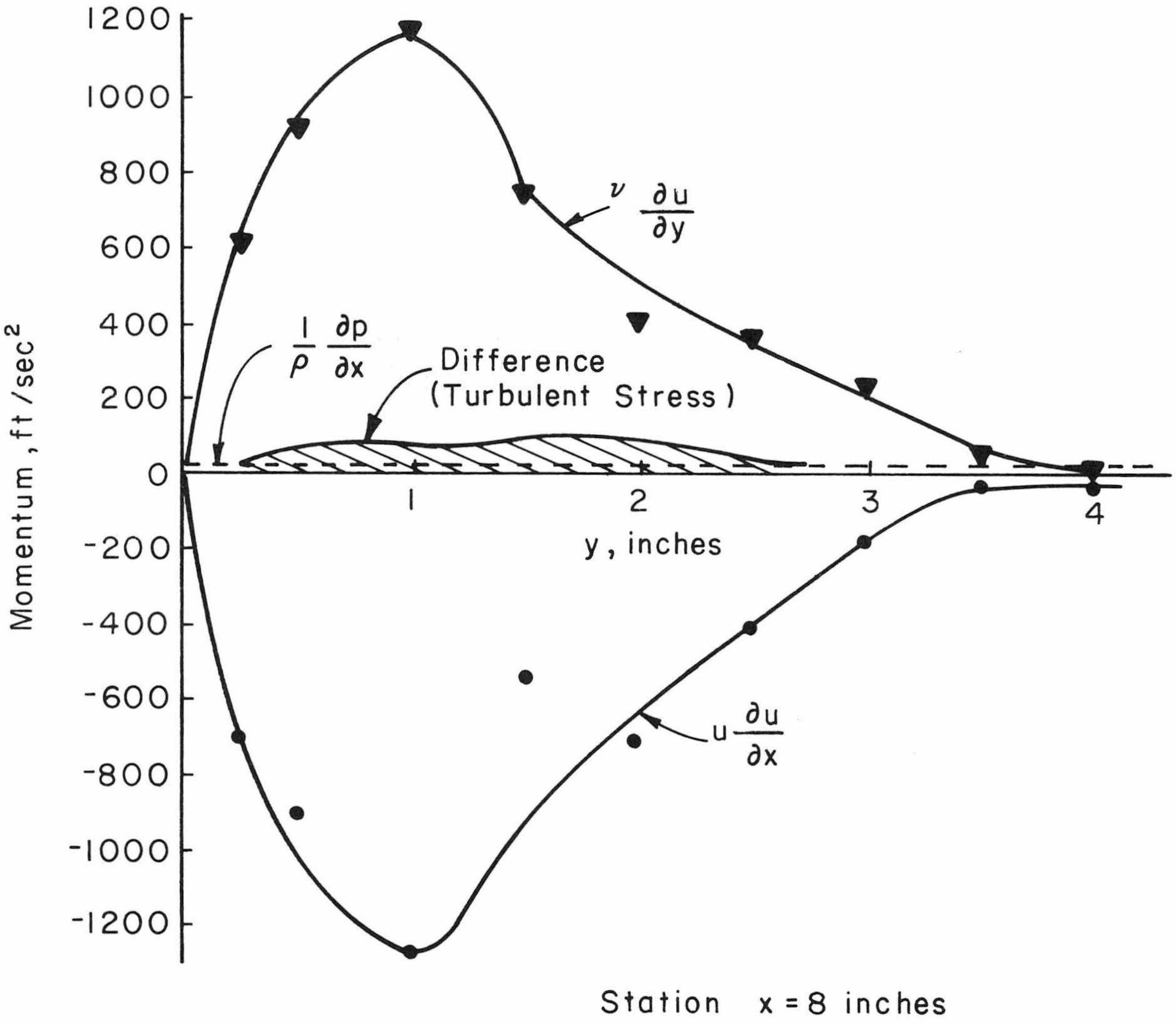

Fig. 54. Estimated momentum balance in X-direction

Unclassified

Security Classification

DOCUMENT CONTROL DATA - R&D

(Security classification of title, body of abstract and indexing annotation must be entered when the overall report is classified)

1. ORIGINATING ACTIVITY *(Corporate author)* Fluid Dynamics & Diffusion Laboratory College of Engineering, Colorado State University Fort Collins, Colorado 80521	2a. REPORT SECURITY CLASSIFICATION Unclassified 2b. GROUP

3. REPORT TITLE

Prediction of the Turbulent Boundary Layer Separation

4. DESCRIPTIVE NOTES *(Type of report and inclusive dates)*

Technical Report

5. AUTHOR(S) *(Last name, first name, initial)*

Chou, Fang-Kuo and Sandborn, Virgil A.

6. REPORT DATE	7a. TOTAL NO. OF PAGES	7b. NO. OF REFS
July 1973	99	39

8a. CONTRACT OR GRANT NO. N00014-68-A-0493-0001 b. PROJECT NO. NR 062-414/6-6-68 (Code 438) c. d.	9a. ORIGINATOR'S REPORT NUMBER(S) CER73-74FKC-VAS3 9b. OTHER REPORT NO(S) *(Any other numbers that may be assigned this report)* THEMIS Tech. Rpt. No. 22

10. AVAILABILITY/LIMITATION NOTICES

"This document has been approved for public release and sale; its distribution is unlimited."

11. SUPPLEMENTARY NOTES	12. SPONSORING MILITARY ACTIVITY
	U. S. Department of Defense Office of Naval Research

13. ABSTRACT A method for the prediction of the location of turbulent boundary layer separation is developed. The method is based on the inner and outer velocity dis-tributions technique developed by Stratford, together with a separation criterion which applies directly to the separation position.

For the inner region, the model employs the empirical one-parameter boundary layer separation profiles proposed by Sandborn and Kline. For the outer region the equivalent velocity distribution for the flow on a flat plate has been used. The resulting formula for predicting the separation position is a simple nonlinear algebraic equation.

The method is tested by comparing with several well documented separation measurements. The results show a good agreement in prediction of the position of turbulent separation. The calculated pressure rise to separation is also in good agreement with experimental results.

An experimental study for a turbulent boundary layer up to and through the separation region has been made to further demonstrate the present method. The measurements were taken along the test wall of a two dimensional diffuser. Mean quantities, turbulent intensities and wall shear stresses were measured. The velocity profile integral parameters were evaluated from the measured data. The results are also compared with the separation model suggested by Sandborn and Kline. At the start of the separation region, the velocity profile correlation falls approximately on the unrelaxed separation correlation curve given by Sandborn and Kline. The velocity profiles in the separation region are well represented by the two-parameter separation profiles suggested by Sandborn.

14. KEY WORDS	LINK A ROLE	LINK A WT	LINK B ROLE	LINK B WT	LINK C ROLE	LINK C WT
Turbulent Boundary Layer Separation						
Flow Separation						
Stratford Method						
Sandborn & Kline Method						
Separation Position						

INSTRUCTIONS

1. ORIGINATING ACTIVITY: Enter the name and address of the contractor, subcontractor, grantee, Department of Defense activity or other organization *(corporate author)* issuing the report.

2*a*. REPORT SECURITY CLASSIFICATION: Enter the overall security classification of the report. Indicate whether "Restricted Data" is included. Marking is to be in accordance with appropriate security regulations.

2*b*. GROUP: Automatic downgrading is specified in DoD Directive 5200.10 and Armed Forces Industrial Manual. Enter the group number. Also, when applicable, show that optional markings have been used for Group 3 and Group 4 as authorized.

3. REPORT TITLE: Enter the complete report title in all capital letters. Titles in all cases should be unclassified. If a meaningful title cannot be selected without classification, show title classification in all capitals in parenthesis immediately following the title.

4. DESCRIPTIVE NOTES: If appropriate, enter the type of report, e.g., interim, progress, summary, annual, or final. Give the inclusive dates when a specific reporting period is covered.

5. AUTHOR(S): Enter the name(s) of author(s) as shown on or in the report. Enter last name, first name, middle initial. If military, show rank and branch of service. The name of the principal author is an absolute minimum requirement.

6. REPORT DATE: Enter the date of the report as day, month, year; or month, year. If more than one date appears on the report, use date of publication.

7*a*. TOTAL NUMBER OF PAGES: The total page count should follow normal pagination procedures, i.e., enter the number of pages containing information.

7*b*. NUMBER OF REFERENCES: Enter the total number of references cited in the report.

8*a*. CONTRACT OR GRANT NUMBER: If appropriate, enter the applicable number of the contract or grant under which the report was written.

8*b*, 8*c*, & 8*d*. PROJECT NUMBER: Enter the appropriate military department identification, such as project number, subproject number, system numbers, task number, etc.

9*a*. ORIGINATOR'S REPORT NUMBER(S): Enter the official report number by which the document will be identified and controlled by the originating activity. This number must be unique to this report.

9*b*. OTHER REPORT NUMBER(S): If the report has been assigned any other report numbers *(either by the originator or by the sponsor)*, also enter this number(s).

10. AVAILABILITY/LIMITATION NOTICES: Enter any limitations on further dissemination of the report, other than those imposed by security classification, using standard statements such as:

(1) "Qualified requesters may obtain copies of this report from DDC."

(2) "Foreign announcement and dissemination of this report by DDC is not authorized."

(3) "U. S. Government agencies may obtain copies of this report directly from DDC. Other qualified DDC users shall request through
______________________________."

(4) "U. S. military agencies may obtain copies of this report directly from DDC. Other qualified users shall request through
______________________________."

(5) "All distribution of this report is controlled. Qualified DDC users shall request through
______________________________."

If the report has been furnished to the Office of Technical Services, Department of Commerce, for sale to the public, indicate this fact and enter the price, if known.

11. SUPPLEMENTARY NOTES: Use for additional explanatory notes.

12. SPONSORING MILITARY ACTIVITY: Enter the name of the departmental project office or laboratory sponsoring *(paying for)* the research and development. Include address.

13. ABSTRACT: Enter an abstract giving a brief and factual summary of the document indicative of the report, even though it may also appear elsewhere in the body of the technical report. If additional space is required, a continuation sheet shall be attached.

It is highly desirable that the abstract of classified reports be unclassified. Each paragraph of the abstract shall end with an indication of the military security classification of the information in the paragraph, represented as *(TS)*, *(S)*, *(C)*, *or (U)*.

There is no limitation on the length of the abstract. However, the suggested length is from 150 to 225 words.

14. KEY WORDS: Key words are technically meaningful terms or short phrases that characterize a report and may be used as index entries for cataloging the report. Key words must be selected so that no security classification is required. Idenfiers, such as equipment model designation, trade name, military project code name, geographic location, may be used as key words but will be followed by an indication of technical context. The assignment of links, rules, and weights is optional.

DISTRIBUTION LIST FOR UNCLASSIFIED TECHNICAL REPORTS ISSUED UNDER CONTRACT N00014-68-A-0493-0001 TASK 062-414

October 1972

All addressees receive one copy unless otherwise specified

Defense Documentation Center
Cameron Station
Alexandria, Virginia 22314 (12 copies)

Technical Library
Naval Ship Research and Development Laboratory
Annapolis, Maryland 21402

Professor Bruce Johnson
Engineering Department
Naval Academy
Annapolis, Maryland 21402

Library
Naval Academy
Annapolis, Maryland 21402

Professor W. P. Graebel
Department of Engineering Mechanics
College of Engineering
University of Michigan
Ann Arbor, Michigan 48108

Professor T. Francis Ogilvie
Department of Naval Architecture and Marine Engineering
University of Michigan
Ann Arbor, Michigan 48108

Professor W. W. Willmarth
Department of Aerospace Engineering
University of Michigan
Ann Arbor, Michigan 48108

AFOSR (REM)
1400 Wilson Boulevard
Arlington, Virginia 22204

Professor S. Corrsin
Department of Mechanics and Materials Science
The Johns Hopkins University
Baltimore, Maryland 21218

Professor R. B. Couch
Department of Naval Architecture and Marine Engineering
The University of Michigan
Ann Arbor, Michigan 48105

Professor L. S. G. Kovasznay
Department of Mechanics and Materials Science
The Johns Hopkins University
Baltimore, Maryland 21218

Professor O. M. Phillips
Department of Mechanics and Materials Science
The Johns Hopkins University
Baltimore, Maryland 21218

Professor M. Holt
Department of Mechanical Engineering
University of California
Berkeley, California 94720

Professor E. V. Laitone
Department of Mechanical Engineering
University of California
Berkeley, California 94720

Librarian
Department of Naval Architecture
University of California
Berkeley, California 94720

Professor P. Lieber
Department of Mechanical Engineering
Institute of Engineering Research
Berkeley, California 94720

Professor J. R. Paulling
Institute of Engineering Research
Department of Naval Architecture
University of California
Berkeley, California 94720

Professor W. C. Webster
College of Engineering
Department of Naval Architecture
University of California
Berkeley, California 94720

Professor J. V. Wehausen
Institute of Engineering Research
Department of Naval Architecture
University of California
Berkeley, California 94720

Commander
Boston Naval Shipyard
Boston, Massachusetts 02129

Director
Office of Naval Research Branch Office
495 Summer Street
Boston, Massachusetts 02210

Commander
Puget Sound Naval Shipyard
Bremerton, Washington 98314

Dr. Alfred Ritter
Cornell Aeronautical Laboratory, Inc.
P. O. Box 235
Buffalo, New York 14221

Professor G. Birkhoff
Department of Mathematics
Harvard University
Cambridge, Massachusetts 02138

Professor G. F. Carrier
Division of Engineering and Applied Physics
Harvard University
Cambridge, Massachusetts 02139

Commanding Officer
NROTC Naval Administrative Unit
Massachusetts Institute of Technology
Cambridge, Massachusetts 02139

Professor M. A. Abkowitz
Department of Ocean Engineering
Massachusetts Institute of Technology
Cambridge, Massachusetts 02139

Professor A. T. Ippen
Department of Civil Engineering
Massachusetts Institute of Technology
Cambridge, Massachusetts 02139

Professor Phillip Mandel
Department of Ocean Engineering
Massachusetts Institute of Technology
Cambridge, Massachusetts 02139

Professor E. W. Merrill
Department of Chemical Engineering
Massachusetts Institute of Technology
Cambridge, Massachusetts 02139

Professor E. Mollo-Christensen
Department of Meteorology
Room 54-1722
Massachusetts Institute of Technology
Cambridge, Massachusetts 02139

Professor J. Nicholas Newman
Department of Ocean Engineering
Room 5-324A
Massachusetts Institute of Technology
Cambridge, Massachusetts 02139

Commander
Charleston Naval Shipyard
Naval Base
Charleston, South Carolina 29408

A. R. Kuhlthau, Director
Research Laboratories for the Engineering Sciences
Thorton Hall, University of Virginia
Charlottesville, Virginia 22903

Director
Office of Naval Research Branch Office
536 South Clark Street
Chicago, Illinois 60605

Library
Naval Weapons Center
China Lake, California 93555

Professor R. V. Edwards
Division of Chemical Engineering
Case Western Reserve University
Cleveland, Ohio 44106

Professor J. M. Burgers
Institute of Fluid Dynamics and Applied Mathematics
University of Maryland
College Park, Maryland 20742

Professor Pai
Institute of Fluid Dynamics and Applied Mathematics
University of Maryland
College Park, Maryland 20742

Acquisition Director
NASA Scientific and Technical Information
P. O. Box 33
College Park, Maryland 20742

Technical Library
Naval Weapons Laboratory
Dahlgren, Virginia 22448

Computation and Analyses Laboratory
Naval Weapons Laboratory
Dahlgren, Virginia 22448

Dr. R. H. Kraichnan
Dublin, New Hampshire 03444

Commanding Officer
Army Research Office
Box CM, Duke Station
Durham, North Carolina 27706

Dr. Martin H. Bloom
Polytechnic Institute of Brooklyn
Long Island Graduate Center
Department of Aerospace Engineering and Applied Mechanics
Farmingdale, New York 11735

Technical Documents Center
Building 315
U. S. Army Mobility Equipment Research and Development Center
Fort Belvoir, Virginia 22060

Professor J. E. Cermak
Department of Atmospheric Sciences
Colorado State University
Fort Collins, Colorado 80521

Professor O. H. Shemdin
Coastal and Oceanographic Engineering Department
University of Florida
Gainesville, Florida 32601

Technical Library
Webb Institute of Naval Architecture
Glen Cove, Long Island, New York 11542

Professor E. V. Lewis
Webb Institute of Naval Architecture
Glen Cove, Long Island, New York 11542

Dr. J. P. Breslin
Davidson Laboratory
Stevens Institute of Technology
Castle Point Station
Hoboken, New Jersey 07030

Mr. C. H. Henry
Stevens Institute of Technology
Davidson Laboratory
Castle Point Station
Hoboken, New Jersey 07030

Dr. D. Savitsky
Davidson Laboratory
Stevens Institute of Technology
Castle Point Station
Hoboken, New Jersey 07030

Dr. A. Strumpf
Davidson Laboratory
Stevens Institute of Technology
Castle Point Station
Hoboken, New Jersey 07030

Dr. J. P. Craven
University of Hawaii
1801 University Avenue
Honolulu, Hawaii 96822

Professor J. F. Kennedy, Director
Iowa Institute of Hydraulic Research
State University of Iowa
Iowa City, Iowa 52240

Professor L. Landweber
Iowa Institute of Hydraulic Research
State University of Iowa
Iowa City, Iowa 52240

Professor E. L. Resler
Graduate School of Aeronautical Engineering
Cornell University
Ithaca, New York 14851

Dr. Y. H. Pao
Flow Research, Inc.
1819 South Central Avenue
Suite 72
Kent, Washington 98031

Dr. D. E. Ordway
Sage Action, Incorporated
P. O. Box 416
Ithaca, New York 14850

Professor John Miles
c/o I.G.P.P.
University of California, San Diego
La Jolla, California 92038

Director
Scripps Institute of Oceanography
University of California
La Jolla, California 92037

Professor A. T. Ellis
University of California, San Diego
Department of Aerospace and
Mechanical Engineering Science
La Jolla, California 92037

Dr. Coda Pan
Mechanical Technology Incorporated
968 Albany-Shaker Road
Latham, New York 12110

Mr. P. Eisenberg, President
Hydronautics, Incorporated
8210 Pindell School Road
Laurel, Maryland 20810

Mr. M. P. Tulin
Hydronautics, Incorporated
8210 Pindell School Road
Laurel, Maryland 20810

Commander
Long Beach Naval Shipyard
Long Beach, California 90802

Professor John Laufer
Department of Aerospace Engineering
University Park
Los Angeles, California 90007

Dr. F. H. Harlow
University of California
Los Alamos Scientific Laboratory
P. O. Box 1663
Los Alamos, New Mexico 87544

Professor J. M. Killen
St. Anthony Falls Hydraulic Laboratory
University of Minnesota
Minneapolis, Minnesota 55414

Lorenz G. Straub Library
St. Anthony Falls Hydraulic Laboratory
University of Minnesota
Minneapolis, Minnesota 55414

Professor J. Ripkin
St. Anthony Falls Hydraulic Laboratory
University of Minnesota
Minneapolis, Minnesota 55414

Dr. E. Silberman
St. Anthony Falls Hydraulic Laboratory
University of Minnesota
Minneapolis, Minnesota 55414

Superintendent
Naval Postgraduate School
Attn: Library
Monterey, California 93940

Professor A. B. Metzner
Department of Chemical Engineering
University of Delaware
Newark, New Jersey 19711

Technical Library
Naval Underwater Systems Center
Newport, Rhode Island 02840

Office of Naval Research
New York Area Office
207 W. 24th Street
New York, New York 10011

Professor V. Castelli
Department of Mechanical Engineering
Columbia University
New York, New York 10027

Professor H. Elrod
Department of Mechanical Engineering
Columbia University
New York, New York 10027

Engineering Societies Library
345 E. 47th Street
New York, New York 10017

Professor J. J. Stoker
Institute of Mathematical Sciences
New York University
251 Mercer Street
New York, New York 10003

Society of Naval Architects and
Marine Engineers
74 Trinity Place
New York, New York 10006

Miss O. M. Leach, Librarian
National Research Council
Aeronautical Library
Montreal Road
Ottawa 7, Canada

Technical Library
Naval Coastal System Laboratory
Panama City, Florida 32401

Dr. J. W. Hoyt
Naval Undersea R & D Center
Pasadena Laboratory
3202 E. Foothill Boulevard
Pasadena, California 91107

Technical Library
Naval Undersea R & D Center
Pasadena Laboratory
3203 E. Foothill Boulevard
Pasadena, California 91107

Professor A. J. Acosta
Department of Mechanical Engineering
California Institute of Technology
Pasadena, California 91109

Professor H. Liepmann
Graduate Aeronautical Laboratory
California Institute of Technology
Pasadena, California 91109

Professor M. S. Plesset
Department of Engineering Science
California Institute of Technology
Pasadena, California 91109

Professor A. Roshko
California Institute of Technology
Graduate Aeronautical Laboratories
Pasadena, California 91109

Professor T. Y. Wu
Department of Engineering Science
California Institute of Technology
Pasadena, California 91109

Director
Office of Naval Research Branch Office
1030 E. Green Street
Pasadena, California 91106

Naval Ship Engineering Center
Philadelphia Division
Technical Library
Philadelphia, Pennsylvania 19112

Technical Library
Philadelphia Naval Shipyard
Philadelphia, Pennsylvania 19112

Professor R. C. MacCamy
Department of Mathematics
Carnegie Institute of Technology
Pittsburgh, Pennsylvania 15213

Dr. Paul Kaplan
Oceanics, Inc.
Technical Industrial Park
Plainview, New York 11803

Technical Library
Naval Missile Center
Point Mugu, California 93441

Technical Library
Naval Civil Engineering Laboratory
Port Hueneme, California 93041

Commander
Norfolk Naval Shipyard
Portsmouth, Virginia 23709

Dr. H. N. Abramson
Southwest Research Institute
8500 Culebra Road
San Antonio, Texas 78228

Editor
Applied Mechanics Review
Southwest Research Institute
8500 Culebra Road
San Antonio, Texas 78206

Dr. Andrew Fabula
Code 600, Building 106
Naval Undersea R & D Center
San Diego, California 92132

Office of Naval Research
San Francisco Area Office
760 Market Street, Room 447
San Francisco, California 94102

Library
Pearl Harbor Naval Shipyard
Box 400, FPO
San Francisco, California 96610

Technical Library
Hunters Point Naval Shipyard
San Francisco, California 94135

Librarian
Naval Ordnance Laboratory
White Oak
Silver Spring, Maryland 20910

Mr. J. Enig
Room 3-252
Naval Ordnance Laboratory
White Oak
Silver Spring, Maryland 20910

Fenton Kennedy Document Library
The Johns Hopkins University
Applied Physics Laboratory
8621 Georgia Avenue
Silver Spring, Maryland 20910

Professor E. Y. Hsu
Department of Civil Engineering
Stanford University
Stanford, California 94305

Dr. Byrne Perry
Department of Civil Engineering
Stanford University
Stanford, California 94305

Dr. R. L. Street
Department of Civil Engineering
Stanford University
Stanford, California 94305

Professor R. C. Di Prima
Department of Mathematics
Rensselaer Polytechnic Institute
Troy, New York 12181

Professor J. Lumley
Department of Aerospace Engineering
Pennsylvania State University
University Park, Pennsylvania 16802

Dr. J. M. Robertson
Department of Theoretical and
Applied Mechanics
University of Illinois
Urbana, Illinois 61803

Technical Library
Mare Island Naval Shipyard
Vallejo, California 94592

Code 438
Office of Naval Research
Department of the Navy
Arlington, Virginia 22217 (3 copies)

Code 461
Office of Naval Research
Department of the Navy
Arlington, Virginia 22217

Code 463
Office of Naval Research
Department of the Navy
Arlington, Virginia 22217

Code 466
Office of Naval Research
Department of the Navy
Arlington, Virginia 22217

Code 468
Office of Naval Research
Department of the Navy
Arlington, Virginia 22217

Code 473
Office of Naval Research
Department of the Navy
Arlington, Virginia 22217

Code 481
Office of Naval Research
Department of the Navy
Arlington, Virginia 22217

Code 2627
Naval Research Laboratory
Washington, D. C. 20390 (6 copies)

Library, Code 2629 (ONRL)
Naval Research Laboratory
Washington, D. C. 20390 (6 copies)

Code 6170
Naval Research Laboratory
Washington, D. C. 20390

Code 4000
Director of Research
Naval Research Laboratory
Washington, D. C. 20390

Code 8030 (Maury Center)
Naval Research Laboratory
Washington, D. C. 20390

Code 8040
Naval Research Laboratory
Washington, D. C. 20390

Code 031
Naval Ship Systems Command
Washington, D. C. 20360

Code 0341
Naval Ship Systems Command
Washington, D. C. 20360

Code 0322 (L. Benen)
Naval Ship Systems Command
Washington, D. C. 20360

Code 0321 (J. Schuler)
Naval Ship Systems Command
Washington, D. C. 20360

Code 2052
Naval Ship Systems Command
Washington, D. C. 20360

Code 6034
Naval Ship Engineering Center
Center Building
Prince George's Center
Hyattsville, Maryland 20782

Code 6101E
Naval Ship Engineering Center
Center Building
Prince George's Center
Hyattsville, Maryland 20782

Code 6110
Naval Ship Engineering Center
Center Building
Prince George's Center
Hyattsville, Maryland 20782

Code 6114
Naval Ship Engineering Center
Center Building
Prince George's Center
Hyattsville, Maryland 20782

Code 6120E
Naval Ship Engineering Center
Center Building
Prince George's Center
Hyattsville, Maryland 20782

Code 6136
Naval Ship Engineering Center
Center Building
Prince George's Center
Hyattsville, Maryland 20782

Dr. A. Powell (Code 01)
Naval Ship Research & Development Center
Bethesda, Maryland 20034

Mr. W. M. Ellsworth (Code 11)
Naval Ship Research & Development Center
Bethesda, Maryland 20034

Dr. W. E. Cummins (Code 15)
Naval Ship Research & Development Center
Bethesda, Maryland 20034

Dr. H. R. Chaplin (Code 16)
Naval Ship Research & Development Center
Bethesda, Maryland 20034

Mr. G. H. Gleissner (Code 18)
Naval Ship Research & Development Center
Bethesda, Maryland 20034

Mr. R. Wermter (Code 152)
Naval Ship Research & Development Center
Bethesda, Maryland 20034

Dr. W. B. Morgan (Code 154)
Naval Ship Research & Development Center
Bethesda, Maryland 20034

Mr. J. B. Hadler (Code 156)
Naval Ship Research & Development Center
Bethesda, Maryland 20034

Library (Code 5641)
Naval Ship Research & Development Center
Bethesda, Maryland 20034

Mr. S. F. Crump (Code 1505)
Naval Ship Research & Development Center
Bethesda, Maryland 20034

Dr. P. Pien (Code 1521)
Naval Ship Research & Development Center
Bethesda, Maryland 20034

Mr. Paul Granville (Code 1541)
Naval Ship Research & Development Center
Bethesda, Maryland 20034

Mr. J. McCarthy (Code 1552)
Naval Ship Research & Development Center
Bethesda, Maryland 20034

Dr. Nils Salvesen (Code 1552)
Naval Ship Research & Development Center
Bethesda, Maryland 20034

Dr. M. Strasberg (Code 1901)
Naval Ship Research & Development Center
Bethesda, Maryland 20034

Code 03
Naval Air Systems Command
Department of the Navy
Washington, D. C. 20360

AIR 5301
Naval Air Systems Command
Department of the Navy
Washington, D. C. 20360

AIR 604
Naval Air Systems Command
Department of the Navy
Washington, D. C. 20360

Code ORD 03
Naval Ordnance Systems Command
Department of the Navy
Washington, D. C. 20360

Code ORD 035
Naval Ordnance Systems Command
Department of the Navy
Washington, D. C. 20360

Code ORD 05413
Naval Ordnance Systems Command
Department of the Navy
Washington, D. C. 20360

Code ORD 9132
Naval Ordnance Systems Command
Department of the Navy
Washington, D. C. 20360

CNM PM-1
Strategic Systems Project Office
Department of the Navy
Washington, D. C. 20360

Technical Division (CNM PM 11-20)
Deep Submergence Systems Project Office
Department of the Navy
Washington, D. C. 20360

Oceanographer of the Navy
Washington, D. C. 20390

Commander
Naval Oceanographic Office
Washington, D. C. 20390

Dr. A. L. Slafkosky
Scientific Advisor
Commandant of the Marine Corps (CODE AX)
Washington, D. C. 20380

Librarian Station 5-2
Coast Guard Headquarters
NASSIF Building
400 7th Street, S.W.
Washington, D. C. 20591

Office of Research and Development
Maritime Administration
441 G Street, N.W.
Washington, D. C. 20235

Division of Ship Design
Maritime Administration
441 G Street, N.W.
Washington, D. C. 20235

National Science Foundation
Engineering Division
1800 G Street, N.W.
Washington, D. C. 20550

Dr. G. Kulin
National Bureau of Standards
Washington, D. C. 20234

Science & Technology Division
Library of Congress
Washington, D. C. 20540

Chief of Research & Development
Office of Chief of Staff
Department of the Army
Washington, D. C. 20310

Professor A. Thiruvengadam
Department of Mechanical Engineering
The Catholic University of America
Washington, D. C. 20017

Dr. A. S. Iberall, President
General Technical Services, Inc.
451 Penn Street
Yeadon, Pennsylvania 19050

Commander
Portsmouth Naval Shipyard
Portsmouth, New Hampshire 03801